



NTNU Trondheim
Norwegian University of Science and Technology
Department of Marine Technology

TMR4240 Marine Control Systems - Project 1

By:

Abubakar Aliyu BADAWI

Ishfaq Ahmad BHAT

Celil YILMAZ

Tayyab TAHIR

Specialization: Marine and Maritime Intelligent Robotics [MIR]

Submitted to:

Prof. Dong Trong Nguyen

Contents

1	Introduction	1
2	Theory	3
2.1	Reference Frame	3
2.2	Process Plant Model	4
2.2.1	Vessel Dynamics	4
2.2.2	Wave-frequency Process Plant Model	4
2.2.3	Kinematics	5
2.3	Control Plant Model	6
2.3.1	Low-frequency Control Plant Model	7
2.3.2	Wave-frequency Control Plant Model	7
2.3.3	Bias Model	8
2.3.4	Measurements	8
3	Environmental Loads	9
3.1	Current Model	9
3.1.1	Surface currents	9
3.1.2	Simulink Implementation of the Current Model	9
3.2	Wind Model	10
3.2.1	Mean Wind Component	11
3.2.2	Slowly Varying Component	11
3.2.3	Simulink Implementation of the Wind Model	12
3.3	Wave Model	14
3.3.1	Simulink Model of the Wave Model	15
4	Reference Model	16
4.1	Implementation of the Reference Model	16
4.2	Tuning of the Reference Model	17
5	Trust Allocation	18
5.1	Part 1	18
5.2	Linear Effector Model	18
5.3	Extended Thrust Approach	19
5.4	Part 2 - Quadratic Programming	20
5.5	Simulink Implementation of the Thrust Allocations	23

6 Observer Design	23
6.1 Extended Kalman Filter	24
6.1.1 Tuning	26
6.1.2 Simulink model of the EKF Observer	26
6.2 Nonlinear Passive Observer	26
6.2.1 Tuning	28
6.2.2 Simulink Model	28
7 Controller Design	29
7.1 Proportional-Integral-Derivative (PID) Control	29
7.2 Implementation of the PID Controller	31
7.3 Tuning of the PID	31
8 Simulation Results [part 1 & part 2]	33
8.1 Simulation 1	33
8.1.1 Simulation 1A - Current set to 0.5[m/s] from east.	34
8.1.2 Discussion	34
8.1.3 Simulation 1B - Wind with average speed of 10[m/s] from south.	35
8.1.4 Discussion	35
8.2 Simulation 2	36
8.2.1 Simulation 2	37
8.2.2 Discussion	37
8.3 Simulation 3	38
8.3.1 Vessel Dynamics Without Reference Model	38
8.3.2 Vessel Dynamics With Reference Model	39
8.3.3 Discussion	40
8.3.4 Reference Model Velocity Trajectories	40
8.3.5 Discussion	41
8.4 Simulation 4	41
8.4.1 4 Corner Test Results	42
8.4.2 Discussion	42
8.4.3 Reference Model Velocity Trajectories	43
8.4.4 Discussion	43
8.5 Simulation 1 - Environmental Loads	44
8.5.1 Simulation 1 results	44

8.5.2	Discussion	45
8.6	Simulation 2 - DP and Thrust Allocation	45
8.6.1	All actuators active	46
8.6.2	Thruster forces	46
8.6.3	Thruster 2 & 4 off	47
8.6.4	Thruster forces	48
8.6.5	Discussion	48
8.7	Simulation 3 - DP and Environmental Forces	49
8.7.1	Discussion	50
8.8	Simulation 4 - Observer Selection	50
8.8.1	Extended Kalman Filter	51
8.8.2	Position Without wave forces [EKF]	51
8.8.3	Velocities Without wave forces [EKF]	52
8.8.4	Position With wave forces [EKF]	52
8.8.5	Velocities With wave forces [EKF]	53
8.8.6	Discussion	54
8.8.7	Non-linear Passive Observer	54
8.8.8	Position Without wave forces [NPO]	54
8.8.9	Velocities Without wave forces [NPO]	55
8.8.10	Position With wave forces [NPO]	56
8.8.11	Velocities With wave forces [NPO]	56
8.8.12	Discussions	57
8.8.13	Observer Performance Comparison	57
8.9	Simulation 5 - Capability Plot	58
8.9.1	Discussion	59
8.10	Simulation 6 - Observer Robustness	60
8.10.1	Observer Robustness using Extended Kalman Filter	60
8.10.2	Observer Robustness using Non-Linear Passive Observer	61
8.10.3	Discussions	61
8.11	Simulation 7 - DP System Functionality	62
8.11.1	DP System Robotness - Nominal	62
8.11.2	DP System Robustness - Q_Matrix 10^{-8} times smaller	62
8.11.3	DP System Robustness - Q_Matrix 10^{-8} times larger	63
8.11.4	DP System Robustness - U-W is 5 times larger	64

8.11.5	Discussion	65
9	Conclusions	65
9.1	Summary of the project	65
9.2	Project Achievements:	65
9.3	New Knowledge and Discoveries:	66
9.4	Limitations	66
9.5	Areas for Improvement	66

List of Figures

1	Vessel Model	1
2	Reference frame	3
3	Low-frequency (LF) and wave-frequency (WF) motion	4
4	6 DOF Motion for Marine Vessels	5
5	Current Simulink Model	10
6	WInd Relative Angle Calculation	11
7	Wind direction variation around mean value	12
8	Wind Simulink Model	12
9	Wind Model Sub-blocks	13
10	Wind direction variation around mean value	13
11	Wave spectrum as a function of frequency and direction.	15
12	Given Simulink wave block	15
13	Simulink Reference Model	17
14	Thrust Allocation Block	23
15	Observer Block	24
16	Extended Kalman Filter Block	26
17	Non-Linear Passive Observer Block	29
18	PID Controller Block	31
19	Simulation 1a Results	34
20	SImlation 1b Results	35
21	Change of <i>North</i> and <i>East</i> current components over time as the current direction varies from 180° to 270° over a 200-second period.	36
22	Simulation 2 Results	37
23	Simulation 3 Results (Without reference model)	39

24	Simulation 3 Results (With reference model)	39
25	Simulation 3 Velocity Trajectories	41
26	Simulation 4 Results	42
27	4 Coner Test Velocity Trajectories	43
28	Time Series of Vessel Position in North & East under Environmental Forces	44
29	North-East Trajectory Plot under Environmental Forces & North-East Trajectory Plot under Environmental Forces	45
30	Vessel Position - All Thrusters Active	46
31	Comparison of Thruster Dynamics - All Thrusters Active	47
32	Vessel Position - Thrusters 1 & 2 Disable	47
33	Comparison of Thruster Dynamics - Thruster 1 & 2 Disable	48
34	Position Tracking Performance under Environmental Forces	50
35	Position Estimation without Wave Forces - EKF	51
36	Velocity Estimation without Wave Forces - EKF	52
37	Position Estimation with Wave Forces - EKF	53
38	Velocity Estimation with Wave Forces - EKF	53
39	Position Estimation without Wave Forces - NPO	55
40	Velocity Estimation without Wave Forces - NPO	55
41	Position Estimation with Wave Forces - NPO	56
42	Velocity Estimation with Wave Forces - NPO	57
43	Thrust Utilization Force Plots	59
44	EKF Performance under Extreme Wave Conditions	60
45	NPO Performance under Extreme Wave Conditions	61
46	System Response with Nominal Parameters	62
47	System Response with Modified R Matrix	63
48	System Response with Modified Q Matrix	64
49	System Response with Increased Wind Disturbance	64

List of Tables

1	Final tuning parameters for the reference model	18
2	Thruster positions and angles	18
3	Thruster specifications and constraints	20

1 Introduction

This project is developed using the MSS Toolbox (Marine Systems Simulator), a MATLAB/Simulink library designed for simulating marine systems. MSS includes models for various marine vessels, such as ships, underwater vehicles, and floating structures. Additionally, it provides guidance, navigation, and control (GNC) blocks for real-time simulations.

The objective of this project is to design a controller, a reference model, and an external load system for the dynamic positioning of a ship. The controller will be tuned to ensure that the system follows the reference model behavior. For this purpose, a PID controller will be implemented.

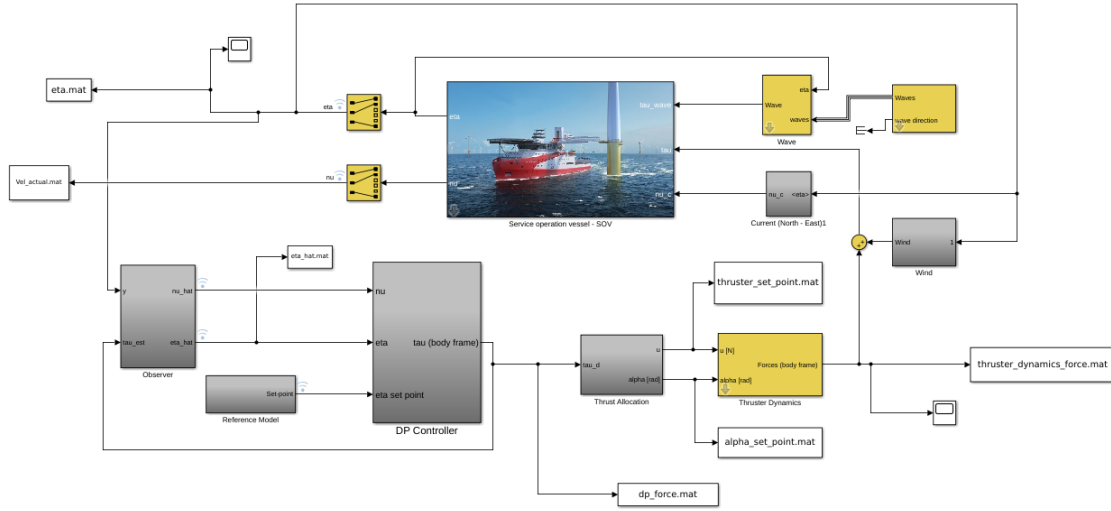


Figure 1: Vessel Model

The vessel's mathematical model, including the equations of motion and the hydrodynamic coefficients utilized in simulations, was prepared in SIMULINK. This report introduces a reference frame employed throughout these simulations. It includes discussions on theories pertinent to process plant modeling and control plant modeling. A mathematical model for the vessel's control plant is proposed, aimed at assisting the design of a potential observer. The reference model used in the simulations is detailed herein. A suitable controller has been selected and implemented for optimizing DP functionality through tuning.

Several tests are necessary to demonstrate the functionality and reliability of the developed systems. These tests are described in the subsequent sections and cover various scenarios that are typical in DP-positioning tasks. Each scenario helps to validate different capabilities of the dynamic positioning system under various conditions and set-point changes.

The document presents a sequence of four simulations for part 1 and seven simulations for part two to evaluate the dynamic positioning (DP) system under diverse conditions:

First Simulations:

- 1. Simulation 1:** Tests the DP system's response to environmental forces with a steady current from the east and varying wind from the south. The objective is to maintain a set-point of $\begin{bmatrix} 0 & 0 & 0 \end{bmatrix}$ and observe the system's stability in xy-plots and individual position and heading

plots until steady state is achieved.

2. **Simulation 2:** Examines the system's performance when the current direction changes linearly, initially from the east, without wind interference. The simulation extends until steady state to ensure the system adjusts and maintains the correct heading and position, depicted in xy and individual plots.
3. **Simulation 3:** Compares vessel position over time from a static starting point to a dynamic setpoint, both with and without a reference model. The scenario excludes environmental forces to isolate control system performance, with results displayed in trajectory and velocity plots.
4. **Simulation 4:** Conducts a DP 4-corner test, challenging the system to accurately navigate and stabilize at sequential setpoints without environmental effects. This critical test confirms the system's precision in transitioning and holding positions and headings as planned.

Second Simulations:

1. Simulation 1: Environmental Loads

This simulation tests the vessel's behavior under environmental forces of current, wind, and waves without thruster activation. The vessel will drift due to these forces, allowing us to observe its natural response over 300 seconds. Current comes from the east at 0.2 m/s, wind from the north at 10 m/s, and waves from the northeast with a significant wave height of 2.5 m and a peak period of 9 seconds. Position and heading are recorded in both individual and xy-plots.

2. Simulation 2: DP and Thrust Allocation

This test examines the DP system's performance during a 4-corner test, moving sequentially between setpoints to observe stability and thruster forces in the absence of environmental forces. We will also conduct a separate simulation disabling thrusters 2 and 4 to evaluate the reconfiguration of thrust allocation. Results will include plots of desired and actual forces, trajectory, and position heading until steady state.

3. Simulation 3: DP and Environmental Forces

This simulation repeats the 4-corner DP test from Simulation 2, but includes environmental forces identical to those in Simulation 1. This test highlights the system's ability to maintain DP under realistic marine conditions, without thruster failure. Position and heading are monitored until steady state, presented in individual and xy-plots.

4. Simulation 4: Observer Selection

Under the same environmental conditions as Simulation 1, this simulation tests two observer designs by comparing their estimates with real measurements before and after wave forces are introduced. The observer that provides the most accurate results will be selected.

5. Simulation 5: Capability Plot

This test generates a thrust utilization plot with weather conditions: wind at 12 m/s, current at 0.2 m/s, significant wave height of 4 m, and peak period of 8 seconds. The vessel holds a stationary setpoint at the origin, with environmental forces from varying directions. Results include average thrust utilization with and without position and heading deviation constraints (3 m and 3°).

6. Simulation 6: Observer Robustness

The robustness of the observer is tested by increasing wave height to 8 m and period to 13 seconds. Vessel position is monitored for 1000 seconds to verify that the observer maintains accurate estimates for station keeping.

7. Simulation 7: DP System Functionality

A custom simulation will demonstrate the DP system's performance in a realistic scenario, chosen to emphasize the system's strengths and limitations. Detailed discussion will follow on observed results, control responses, and areas for improvement.

These simulations collectively verify the DP system's capability to handle a range of operational conditions, ensuring its reliability and precision in real-world maritime tasks.

2 Theory

2.1 Reference Frame

As a reference frame for the vessels motions, the North-East-Down- (NED), and body-fixed frame were used. The NED-frame is a tangent plane to the earth's surface and is denoted as:

$$\{n\} = [x_n, y_n, z_n]^T \quad (1)$$

where x_n follows true north, y_n follows east and z_n is positive pointing downwards.

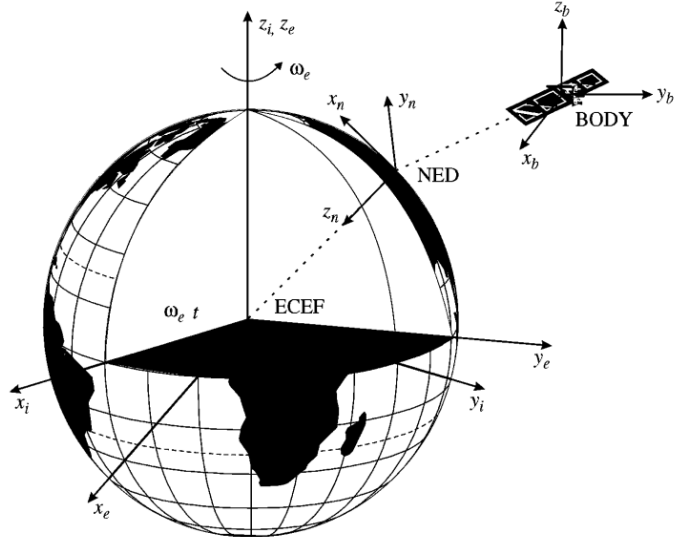


Figure 2: Reference frame
Taken from: *handbook of marine craft hydrodynamics and motion control*

The body-fixed frame corresponds to the vessels different directions and is denoted as:

$$\{b\} = [x_b, y_b, z_b]^T \quad (2)$$

where x_b corresponds to the vessels longitudinal direction, y_b corresponds to transverse directions and

z_b points in a direction normal to x_b and y_b .

The Earth-centered Earth-fixed (ECEF) frame (x_e, y_e, z_e) is rotating with an angular rate ω_e with respect to an Earth-centered inertial (ECI) frame (x_i, y_i, z_i) fixed in space.

2.2 Process Plant Model

The process plant model, or simulation model, is a mathematical model of the physical process. In the case of a supply vessel there is a desire to simulate the real world dynamics. The process plant model gives the necessary detailed descriptions of the vessels dynamics as well as external forces and moments from thrusters and environmental loads.

2.2.1 Vessel Dynamics

When modeling vessel dynamics, it is common to separate the total model into two components using superposition. The first is a wave-frequency model and the second is a low-frequency model, which is referred to as the wave frequency (WF) and low frequency (LF) model respectively. Thus, the total motion becomes a sum of the WF and LF models.

The WF-motions are caused by first order wave loads, while the LF-motions are assumed to be the result of second-order mean and slowly varying wave loads, current loads, wind loads, and thrust forces.

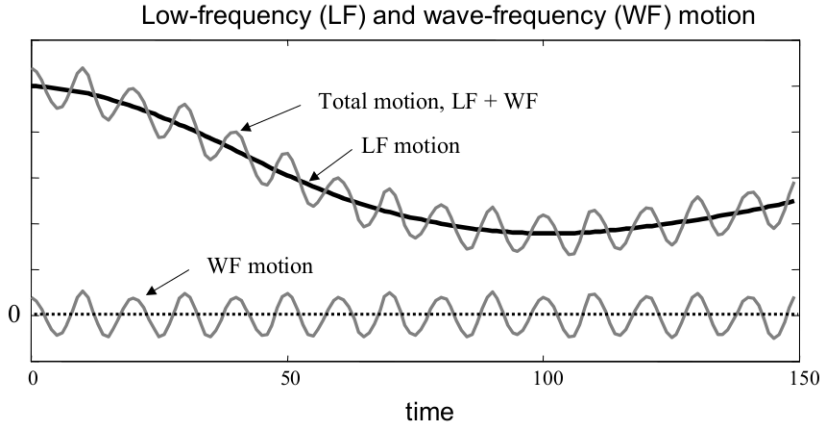


Figure 3: Low-frequency (LF) and wave-frequency (WF) motion
Taken from: *handbook of marine craft hydrodynamics and motion control*

2.2.2 Wave-frequency Process Plant Model

The behavior of first order linear waves is solved as two separate sub-problems, wave reaction and wave excitation. Which is respectively forces due to the vessel being forced to oscillate with the waves and forces due to the vessel being restrained from oscillation. The lecture notes (Sørensen [2018]) express the solution to the respective problems by:

$$M(\omega)\ddot{\eta}_{Rw} + D_p(\omega)\dot{\eta}_{Rw} + G\eta_{Rw} = \tau_{wave1} \quad (3)$$

$$\eta_w = J(\eta_2)\dot{\eta}_{Rw} \quad (4)$$

Where $\eta_2 = [0, 0, \psi_d]^T$

2.2.3 Kinematics

The study of the dynamics of a vessel can be divided into kinematics and kinetics. Kinematics focuses on the geometrical aspects of motion, while kinetics deals with the analysis of forces that cause motion. This section defines the motion variables, reference frames, and the transformations between these frames (Fossen, 2011, Chapter 2).

DOF	Forces and moments	Linear and angular velocities	Positions and Euler angles
1	motions in the x direction (surge)	X	u
2	motions in the y direction (sway)	Y	v
3	motions in the z direction (heave)	Z	w
4	rotation about the x axis (roll, heel)	K	p
5	rotation about the y axis (pitch, trim)	M	q
6	rotation about the z axis (yaw)	N	r

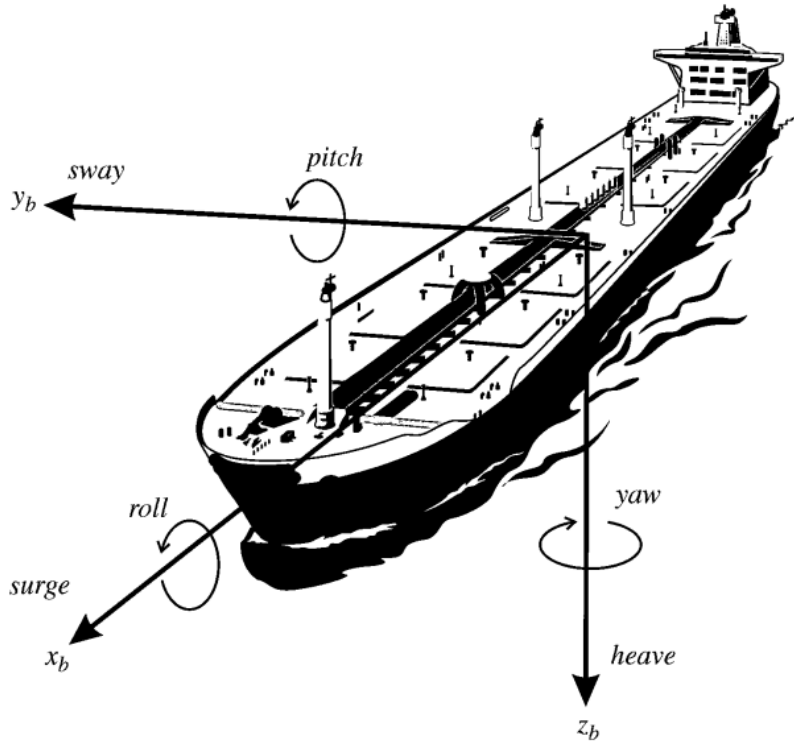


Figure 4: 6 DOF Motion for Marine Vessels
Taken from: *handbook of marine craft hydrodynamics and motion control*

For marine craft moving in six degrees of freedom (DOF), six independent coordinates are required to determine the position and orientation. The first three coordinates and their time derivatives correspond to position and translational motion along the x , y , and z axes. The last three coordinates, along with their time derivatives, describe the orientation and rotational movement (Fossen T.I., page 15) [3]. These variables lead to the SNAME notation for marine vessels, as shown in Table 1. The

vectors η , representing position and Euler angles, and ν , representing linear and angular velocities, are used to describe the motion.

When analyzing the motion of marine craft in 6 DOF, it is useful to define two Earth-centered coordinate frames, along with several geographic reference frames. Fossen defines the Earth-centered frames as the "Earth-Centered Inertial" (ECI) frame and the "Earth-Centered, Earth-Fixed" (ECEF) frame.

The following coordinate frames are commonly used in marine navigation and control:

- **ECI** $i = (x_i, y_i, z_i)$: An inertial frame used for terrestrial navigation. It is non-accelerating and follows Newton's laws of motion, with its origin at the center of the Earth.
- **ECEF** $e = (x_e, y_e, z_e)$: This frame has its origin at the Earth's center but rotates relative to the ECI frame. It is typically used for global navigation and control, such as intercontinental travel.
- **NED** $n = (x_n, y_n, z_n)$: A local coordinate system often defined as a tangent plane at the Earth's surface. The x and y axes point towards true North and East, while the z axis points downwards. The position of n relative to e is determined by the latitude (l) and longitude (μ).
- **BODY** $b = (x_b, y_b, z_b)$: A coordinate frame fixed to the vessel, moving with it. The x_b axis represents the longitudinal axis (aft to fore), y_b the transverse axis (to starboard), and z_b the normal axis (top to bottom). This frame is typically used to express the vessel's linear and angular velocities.

2.3 Control Plant Model

Compared to the process plant model in Section 3, the purpose of a control plant model is to capture the essential behavior of the system, i.e., the most necessary physical characteristics of the model, and not the details. These models are formulated based on careful model reduction or simplification, resulting in a low-fidelity model. The control plant model can constitute a part of the controller and can be used for analytical stability analysis.

In this project, the control plant model is divided into four sub-problems: low-frequency (LF), high-frequency (or wave-frequency, WF), bias, and measurements. While part 1 only considered the low-frequency components, part 2 expands to include all four sub-models.

The system of equations representing the control plant model is given by:

$$\dot{\zeta} = \mathbf{A}_w \zeta + \mathbf{E}_w \mathbf{w}_w \quad (5)$$

$$\dot{\eta} = \mathbf{R}(\psi) \nu \quad (6)$$

$$\dot{\mathbf{b}} = -\mathbf{T}_b^{-1} \mathbf{b} + \mathbf{E}_b \mathbf{w}_b \quad (7)$$

$$\dot{\nu} = -\mathbf{M}^{-1} \mathbf{D} \nu + \mathbf{M}^{-1} \mathbf{R}^T(\psi) \mathbf{b} + \tau \quad (8)$$

$$\mathbf{y} = \eta + \eta_w + \mathbf{w} \quad (9)$$

The variables and matrices used in these equations are described in the following subsections:

- **Equation (5)** describes the wave-frequency dynamics with ζ as the state variable, \mathbf{A}_w as the system matrix, and $\mathbf{E}_w \mathbf{w}_w$ representing the wave input disturbance.

-
- **Equation (6)** represents the kinematic equation, where η is the position and orientation vector, $\mathbf{R}(\psi)$ is the rotation matrix as a function of the yaw angle ψ , and ν is the velocity vector.
 - **Equation (7)** models the dynamics of the bias, where \mathbf{b} is the bias vector, \mathbf{T}_b^{-1} is the inverse time constant matrix, and $\mathbf{E}_b \mathbf{w}_b$ represents the input disturbance for the bias.
 - **Equation (8)** describes the low-frequency velocity dynamics, where \mathbf{M} is the mass matrix, \mathbf{D} is the damping matrix, and τ represents external forces acting on the system.
 - **Equation (9)** defines the measurement equation, where \mathbf{y} is the measured output, including the true position η , wave-induced motion η_w , and a measurement noise term \mathbf{w} .

This is a linear model based on assumptions of small waves and motion amplitudes. By including wave excitation and reaction forces, one can solve the hydrodynamic problem of the vessel. This approach assumes potential theory and neglects viscous effects.

2.3.1 Low-frequency Control Plant Model

Low-frequency (LF) motions are assumed to be caused by second-order mean, slowly-varying loads from wind, current, waves, and forces from the mooring and thrust.

In the low-frequency model, Equation (4) is reduced from 6 DOF to 3 DOF of interest: surge, sway, and yaw (all in the horizontal plane). This simplification is appropriate due to the large vessel size, which results in self-stabilizing behavior in vertical motion. Therefore, it is more convenient for controller design and analysis to derive this nonlinear LF control plant model.

By simplifying Equation (4), we obtain the following reduced equations for the LF model:

$$\dot{\eta} = \mathbf{R}(\psi)\nu \quad (10)$$

$$\mathbf{M}\dot{\nu} + \mathbf{D}\nu + \mathbf{R}^T(\psi)\mathbf{G}(\eta) = \tau + \mathbf{R}^T(\psi)\mathbf{b} \quad (11)$$

where $\nu = [u, v, r]^T$, $\eta = [x, y, \psi]^T$, and $\mathbf{b} \in R^3$ is the bias vector. Additionally, $\eta = [\eta_x, \eta_y, \eta_\psi]^T$ represents the control input vector.

The Coriolis and centripetal forces, $\mathbf{C}_{RB}(\nu_r)\nu_r$ and $\mathbf{C}_A\nu_r$, from Equation (4) are neglected due to the small changes in the body frame when the vessel's velocity is low. Similarly, the damping and current forces, $\mathbf{D}(\kappa, \nu_r)$, can be set to zero because of the small angles involved in low-frequency motion.

2.3.2 Wave-frequency Control Plant Model

To model the wave-frequency (WF) motions, fewer assumptions and simplifications are needed compared to the low-frequency (LF) model. The WF motions can be effectively represented by a harmonic oscillator in state-space form, as shown in Equations (4.7) and (4.8):

$$\dot{\zeta}_w = A_w \zeta_w + E_w w_w \quad (4.7)$$

$$\eta_w = C_w \zeta_w \quad (4.8)$$

Here, $\dot{\zeta}_w$ is the wave-induced motion vector, A_w is the system matrix, E_w is the disturbance matrix, w_w is a zero-mean Gaussian white noise vector, and C_w is the measurement matrix. The matrices are defined mathematically in Equation (4.9):

$$A_w = \begin{bmatrix} \mathbf{0}_{3 \times 3} & \mathbf{I}_{3 \times 3} \\ -\Omega^2 & -2\Lambda\Omega \end{bmatrix}, \quad E_w = \begin{bmatrix} \mathbf{0}_{3 \times 3} \\ K_w \end{bmatrix}, \quad C_w = \begin{bmatrix} \mathbf{0}_{3 \times 3} & \mathbf{I}_{3 \times 3} \end{bmatrix} \quad (4.9)$$

Where:

- $\Omega = \text{diag}(\omega_1, \omega_2, \omega_3)$ is the diagonal matrix of natural frequencies.
- $\Lambda = \text{diag}(\zeta_1, \zeta_2, \zeta_3)$ is the diagonal matrix of damping ratios.
- $K_w = \text{diag}(K_{w1}, K_{w2}, K_{w3})$ is the diagonal matrix of wave disturbance gains.

For more detailed explanations and derivations, refer to Sørensen [2018].

2.3.3 Bias Model

The bias model captures the slowly-varying forces and moments caused by second-order wave loads, ocean currents, wind, and any errors in the modeling process. A commonly used bias model is the Markov model, where the bias vector $\mathbf{b} \in R^3$ is governed by the following equation:

$$\dot{\mathbf{b}} = -\mathbf{T}_b^{-1}\mathbf{b} + \mathbf{E}_b\mathbf{w}_b \quad (15)$$

In this equation, \mathbf{b} represents the bias vector, \mathbf{w}_b is a vector of zero-mean Gaussian white noise, \mathbf{T}_b is a diagonal matrix of bias time constants, and \mathbf{E}_b is a diagonal scaling matrix.

An alternative bias model is the Wiener process, which is described by the following equation:

$$\dot{\mathbf{b}} = \mathbf{E}_b\mathbf{w}_b \quad (16)$$

In this model, the bias evolves purely as a stochastic process driven by the noise vector \mathbf{w}_b and scaled by \mathbf{E}_b .

2.3.4 Measurements

The measurement equation is given by:

$$\mathbf{y} = \boldsymbol{\eta} + \boldsymbol{\eta}_\omega + \mathbf{v}$$

In this equation, \mathbf{y} represents the output, which is composed of the low-frequency (LF) motion $\boldsymbol{\eta}$, the wave-frequency (WF) motion $\boldsymbol{\eta}_\omega$, and the measurement noise $\mathbf{v} \in R^3$. The noise vector \mathbf{v} is assumed to be zero-mean Gaussian noise.

3 Environmental Loads

Models of environmental loads are essential for achieving realistic simulations of a marine vessel. For Project 1, we will look at only the current and the wind models; in the next project, we will also implement the wave model.

3.1 Current Model

Water currents can behave as disturbances on the vessel and must be taken into account when designing and implementing the controller.

When talking about current modeling, we are looking at two levels of detail:

- Surface current: used for modeling the surface vessel response
- Full current profile: for use in modeling of riser, anchor lines, etc.

A two-dimensional (2D) current model (surface current) is sufficient when modeling a surface vessel, and this approach is described in the following subsection.

3.1.1 Surface currents

For the current velocity vector ν_c in NED frame, we get the following equation:

$$\nu_c = \begin{bmatrix} V_c \cos \psi_c \\ V_c \sin \psi_c \\ 0 \end{bmatrix} \quad (5)$$

Where V_c is the magnitude and ψ_c is the direction in the NED frame. Recall that the down component is zero.

The variation in current velocity, V_c , may be implemented by a first order Gauss-Markov Process, where ω represents the white noise and the constant $\mu \geq 0$.

$$\omega = \dot{V}_c + \mu V_c$$

Similarly, the variation in current direction, ψ_c , may be implemented as

$$\omega = \dot{\psi}_c + \mu \psi_c$$

3.1.2 Simulink Implementation of the Current Model

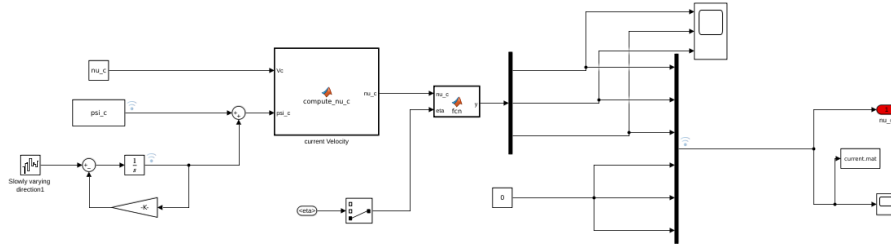


Figure 5: Current Simulink Model

The Simulink current model provides a detailed representation of ocean current dynamics, combining both predictable and random elements. The model has three main inputs: the mean current velocity (ν_c), the current direction (ψ_c), and a slowly changing directional component created using a first-order Gauss-Markov process. This directional component uses a white noise input processed through an integrator ($\frac{1}{s}$) and a feedback loop with a gain (K) to produce realistic directional variations. These inputs come together in the current velocity computation block, which processes the magnitude and direction to create a current velocity vector. The model uses various signal pathways and bus structures to handle the different parts of the current model, with outputs available for visualizing the current magnitude and the computed current forces. The model computes current forces through several steps. First, it calculates the current velocity vector (ν_c) in the North-East-Down (NED) frame using the expression:

$$\nu_c = \begin{bmatrix} V_c \cos \psi_c \\ V_c \sin \psi_c \\ 0 \end{bmatrix}$$

where V_c is the current speed and ψ_c is the current direction. This vector is then transformed into the body frame (the vessel's local frame of reference) by a "From NED to Body" block, which takes the vessel's heading into account and provides the body-frame current velocities. The model includes scopes and output blocks for tracking key parameters. The rightmost blocks handle the computation of the current magnitude and routing signals for integration with the vessel's control system.

3.2 Wind Model

Wind is the movement of air and is typically divided into two components: a mean value and a fluctuating component (gusts). Although wind forces are often smaller compared to wave and current forces, they cannot be neglected. While wind is inherently a three-dimensional phenomenon, the commonly used models restrict the analysis to horizontal plane velocities, characterized by the wind speed U and direction ψ [6].

In this project, wind loads are computed as generalized forces acting on the body frame across all six degrees of freedom (DOFs). The wind model utilizes a coefficient table, where the generalized wind forces are calculated as:

$$F_{\text{wind}} = |V_w|^2 \cdot C_w(\alpha_{rw}) \quad (21)$$

Here, F_{wind} represents the generalized wind forces, V_w is the wind velocity magnitude, $C_w(\alpha_{rw})$ is the wind coefficient matrix, and α_{rw} is the relative angle between the wind direction and the vessel

heading.

NOTE: $C_w(\alpha_{rw})$ is the wind coefficient matrix and in our case is in degree inside the init file and we then convert the angle we get from the measurement to degree because the wind coefficient were in degrees

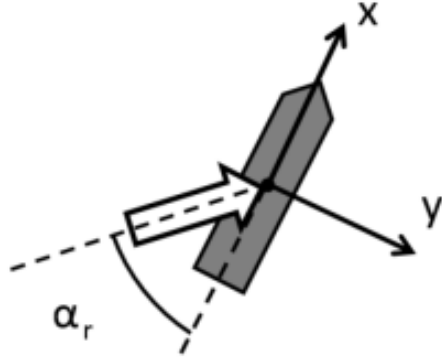


Figure 6: WInd Relative Angle Calculation

Figure 5 shows how the relative wind angle is calculated. The detailed procedure for calculating the relative incidence angle is provided in Appendix A of the project description for part 2.

3.2.1 Mean Wind Component

The mean wind velocity at elevation z is expressed as:

$$\begin{aligned}\frac{\bar{U}(z)}{\bar{U}_{10}} &= \frac{5}{2} \sqrt{\kappa} \ln \left(\frac{z}{z_0} \right) \\ z_0 &= 10 \times \exp \left(-\frac{2}{5\sqrt{\kappa}} \right)\end{aligned}\quad (22)$$

where \bar{U}_{10} is the one-hour wind speed at an elevation of 10 meters, κ is the sea surface drag coefficient, and z is the elevation.

3.2.2 Slowly Varying Component

Slowly-varying changes in the mean wind velocity can be modeled using a first-order Gauss-Markov process [6]:

$$\dot{\bar{U}} + \mu \bar{U} = w \quad (23)$$

where w is Gaussian white noise and μ is a constant ($\mu \geq 0$). If $\mu = 0$, the process becomes a random walk. The wind velocity is constrained by saturation limits:

$$0 \leq \bar{U}_{\min} \leq \bar{U} \leq \bar{U}_{\max} \quad (24)$$

Variations in wind direction can be modeled similarly:

$$\dot{\psi} + \mu_2 \psi = \omega_2 \quad (25)$$

$$\psi_{\min} \leq \psi \leq \psi_{\max} \quad (26)$$

where ω_2 is Gaussian white noise, and μ_2 is a positive constant.

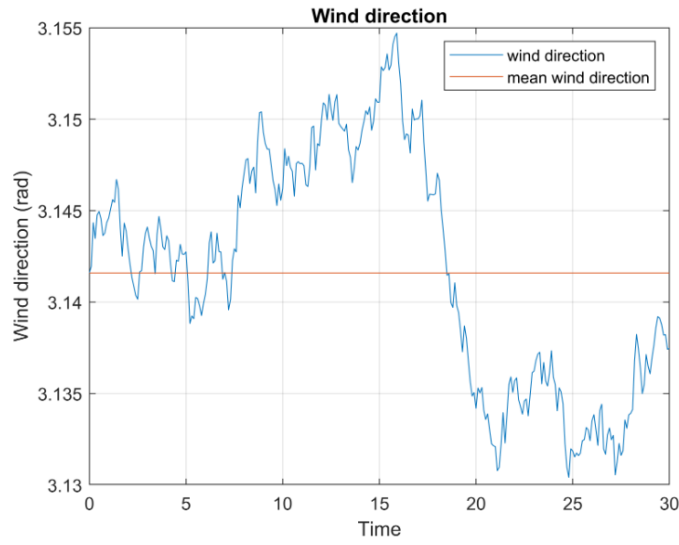


Figure 7: Wind direction variation around mean value

3.2.3 Simulink Implementation of the Wind Model

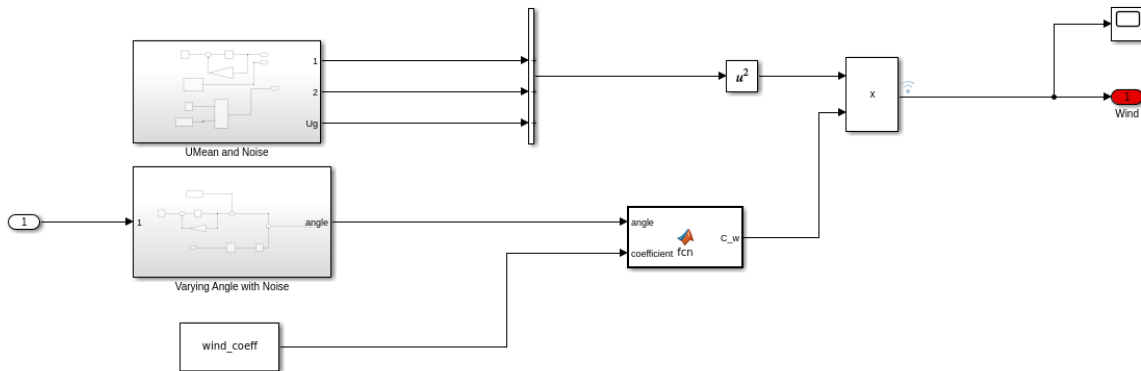


Figure 8: Wind Simulink Model

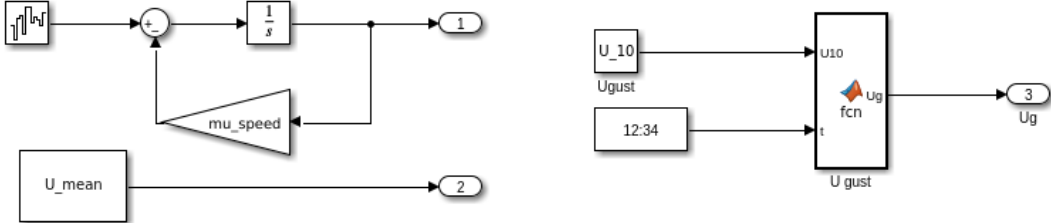


Figure 9: Wind Model Sub-blocks

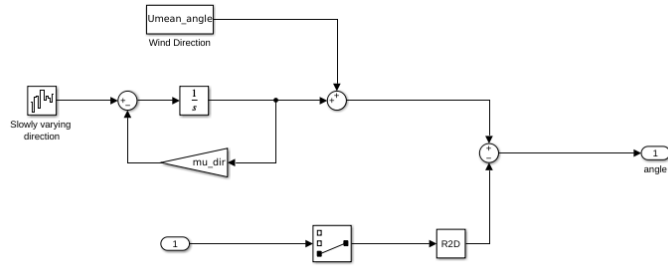


Figure 10: Wind direction variation around mean value

The Simulink model for wind includes both steady and fluctuating wind components, combining multiple subsystems to simulate wind effects on a vessel. The main part of the model uses a steady wind speed, U_{mean} , which combines with three random noise signals through separate channels. This setup allows for different types of wind turbulence and disturbances to be represented in a more detailed way. For gradual changes in wind speed, the model uses a first-order Gauss-Markov process, which smooths out the noise to simulate slow wind variations. This is controlled by the parameter μ_{speed} , which adjusts the rate of these changes. Additional feedback loops and gains further modify these noise characteristics, helping the model achieve realistic wind patterns. The model also includes a system for wind angle variations, which brings in its own noise inputs and variation patterns. These components are processed to create more realistic directional changes in the wind profile over time. Together, these parts create a comprehensive wind profile that includes both wind speed and direction changes.

To compute the wind forces, the model calculates the relative wind angle, α_{rw} , by accounting for both the steady wind direction, ψ , and the vessel's heading, while also considering the vessel's movement. A wind coefficient function block uses tables of wind force coefficients, C_w , for the vessel's motion in three directions: surge, sway, and yaw. The wind force model calculates forces based on air density, the vessel's reference area, wind speed, and wind coefficients. It then transforms these forces into the vessel's body frame, which makes it easier to use within the vessel's control system. Additionally, the model includes scope outputs and visualization blocks for monitoring different parts of the wind model and the final computed wind forces, making it easier to analyze and validate the model's performance.

3.3 Wave Model

Irregular waves are commonly described by a wave spectrum $S(\omega, \psi)$, which generally depends on both frequency ω and direction ψ (Faltinsen, 1993). The wave spectrum is often divided into a frequency spectrum $S(\omega)$ and a directional spreading function $D(\omega, \psi)$, such that

$$S(\omega, \psi) = S(\omega)D(\omega, \psi)$$

The total energy in the sea state, S_{tot} , is given by integrating over all frequencies and directions:

$$S_{\text{tot}} = \int_0^\infty \int_0^{2\pi} S(\omega, \psi) d\psi d\omega$$

Frequency Spectrum $S(\omega)$: Irregular waves are described by a wave spectrum $S(\omega, \psi)$, which depends on both frequency ω and direction ψ . This spectrum can be divided into a frequency spectrum $S(\omega)$ and a directional spreading function $D(\omega, \psi)$. The frequency spectrum describes the energy distribution of waves across different frequencies. Harmonic wave components can be derived from the spectrum using selected frequencies ω_q and frequency intervals $\Delta\omega_q$. The amplitude ζ_{aq} of a wave component is calculated as $\zeta_{aq} = \sqrt{2S(\omega_q)\Delta\omega_q}$. The harmonic waves are represented as $\zeta_q(t) = \zeta_{aq} \cos(\omega_q t + \phi_q)$.

Spreading Function $D(\omega, \psi)$: The spreading function $D(\omega, \psi)$ represents the directional distribution of wave energy. It is often simplified to depend only on the direction and ensures conservation of total wave energy.

Wave Spectrum $S(\omega, \psi)$: The wave spectrum $S(\omega, \psi)$ combines the frequency spectrum and the spreading function, representing the energy distribution over both frequencies and directions. Integration over all directions results in the frequency spectrum $S(\omega)$.

Implementation Considerations: Modifications can be applied to the wave spectrum to reduce computational effort while preserving realism. Common wave spectra include Pierson-Moskowitz (PM), ITTC/ISSC, JONSWAP, and Torsethaugen spectra. PM spectra are characterized by parameters A and B and are applicable to fully developed sea states. ITTC/ISSC spectra are defined using significant wave height H_s and peak wave frequency ω_p to determine parameters A and B . Adjusting parameters like the frequency cutoff ξ , direction limit ψ_{lim} , and energy limit k can reduce the number of wave components without significantly impacting realism.

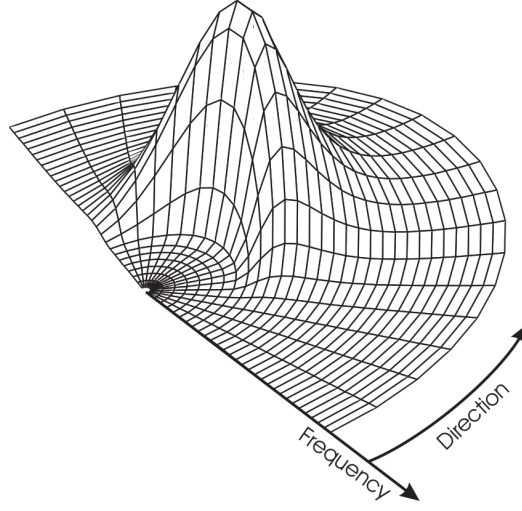


Figure 11: Wave spectrum as a function of frequency and direction.

In this project, the wave model was provided, and only minor parameter adjustments, such as wave height and wave period, were required to simulate various wave conditions.

Waves are generated by wind blowing over a fluid surface. The spectrum $S(\omega, \psi)$ is often divided into two parts: a frequency spectrum $S(\omega)$ and a directional spreading function $D(\psi, \omega)$, resulting in

$$S(\omega, \psi) = S(\omega)D(\psi, \omega) \quad (30)$$

There are three commonly used frequency spectra for waves: Pierson-Moskowitz (PM), ITTC/ISSC, and JONSWAP. In this project, the ITTC spectrum is used, but it is possible to change the spectrum type in the wave block. The ITTC spectrum is defined as:

$$S(\omega) = \frac{A}{\omega^5} \exp\left(-\frac{B}{\omega^4}\right) \quad (31)$$

where $A = 0.31H_s^2\omega_p^4$ and $B = 1.25\omega_p^4$. Here, H_s is the significant wave height, and ω_p is the peak wave frequency.

3.3.1 Simulink Model of the Wave Model

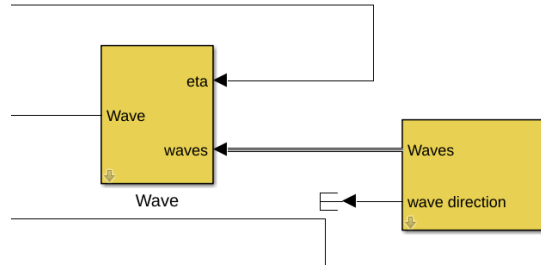


Figure 12: Given Simulink wave block

NOTE: The wave loads were implemented in the Simulink model using a given wave block from the

MSS toolbox.

4 Reference Model

A reference model is essential for the Dynamic Positioning (DP) control system, as the controller must function in both stationkeeping and trajectory-following modes. When the vessel is required to follow multiple reference points, an autopilot is used. The reference model is implemented in the NED-frame (North-East-Down) and allows us to select a global position.

The reference model is designed to smooth the reference signal and minimize abrupt transitions. This is particularly useful in preventing large, sudden changes in reference signals, such as an immediate shift from 0 to 50 meters, which can destabilize the controller or vessel.

4.1 Implementation of the Reference Model

The chosen reference model is a cascade reference model (see pages 181-182), which combines a first-order low-pass filter with a mass-spring-damper system. The low-pass filter smooths the signal and prevents step changes in the controller's output, while the mass-spring-damper system captures the dynamics necessary for the vessel to follow the trajectory. The reference model is described by the following equations:

$$\mathbf{a}_d^e + \boldsymbol{\Omega} \mathbf{v}_d^e + \boldsymbol{\Gamma} \mathbf{x}_d^e = \boldsymbol{\Gamma} \mathbf{x}_{ref} \quad (25)$$

$$\dot{\mathbf{x}}_{ref} = -\mathbf{A}_f \mathbf{x}_{ref} + \mathbf{A}_f \boldsymbol{\eta}_r \quad (26)$$

The matrices in these equations are defined as:

$$\boldsymbol{\Omega} = \text{diag} \{2\zeta_i \omega_i\}, \quad i = 1, 2, 3 \quad (27)$$

$$\boldsymbol{\Gamma} = \text{diag} \{\omega_i^2\}, \quad i = 1, 2, 3 \quad (28)$$

$$\mathbf{A}_f = \text{diag} \left\{ \frac{1}{t_i} \right\}, \quad i = 1, 2, 3 \quad (29)$$

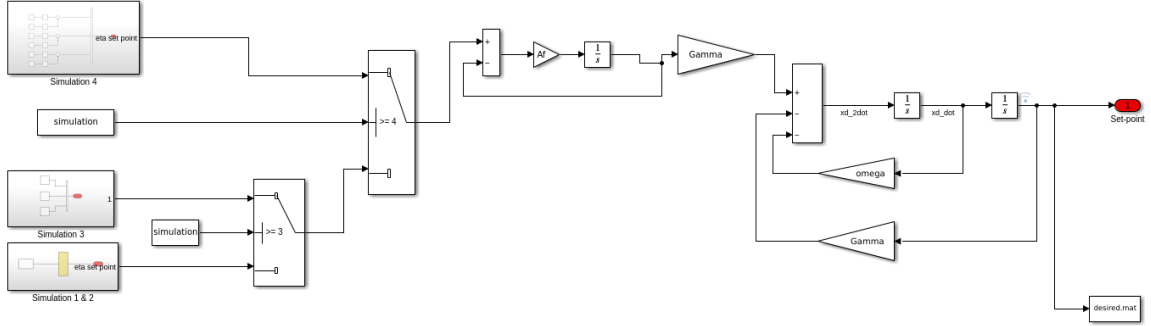


Figure 13: Simulink Reference Model

The Simulink implementation of the reference model is essential for ensuring smooth and stable performance of the Dynamic Positioning (DP) control system. The model is designed to provide reference signals for both stationkeeping and trajectory-following modes. To achieve this, the reference signal is processed using a cascade reference model, which combines a low-pass filter and a mass-spring-damper system. This setup ensures that sudden changes in the reference signals, such as abrupt position shifts, are filtered, preventing destabilization of the vessel or controller.

The reference model begins by inputting the desired reference set points. Depending on the simulation scenario, the model checks which set point to use. The chosen set point then passes through a low-pass filter (represented by the integrator and Af blocks) to ensure smooth transitions. The mass-spring-damper system, represented by the Gamma and Omega blocks, is responsible for adding necessary dynamics that enable the vessel to follow the reference trajectory. The output of the model provides smoothed reference signals for position and velocity (xd_dot and xd_2dot) in the NED frame. These reference signals are then fed into the control system to guide the vessel's movement toward the desired set points in a controlled and stable manner.

4.2 Tuning of the Reference Model

The reference model is tuned by observing each position trajectory and comparing it with the input reference trajectory. To avoid oscillations, the damping coefficient ζ_i is adjusted to achieve either critical or over-damping. For a critically damped system, $\zeta = 1$, and for an over-damped system, $\zeta > 1$. Initially, ζ_i is set to 1, and increased if oscillations are observed. This tuning is performed for each state individually, and adjustments to the controller are made if necessary.

The natural period corresponding to ω_i typically ranges from 50 to 200 seconds for vessels of this size. Initially, ω_i is set using the relation $\omega_i = \frac{2\zeta_i 2\pi}{T}$, where T is the desired period in seconds. For this system, the period is chosen as $T = 10$ seconds, giving an initial value of $\omega_i = \frac{2\pi}{10}$ for each state. The values of ω_i are adjusted during tuning to ensure the best system response.

The filter gain $\mathbf{A}_f = [0.1, 0.1, 0.01]$ is applied to the system to smoothen the response, reducing the impact of high-frequency disturbances. The time constant for the low-pass filter is set such that the filter reaches 63.2% of its maximum value at time t_i for each state.

The damping ratio is set to $\zeta_i = 1$ for all states to ensure critical damping. The natural frequency ω_i is initially set to $\frac{2\pi}{10}$, corresponding to a period of 10 seconds, and adjusted as needed based on system performance.

i	A_{fi}	t_i (s)	ζ_i	ω_i
1	0.1	10	1.0	$\frac{2\pi}{t_i}$
2	0.1	10	1.0	$\frac{t_i}{2\pi}$
3	0.01	100	1.0	$\frac{2\pi}{t_i}$

Table 1: Final tuning parameters for the reference model

5 Trust Allocation

The control algorithm outputs the total forces and moments required to move the vessel to the desired reference point. However, these forces cannot be directly applied to the ship, as there is no way to distribute the generalized forces to its individual thrusters. Therefore, we need to implement a thrust allocation system that decomposes the generalized forces calculated by the PID controller into individual commands for each thruster. This process is known as Thrust Allocation.

Since the system is over-actuated, several approaches are possible for thrust allocation. An extended thrust alloInitially, a quadratic programming-based optimization approach was used in the second part.

5.1 Part 1

The supply vessel is equipped with five thrusters: one tunnel thruster located at the bow, and four azimuth thrusters. Two are positioned at the stern and two at the bow.

As with any physical system, the thrusters are subject to limitations, such as maximum thrust, thrust ramp rate, and the rotation rate of the azimuth thrusters. Table 8.1 outlines the key specifications and limitations for each thruster. Thrusters 2, 4, and 5 are azimuth thrusters that can rotate freely.

Thruster Number	Position X [m]	Position Y [m]	Angle [deg]
1	39.3	0	90
2	35.6	0	α_2
3	31.3	0	90
4	-28.5	5	α_4
5	-28.5	-5	α_5

Table 2: Thruster positions and angles.

5.2 Linear Effector Model

The relationship between the thrust exerted by the actuators and the generalized forces is described by the Linear Effector Model (Eq. 8.1):

$$\boldsymbol{\tau} = \mathbf{B}\mathbf{u} \quad (8.1)$$

Here, $\boldsymbol{\tau}$ is the vector of generalized forces, \mathbf{u} is the vector of thruster commands, and $\mathbf{B} \in R^{m \times p}$ is the effectiveness matrix that describes how the thrusters generate the forces $\boldsymbol{\tau}$. In this case, $p = 5$ represents the number of thrusters, and $m = 3$ corresponds to the degrees of freedom (surge, sway, and yaw).

To allocate thrust, we need to compute the inverse of the matrix \mathbf{B} , or more practically, its pseudo-inverse, since \mathbf{B} is generally not square. The thruster commands can then be computed as:

$$\mathbf{u} = \mathbf{B}^{-1} \boldsymbol{\tau} \quad (8.2)$$

The vector \mathbf{u} is given by:

$$\mathbf{u} = [u_1 \ u_2 \ u_3 \ u_4 \ u_5]^T \quad (8.3)$$

Each thruster's contribution to the forces is described in the \mathbf{B} matrix. The tunnel thruster generates forces only in the sway direction, with a corresponding moment in yaw, as shown in Eq. 8.4:

$$b_1 = [0 \ 1 \ l_{x,1}]^T \quad (8.4)$$

Azimuth thrusters generate both surge and sway forces, as well as moments. The forces depend on the angular position of the thruster, and they are expressed as body-fixed forces in Eq. 8.5:

$$b_i = [\cos(\alpha_i) \ \sin(\alpha_i) \ l_{x,i} \sin(\alpha_i) - l_{y,i} \cos(\alpha_i)]^T, \quad i = \{2, 3, 4, 5\} \quad (8.5)$$

Thus, the full \mathbf{B} matrix is:

$$\mathbf{B} = \begin{bmatrix} 0 & \cos(\alpha_2) & 0 & \cos(\alpha_4) & \cos(\alpha_5) \\ 1 & \sin(\alpha_2) & 1 & \sin(\alpha_4) & \sin(\alpha_5) \\ l_{x,1} & l_{x,2} \sin(\alpha_2) - l_{y,2} \cos(\alpha_2) & l_{x,3} & l_{x,4} \sin(\alpha_4) - l_{y,4} \cos(\alpha_4) & l_{x,5} \sin(\alpha_5) - l_{y,5} \cos(\alpha_5) \end{bmatrix} \quad (8.6)$$

The expanded form of Eq. 8.1 for our vessel is:

$$\begin{bmatrix} F_X \\ F_Y \\ M \end{bmatrix} = \begin{bmatrix} 0 & \cos(\alpha_2) & 0 & \cos(\alpha_4) & \cos(\alpha_5) \\ 1 & \sin(\alpha_2) & 1 & \sin(\alpha_4) & \sin(\alpha_5) \\ 39.5 & 35.3 \sin(\alpha_2) - 0 \cos(\alpha_2) & 31.3 & 28.5 \sin(\alpha_4) - 5 \cos(\alpha_4) & 28.5 \sin(\alpha_5) - 5 \cos(\alpha_5) \end{bmatrix} \begin{bmatrix} u_1 \\ u_2 \\ u_3 \\ u_4 \\ u_5 \end{bmatrix} \quad (8.7)$$

5.3 Extended Thrust Approach

In Equation (8.7), the effectiveness matrix \mathbf{B} depends on the thruster angles $\boldsymbol{\alpha}$. This creates a challenge because the thruster angles are variables we aim to compute in the thrust allocation algorithm, rather than known inputs. To address this, we adopt an extended thrust approach. In this method, we decompose the control inputs for the azimuth thrusters into longitudinal and lateral components and treat each component as a separate thruster.

Figure 8.1: Decomposition of azimuth thrust

The extended thrust vector is then expressed as:

$$\begin{aligned}\mathbf{u}_{\text{exp}} &= [\mathbf{u}_1, \mathbf{u}_{2,x}, \mathbf{u}_{2,y}, \mathbf{u}_3, \mathbf{u}_{4,x}, \mathbf{u}_{4,y}, \mathbf{u}_{5,x}, \mathbf{u}_{5,y}]^T \\ &= [\mathbf{u}_1, \mathbf{u}_2, \mathbf{u}_3, \mathbf{u}_4, \mathbf{u}_5, \mathbf{u}_6, \mathbf{u}_7, \mathbf{u}_8]^T\end{aligned}\quad (8.8)$$

The \mathbf{B} matrix must also be expanded. Each x -component contributes to surge and moment, while each y -component affects sway and moment. The components are given by:

$$\begin{aligned}b_i &= [0, 1, l_{x,i}]^T, \quad i = \{1, 2, 4, 6, 8\} \\ b_i &= [1, 0, l_{y,i}]^T, \quad i = \{3, 5, 7, 9\}\end{aligned}$$

This results in the expanded \mathbf{B} matrix for the system:

$$\begin{aligned}\mathbf{B} &= \begin{bmatrix} 0 & 1 & 0 & 0 & 1 & 0 & 1 & 0 \\ 1 & 0 & 1 & 1 & 0 & 1 & 0 & 1 \\ 39.3 & 0 & 35.6 & 31.3 & -5 & -28.5 & -5 & -28.5 \end{bmatrix} \quad (8.10) \\ \Rightarrow \begin{bmatrix} F_X \\ F_Y \\ M \end{bmatrix} &= \begin{bmatrix} 0 & 1 & 0 & 0 & 1 & 0 & 1 & 0 \\ 1 & 0 & 1 & 1 & 0 & 1 & 0 & 1 \\ 39.3 & 0 & 35.6 & 31.3 & -5 & -28.5 & -5 & -28.5 \end{bmatrix} \begin{bmatrix} u_1 \\ u_2 \\ u_3 \\ u_4 \\ u_5 \\ u_6 \\ u_7 \\ u_8 \end{bmatrix} \quad (8.11)\end{aligned}$$

5.4 Part 2 - Quadratic Programming

In the model for Project Part 2, additional constraints have been applied to the thruster dynamics, specifically addressing rotational speed, maximum thrust, and ramp-up time. These constraints have been incorporated into the "thruster dynamics" block, as shown in Table 3.

#	X [m]	Y [m]	Angle	RPM	Max [kN]	Ramp [s]
1	39.3	0	90	-	125	8
2	35.6	0	α_2	2	150	8
3	31.3	0	90	-	125	8
4	-28.5	5	α_4	2	300	10
5	-28.5	-5	α_5	2	300	10

Table 3: Thruster specifications and constraints

The angle of each thruster is defined in the body frame, with zero degrees pointing towards the bow, and angles measured clockwise. Note that thrusters 2, 4, and 5 are azimuth capable of rotating freely. An enhanced thrust allocation algorithm is essential to fully address these constraints.

Thrust System Configuration:

The supply vessel utilizes five thrusters for manoeuvring:

- **Two tunnel thruster** located at the bow.
- **Three azimuth thrusters** – two positioned at the stern and two at the bow.

Each thruster is constrained by physical limitations such as maximum thrust, ramp rate, and rotation rate for the azimuth thrusters. Table 3 details these specifications and limitations. Note that thrusters 2, 4, and 5 can free rotation, enabling greater flexibility in thrust allocation strategies.

For our over-actuated thruster system, we aim to optimize the thruster outputs to achieve the desired control input τ . This optimization problem can be formulated with a control allocation algorithm that computes an input vector u to yield the most efficient thruster output.

Objective Function

The objective function for our Quadratic Programming (QP) formulation is:

$$\min_{u,s} \left(\sum_{i=1}^8 q_i u_i^2 + \sum_{j=1}^3 s_j^2 \cdot \text{weight}_{\text{slack}} \right)$$

where:

- q_i are weighting factors for the thrust control variables u_i .
- s represents slack variables to ensure a feasible solution.

Constraints

The optimization is subject to the following constraints:

- **Equality Constraint:** $Bu = \tau + s$
- **Saturation Constraint:** $u_{\min} \leq u \leq u_{\max}$

where B is the control effectiveness matrix, and s are the slack variables used to manage feasible solutions.

MATLAB Implementation

To solve this problem, we use the MATLAB ‘quadprog’ function. The constraints and inputs are structured as follows:

- **Initial Point x_0 :** We initialize x_0 as:

$$x_0 = \begin{bmatrix} u^+ \\ u^- \\ s \end{bmatrix}$$

where:

- u^+ and u^- represent positive and negative thrust values for each thruster.
- s is a slack variable vector for each controlled degree of freedom.

- **Quadratic Objective Term H :** The matrix H includes weighting terms for u and s . In our case, we set:

$$H = 2 \cdot \text{diag}(q_1, q_2, \dots, q_8, \text{weight}_{\text{slack}}, \text{weight}_{\text{slack}}, 10 \cdot \text{weight}_{\text{slack}})$$

where q and **weight** values are:

$$q = [2, 2, 2, 2, 0.9, 0.9, 0.9, 0.9], \quad \text{weight}_{\text{slack}} = 1 \times 10^5$$

- **Linear Objective Term f :** Since there is no linear term in the objective function, we set $f = 0$.
- **Linear Inequality Constraint Matrix A :** To handle the inequality constraints, A is formulated as:

$$A = \begin{bmatrix} -I_8 & O_{8 \times 3} \\ I_8 & O_{8 \times 3} \end{bmatrix}$$

- **Linear Inequality Constraint Vector b :** This vector ensures that thrust values stay within the bounds u_{\min} and u_{\max} . We set:

$$b = \begin{bmatrix} -\max(u_{\min}, \text{lim_min}) \\ \min(u_{\max}, \text{lim_max}) \end{bmatrix}$$

- **Linear Equality Constraints Matrix A_{eq} and Vector b_{eq} :** For the equality constraint, we set:

$$A_{eq} = \begin{bmatrix} B & -I_3 \end{bmatrix}, \quad b_{eq} = \tau$$

- **Optimization Options:** The options for ‘quadprog’ are set to use the ‘active-set’ method:

```
options = optimoptions('quadprog', 'Algorithm', 'active-set', 'Display', 'off', ...
    'StepTolerance', 1e-30, 'OptimalityTolerance', 1e3);
```

After running the optimization using the ‘quadprog’ function, we obtain the optimized variables u^+ , u^- , s^+ , and s^- . The final thruster allocation variable u is found by subtracting u^- from u^+ :

$$u = u^+ - u^-$$

Since the thruster allocation vector u is also in a redistributed form, the azimuth angles α can be determined as:

$$\begin{aligned} a_2 &= \text{atan2}(T_d(3), T_d(2)) \\ a_4 &= \text{atan2}(T_d(6), T_d(5)) \\ a_5 &= \text{atan2}(T_d(8), T_d(7)) \end{aligned}$$

In MATLAB, it is recommended to use the ‘atan2’ function instead of ‘atan’ for computing the azimuth angle α . This is because the atan() function returns a value in the range $-\frac{\pi}{2}$ to $\frac{\pi}{2}$ radians, while the

`atan2()` function returns a value in the range $-\pi$ to π radians, which is more appropriate for azimuth angle calculations.

5.5 Simulink Implementation of the Thrust Allocations

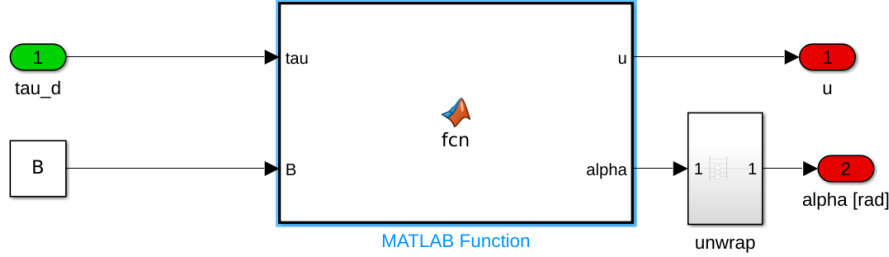


Figure 14: Thrust Allocation Block

This implementation effectively handles the over-actuation of the vessel by optimizing the allocation of thrust across multiple thrusters. The quadratic programming approach ensures that the allocation is optimal, minimizing unnecessary thrust usage while meeting the control demands.

6 Observer Design

Filtering and state estimation play a crucial role in control systems, as measured signals often contain noise that can negatively impact controller performance. Therefore, it is essential to implement precautionary measures in the DP (Dynamic Positioning) and PM (Position Mooring) systems. The primary objectives of state estimators (observers) in positioning systems are:

1. Reconstruction of non-measured data
2. Dead reckoning
3. Wave filtering

It is possible to create an observer using the measured states of the vessel and its estimated generalized forces over the vessel hull. To verify observability, one can calculate the rank of the observability matrix, denoted as:

$$\mathbf{Q}_0 = \left[\mathbf{C}^T \ \mathbf{A}^T \mathbf{C}^T : (\mathbf{A}^T)^{n-1} \mathbf{C}^T \right]$$

where \mathbf{A} and \mathbf{C} are equal to $\mathbf{A}3$ and $\mathbf{C}3$ from the state-space model derived in Section 8. For the given system, the observability matrix has full rank, indicating that the system is observable. In this project, two different observers are implemented:

1. Extended Kalman Filter (EKF)
2. Nonlinear Passive Observer (NPO)

The objective is to estimate position and velocity while filtering the wave frequency of the ship motion. Velocity measurements are usually not directly measured but can be estimated by the observer.

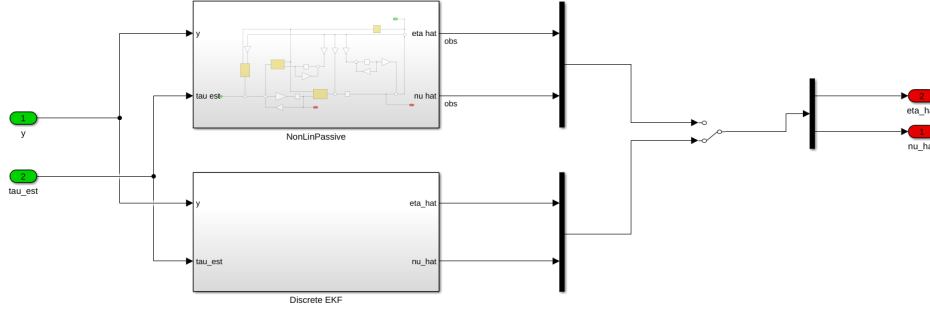


Figure 15: Observer Block

6.1 Extended Kalman Filter

The discrete-time Kalman filter is a recursive filter used for state estimation and noise reduction in measurements. It is widely used among engineers for its convenience in providing accurate state estimates while removing measurement noise. The traditional Kalman filter is linear and assumes a linear time-invariant system, but since our system is nonlinear, we require a nonlinear state estimator. The extended Kalman filter (EKF) accommodates this need by linearizing the system around the current state. The EKF design is based on the nonlinear model:

$$\dot{\mathbf{x}} = \mathbf{f}(\mathbf{x}) + \mathbf{B}\mathbf{u} + \mathbf{E}\mathbf{w} \quad (48)$$

$$\mathbf{y} = \mathbf{H}\mathbf{x} + \mathbf{v} \quad (49)$$

where $\mathbf{f}(\mathbf{x})$, \mathbf{B} , \mathbf{E} , and \mathbf{H} are defined as follows. We assume \mathbf{w} and \mathbf{v} are mutually independent, zero-mean white noise processes with covariance matrices \mathbf{Q} and \mathbf{R} .

$$\mathbf{f}(\mathbf{x}) = \begin{bmatrix} \mathbf{A}_w\xi \\ \mathbf{R}(\psi)\nu \\ -\mathbf{T}_b^{-1}\mathbf{b} \\ -\mathbf{M}^{-1}\mathbf{D}\nu - \mathbf{M}^{-1}\mathbf{R}^T(\psi)\mathbf{G}\eta + \mathbf{M}^{-1}\mathbf{R}^T(\psi)\mathbf{b} \end{bmatrix} \quad (50)$$

$$\mathbf{B} = \begin{bmatrix} \mathbf{0}_{6 \times 3} \\ \mathbf{0}_{3 \times 3} \\ \mathbf{0}_{3 \times 3} \\ \mathbf{M}^{-1} \end{bmatrix} \quad (51)$$

$$\mathbf{E} = \begin{bmatrix} \mathbf{E}_w & \mathbf{0}_{6 \times 3} \\ \mathbf{0}_{3 \times 3} & \mathbf{0}_{3 \times 3} \\ \mathbf{0}_{3 \times 3} & \mathbf{E}_b \\ \mathbf{0}_{3 \times 3} & \mathbf{0}_{3 \times 3} \end{bmatrix} \quad (52)$$

$$\mathbf{H} = \begin{bmatrix} \mathbf{C}_w & \mathbf{I}_{3 \times 3} & \mathbf{0}_{3 \times 3} & \mathbf{0}_{3 \times 3} \end{bmatrix} \quad (53)$$

We have a system with $n = 15$ states where $\mathbf{x} = \begin{bmatrix} \xi^T, & \eta^T, \mathbf{b}^T, \nu^T \end{bmatrix}^T$, $\mathbf{w} = \begin{bmatrix} \mathbf{w}_w^T, & \mathbf{w}_b^T \end{bmatrix}^T$, and $\mathbf{u} = \tau = [\tau_x, \tau_y, \tau_\psi]^T$. We have \mathbf{A}_w , \mathbf{E}_w , and \mathbf{C}_w given from the WF control plant model in (14). \mathbf{E}_b is the diagonal scaling matrix mentioned in subsection 4.3.

The EKF algorithm consists of two stages: prediction and correction. In the prediction step, the covariance and the state variables are estimated. It then observes the next measurement and corrects the covariance and state estimates. Estimates with lower uncertainty are weighted higher. The discrete-time EKF equations are given below.

Initial values:

$$\bar{\mathbf{x}}_{k=0} = \mathbf{x}_0 = \mathbf{0}_{15 \times 1} \quad (54)$$

Since the initial position and velocity are, respectively, $\eta = [0 \ 0 \ 0]^T$ and $\nu = [0 \ 0 \ 0]^T$, and

$$\bar{\mathbf{P}}_{k=0} = E[(\mathbf{x}(0) - \hat{\mathbf{x}}(0))(\mathbf{x}(0) - \hat{\mathbf{x}}(0))^T] = \mathbf{P}_0 = \mathbf{I}_{15} \quad (55)$$

since the deviation between initial states and the true states is unknown.

Corrector:

$$\mathbf{K}_k = \bar{\mathbf{P}}_k \mathbf{H}^T [\mathbf{H} \bar{\mathbf{P}}_k \mathbf{H}^T + \mathbf{R}]^{-1} \quad (56)$$

$$\hat{\mathbf{P}}_k = (\mathbf{I} - \mathbf{K}_k \mathbf{H}) \bar{\mathbf{P}}_k (\mathbf{I} - \mathbf{K}_k \mathbf{H})^T + \mathbf{K}_k \mathbf{R} \mathbf{K}_k^T \quad (57)$$

$$\hat{\mathbf{x}}_k = \bar{\mathbf{x}}_k + \mathbf{K}_k (\mathbf{y}_k - \mathbf{H} \bar{\mathbf{x}}_k) \quad (58)$$

where \mathbf{K}_k is the Kalman gain, and $\mathbf{R} = \mathbf{E}(\mathbf{v}\mathbf{v}^T)$ is the position and heading measurement noise covariance matrix.

Predictor:

$$\bar{\mathbf{P}}_{k+1} = \Phi_k \hat{\mathbf{P}}_k \Phi_k^T + \Gamma_k \mathbf{Q} \Gamma_k^T \quad (59)$$

$$\bar{\mathbf{x}}_{k+1} = \mathbf{f}_k(\hat{\mathbf{x}}_k, \mathbf{u}_k) \quad (60)$$

where $\mathbf{Q} = \mathbf{E}(\mathbf{w}\mathbf{w}^T)$ is the process noise covariance matrix, and $\mathbf{f}_k(\hat{\mathbf{x}}_k, \mathbf{u}_k)$, Φ_k , and Γ_k can be determined using, e.g., the forward Euler method:

$$\mathbf{f}_k(\hat{\mathbf{x}}_k, \mathbf{u}_k) = \hat{\mathbf{x}}_k + T[\mathbf{f}(\hat{\mathbf{x}}_k) + \mathbf{B}\mathbf{u}_k] \quad (61)$$

$$\Phi_k = \mathbf{I} + T \frac{\partial \mathbf{f}(\hat{\mathbf{x}}_k, \mathbf{u}_k)}{\partial \mathbf{x}_k} \Big|_{\mathbf{x}_k=\hat{\mathbf{x}}_k} \quad (62)$$

$$\Gamma_k = T\mathbf{E} \quad (63)$$

where T is the sampling period, set to 0.1.

6.1.1 Tuning

One drawback of the Kalman filter observer is that it can be intricate to tune due to the number of tuning parameters involved. To simplify the tuning process, the matrices \mathbf{Q} and \mathbf{R} are typically treated as positive definite diagonal matrices. The difficulty of defining these covariance matrices depends on the system knowledge. We began with constant values for \mathbf{R} and \mathbf{E}_b and adjusted \mathbf{Q} until reaching near-optimal results. Then, \mathbf{R} was fine-tuned. Initially, the three matrices were set to:

$$\mathbf{E}_b = \mathbf{I}_{3 \times 3} \quad (64)$$

$$\mathbf{R} = \mathbf{I}_{3 \times 3} \quad (65)$$

$$\mathbf{Q} = \mathbf{I}_{6 \times 6} \quad (66)$$

The final tuning parameters for simulation 4 are shown below (68) and (69) and were later adjusted for simulation 7 to test the DP robustness:

$$\mathbf{E}_b = \text{diag}\{0.1, 0.1, 0.1\} \quad (67)$$

$$\mathbf{R} = \text{diag}\{0.000001, 0.000001, 0.2\} \quad (68)$$

$$\mathbf{Q} = \text{diag}\{0.8, 0.1, 0.1, 10^6, 10^6, 10^6\} \quad (69)$$

6.1.2 Simulink model of the EKF Observer

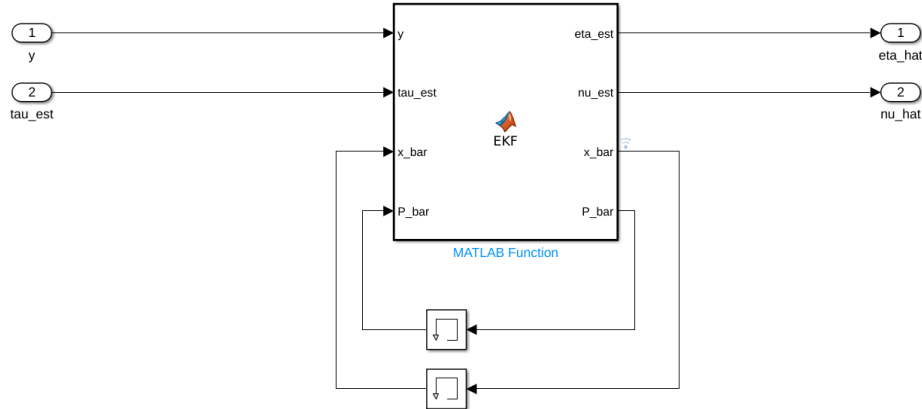


Figure 16: Extended Kalman Filter Block

6.2 Nonlinear Passive Observer

The Nonlinear Passive Observer (NPO) is implemented as an alternative to the EKF. The state estimator in EKF is time-consuming and difficult to tune because of the numerous covariance parameters that are challenging to match with the model's physical quantities. With an NPO, global convergence of all estimated states is guaranteed. Only one set of observer gains is needed to cover the entire state-space, requiring a single set of parameters to be tuned. The design of an NPO uses SPR-Lyapunov

analysis to ensure passivity and stability of the nonlinear observers. The Lyapunov analysis makes the following assumptions:

- **A1:** Position and heading sensor noise is neglected, i.e., $v = 0$, as this term is negligible compared to wave-induced motion.
- **A2:** The amplitude of the wave-induced yaw motion ϕ_w is assumed to be small—less than 1 degree during normal operation and less than 5 degrees in extreme weather conditions. Thus, $\mathbf{R}(\psi) \approx \mathbf{R}(\psi + \psi_w)$. With **A1**, this implies $\mathbf{R}(\psi) \approx \mathbf{R}(\psi_y)$, where $\psi_y\psi + \psi_w$ denotes the measured heading.

The observer is given by

$$\begin{aligned}\dot{\hat{\xi}} &= \mathbf{A}_w \hat{\xi} + \mathbf{K}_1(\omega_0) \tilde{\mathbf{y}} \\ \dot{\hat{\eta}} &= \mathbf{R}(y_3) \hat{\nu} + \mathbf{K}_2 \tilde{\mathbf{y}} \\ \dot{\hat{\mathbf{b}}} &= -\mathbf{T}_b^{-1} \hat{\mathbf{b}} + \mathbf{K}_3 \tilde{\mathbf{y}} \\ \mathbf{M} \dot{\hat{\nu}} &= -\mathbf{D} \hat{\nu} - \mathbf{R}^T(y_3) \hat{\mathbf{b}} + \tau + \tau_{wind} + \mathbf{R}^T(y_3) \mathbf{K}_4 \tilde{\mathbf{y}} \\ \hat{\mathbf{y}} &= \hat{\eta} + \mathbf{C}_w \hat{\xi}\end{aligned}$$

Where $\tilde{\mathbf{y}} = \mathbf{y} - \hat{\mathbf{y}}$ is the estimation error, $\hat{\xi}$ is the first order wave estimation, $\hat{\mathbf{b}}$ is the bias estimation and $\mathbf{K}_1, \mathbf{K}_2, \mathbf{K}_3, \mathbf{K}_4$ are observer gain matrices. The matrices are given as:

The observer equations are given by:

$$\mathbf{K}_1(\omega_0) = \begin{bmatrix} \text{diag}\{K_{11}(\omega_{01})\} & \text{diag}\{K_{12}(\omega_{02})\} & \text{diag}\{K_{13}(\omega_{03})\} \\ \text{diag}\{K_{14}(\omega_{01})\} & \text{diag}\{K_{15}(\omega_{02})\} & \text{diag}\{K_{16}(\omega_{03})\} \end{bmatrix} \quad (71a)$$

$$\mathbf{K}_2 = \text{diag}\{K_{21}, K_{22}, K_{23}\} \quad (71b)$$

$$\mathbf{K}_3 = \text{diag}\{K_{31}, K_{32}, K_{33}\} \quad (71c)$$

$$\mathbf{K}_4 = \text{diag}\{K_{41}, K_{42}, K_{43}\} \quad (71d)$$

For $\mathbf{K}_1(\omega_0)$, the wave spectra frequencies are $\omega_0 = [\omega_{01}, \omega_{02}, \omega_{03}]^T$ in surge, sway, and yaw. The matrices are tuned as follows, according to the Kalman-Yakubovich-Popov.

$$k_i(\omega_{0i}) = -2(\zeta_{ni} - \zeta_i) \frac{\omega_{ci}}{\omega_i}, \quad i = 1, 2, 3 \quad (72)$$

$$k_i = 2\omega_i(\zeta_{ni} - \zeta_i), \quad i = 4, 5, 6 \quad (73)$$

$$k_i = \omega_{ci}, \quad i = 7, 8, 9 \quad (74)$$

6.2.1 Tuning

In order to ensure passivity and to relate the observer gains of equation 22 to the dominating wave response frequencies, it is proposed that:

$$\begin{aligned} k_i &= -2(\zeta_{ni} - \zeta_i) \frac{\omega_{ci}}{\omega_i} \quad i = 1, 2, 3 \\ k_i &= 2\omega(\zeta_{ni} - \zeta_i) \frac{\omega_{ci}}{\omega_i} \quad i = 4, 5, 6 \\ k_i &= \omega_{ci} \quad i = 7, 8, 9 \end{aligned}$$

where $\omega_{ci} > \omega_i$ is the filter cut-off frequency. $\zeta_{ni} > \zeta_i$ are tuning parameters to set between 0.1 – 1.0. $k_{10} - k_{12}$ should be high enough to ensure a proper bias estimation.

At initial step, we have set the tuning parameters to these values, subject to further tuning as seen in the init.m file:

$$\begin{aligned} \zeta_{ni} &= [1.0, 1.0, 1.0] \\ \zeta_n &= [0.1, 0.1, 0.1] \\ \omega_i &= \frac{2\pi}{T_n} \text{ where } T_n \text{ is the period of interest chosen as 20 s} \\ \omega_{ci} &= 1.3\omega_i \\ K_4 &\approx \text{diag}(\text{Mass of vessel}) \\ K_3 &= 0.1K_4 \\ \Omega &= \text{diag}(\omega_1, \omega_2, \omega_3) \\ \Lambda &= \text{diag}(\zeta_1, \zeta_2, \zeta_3) \end{aligned}$$

Further tuning of these parameters is done to ensure good results in the estimation of the states. After tuning, the final values are:

$$\begin{aligned} T_n &= [9, 1.8, 9] \text{ s} \\ K_4 &= 10000 \times [30, 30, 1000] \\ K_3 &= 0.08 \times K_4 \end{aligned}$$

6.2.2 Simulink Model

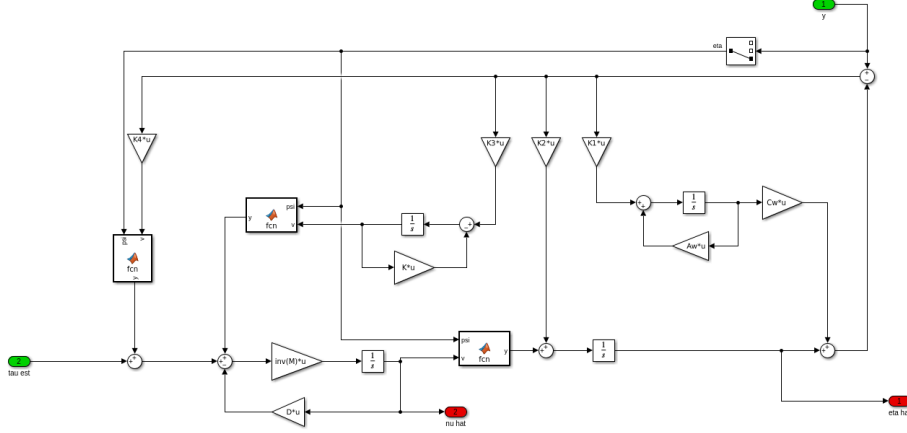


Figure 17: Non-Linear Passive Observer Block

The Nonlinear Proportional Observer (NPO) block diagram shown represents a control system designed to estimate states such as position (η_{hat}) and velocity (ν_{hat}) in a nonlinear dynamic system. The main input, denoted as τ_{est} , likely represents control forces or torques applied to the system. This input is scaled by various gains (K_1, K_2, K_3 , etc.), which are multiplied by the control signal u to adjust the system's response. The system contains nonlinear function blocks (represented as ‘fcn’) that might model transformations, nonlinear disturbances, or system uncertainties, processing the scaled signals to generate state estimates. Integrators ($\frac{1}{s}$) accumulate these signals over time, providing state estimations by modeling velocity and position changes. The summation points (+ and -) allow feedback from estimated values, enabling error correction by comparing observed and estimated states. Feedback loops further refine the estimation, adjusting η_{hat} and ν_{hat} to closely match the actual states. Thus, the NPO block aims to produce accurate state estimates, which can be used for control or monitoring in real-time operations.

7 Controller Design

The controller’s main objective is to align the state variables with the desired setpoints using a feedback loop. It compares the system’s current state with the desired state and generates an input to reduce the error.

In this case, the controller receives a target trajectory from the reference model, as well as the current state variables—surge, sway, yaw, and their rates of change. Based on this, the controller produces a control input τ , which is applied to the ship model after adjusting for the reference frame.

The desired Earth-fixed position and velocity are represented by η_d and ν_d , respectively. Each term in the control law involves a diagonal gain matrix and an error term, with the goal of minimizing the error $e(t)$, defined as the difference between the desired position $y_0(t)$ and the current position $y(t)$.

7.1 Proportional-Integral-Derivative (PID) Control

The PID controller, although a straightforward solution to the Dynamic Positioning (DP) challenge, provides a reliable and robust method. Its ease of implementation, widespread use in various fields, and efficiency make it a strong candidate for the DP control system. Each term in the PID controller

serves a vital function: the integral term corrects steady-state errors, defined as $e_\infty = \eta_{d\infty} - \eta_\infty$, while the derivative term helps introduce damping into the system to stabilize the response.

The controller is expressed in Eq. 50, in a reduced vector form:

$$\tau^{(b)}(1, 2, 6) = \begin{bmatrix} \tau_u \\ \tau_v \\ \tau_\psi \end{bmatrix} = R^T(\psi)\tau^n = R^T(\psi) \left[K_p e - K_d \dot{\eta} + K_i \int_0^\infty e(x) dx \right] \quad (50)$$

Here, the vector $\tau^{(b)}$ is reduced from a 6×1 to a 3×1 vector based on the assumption that roll, pitch, and heave motions are already stabilized and remain constant (set to zero) within the DP controller block, as shown in Figure 18.

The error between the desired position η_d and the current position η is defined as:

$$e = \eta_d - \eta$$

The derivative of the position vector η is expressed as:

$$\dot{\eta} = R(\psi)\nu = \begin{bmatrix} \dot{x} & \dot{y} & \dot{z} & \dot{\phi} & \dot{\theta} & \dot{\psi} \end{bmatrix}^T$$

The controller gains, denoted by K_j , where j represents the proportional (p), integral (i), and derivative (d) terms, are structured as diagonal matrices:

$$K_j = \begin{bmatrix} K_{ju} & 0 & 0 \\ 0 & K_{jv} & 0 \\ 0 & 0 & K_{jr} \end{bmatrix}$$

The implementation of the DP controller along with its corresponding PID controller was carried out in Simulink, as illustrated in Figures 18 and 19.

Proportional Term: The proportional term is the product of the proportional gain and the error. It dictates the speed of the controller's response. A high proportional gain may lead to instability, while a low gain results in slow responses. Using only the proportional term can cause the vessel to never fully reach the setpoint due to steady-state error, which can be corrected by adding the integral term.

Integral Term: The integral term corrects steady-state error by accumulating the error over time. However, if the integral gain is too large, it may cause overshooting or instability (integral windup), leading to oscillations.

Derivative Term: The derivative term predicts future errors based on the current rate of change. A high rate of error change results in a larger output, leading to faster controller responses. However, rapid small fluctuations can be problematic and are often mitigated with an input filter.

7.2 Implementation of the PID Controller

The Simulink implementation of the Proportional-Integral-Derivative (PID) controller for the Dynamic Positioning (DP) system is shown in the figure. The PID controller calculates the control input, τ (in the body frame), to adjust the vessel's position and heading according to the desired setpoints. The controller uses the error between the desired position, $\eta_{\text{set point}}$, and the current position, η , which is processed in the NED to body frame transformation block to account for the vessel's orientation (yaw, ψ). The error is then used to compute the PID terms.

The proportional term, K_p , corrects the error based on its current magnitude. The integral term, K_i , accumulates the error over time to remove any steady-state error, while the derivative term, K_d , helps stabilize the system by counteracting rapid changes in the error signal. The integral and derivative actions are applied using the integrator and gain blocks. The outputs of the proportional, integral, and derivative terms are summed together to produce the control signal, τ , which is then sent to the vessel to adjust its motion in the body frame.

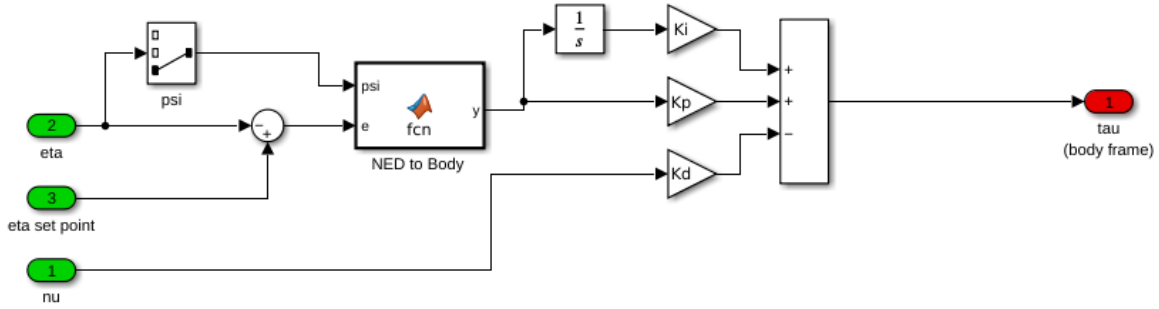


Figure 18: PID Controller Block

The PID controller provides a straightforward yet robust solution for dynamic positioning. By adjusting the gains, K_p , K_i , and K_d , the system can be tuned to achieve the desired balance between responsiveness and stability. The proportional gain ensures a quick reaction to the error, while the integral term eliminates steady-state offsets. The derivative term further smooths the response by damping rapid changes in the error, preventing overshooting or oscillations.

7.3 Tunning of the PID

Several methods are available to tune the three parameters. One of them is to treat the system like a mass-spring-damper system.

First, we observe that the control plant model for a DP system is given as:

$$M\dot{v} + Dv = \tau_{\text{thrusters}}$$

$$\tau_{PID} = -K_P \cdot e - K_I \int e dt - K_D \dot{e}$$

where M is the mass of the vessel, D is the damping coefficient, v is the velocity, \dot{v} is the acceleration, and e and \dot{e} are the error and its derivative, defined as:

$$e = \eta_{sp} - \eta = \begin{bmatrix} x_{sp} \\ y_{sp} \\ \psi_{sp} \end{bmatrix} - \begin{bmatrix} x \\ y \\ \psi \end{bmatrix}$$

$$\dot{e} = \dot{\eta}_{sp} - \dot{\eta} = v = nu_{sp} - nu$$

Since we want to control the thrusters with the PID output, equation (23) becomes:

$$\begin{aligned} M\dot{v} + Dv &= -K_P R^T e - K_I \int R^T e dt - K_D v \\ M\dot{v} + (D + K_D)v + K_P R^T e &= -K_I \int e dt \\ \dot{v} + \frac{K_P}{M} R^T e + \left(\frac{D + K_D}{M} \right) v &= \frac{-K_I}{M} \int R^T e dt \end{aligned}$$

The coefficient of the second term describes the natural frequency component of the DP system, expressed as:

$$\frac{K_P}{M} = \omega_n^2 = \left(\frac{2\pi}{T_n^{DP}} \right)^2$$

where T_n^{DP} is the period of interest, chosen between 50 – 200 s. We initially set $T_n^{DP} = 70$ s.

For K_I , we aim to make the integral term slower than the proportional term. One rule of thumb is:

$$K_I = \frac{\omega_n}{10} K_P$$

The factor of 10 is the rise time factor, meaning K_I is 10 seconds slower than K_P , allowing for adjustment of K_I .

For K_D , the coefficient of the second part is related to the damping frequency, expressed as:

$$\frac{D + K_D}{M} = 2\xi\omega_n^{DP}$$

The ξ term represents the damping frequency, often set to 1. In this case, since we may have a noisy velocity estimate, we set $\xi = 0.7$.

With the given Mass and Damping matrices, we compute initial values for K_P , K_I , and K_D .

The MATLAB implementation is shown below:

```
%>> % PID Parameters
Mass = diag([vesselABC.MRB(1,1), vesselABC.MRB(2,2), vesselABC.MRB(6,6)]); %
    vesselABC.MRB(1:3,1:3);
Damping = diag([2.6486e5, 8.8164e5, 3.3774e8]);
T_n = 70; %period of interest -- can tune
omega_n_dp = 2*pi / T_n;
xi = 0.7; %--- can tune
rise_time = 10; %--- can tune
%%PID values
Kp = Mass .* omega_n_dp.^2;
Ki = omega_n_dp/10 .*Kp;
Kd = (2 * zeta * omega_n_dp .* Mass) - Damping;
```

For analysis, we used the reference to be a step input with constant values on the three motions. This gives us initial values of the K_p , K_i , and K_d for $[x, y, \psi]$ as:

$$K_P = \begin{bmatrix} 51259.1681732638 & 51259.1681732638 & 21964043.2251420 \end{bmatrix}$$

$$K_I = \begin{bmatrix} 460.101217606426 & 460.101217606426 & 197148.790969242 \end{bmatrix}$$

$$K_D = \begin{bmatrix} 799498.699368261 & 799498.699368261 & 342577232.857410 \end{bmatrix}$$

We observe that these parameters serve as a good starting point to tune our K_d , K_i , and K_p values, as the controllers try to follow our reference points. Upon further tuning, we can perform the simulation tasks required of us. After repetitive tuning, we found well-tuned values that do not overshoot the output and follow the reference smoothly. However, it takes a bit more time to converge, which comes down to the trade-off issue we have in the control system. The new plot is shown below.

The final tuned values are:

$$K_P = \begin{bmatrix} 44440.8471205421 & 174748.115243117 & 56099945.0910478 \end{bmatrix}$$

$$K_I = \begin{bmatrix} 540.64009360768 & 3153.2361136748 & 1036593.12054623 \end{bmatrix}$$

$$K_D = \begin{bmatrix} 885551.128894883 & 1413618.40984523 & 582749740.806195 \end{bmatrix}$$

We can see that the tuned values are in the order of 10,000 to 100,000, which corresponds to the thruster values that have an order of magnitude of 10 kN(m) to 100 kN(m) in Force and Torque.

8 Simulation Results [part 1 & part 2]

Several tests have been performed to show that our system is working properly. They are described in the following sections. The results contains separate sections for part 1 and part 2 of the assignment.

Part 1 Simulation Test

8.1 Simulation 1

Scenario

This simulation tests the DP system's performance under two different environmental conditions. First, the vessel is subjected to a current of 0.5 [m/s] coming from the east, and in the second case, a wind with an average speed of 10 [m/s] from the south is applied. The DP setpoint is set to $[0, 0, 0]$, and the vessel's position and heading are plotted until steady state is reached for both cases. The results are presented as individual time-series plots and combined xy-plots for each scenario.

8.1.1 Simulation 1A - Current set to 0.5[m/s] from east.

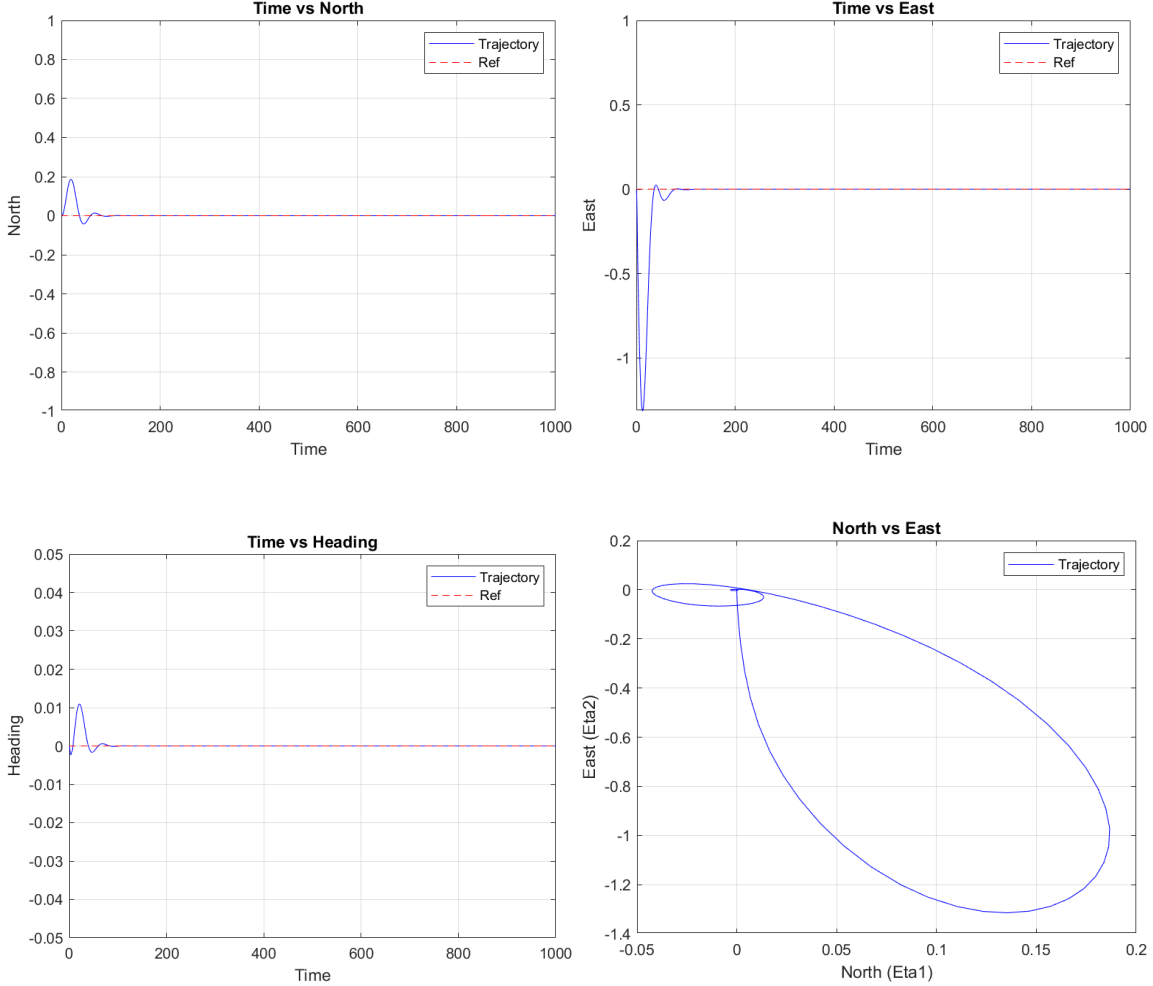


Figure 19: Simulation 1a Results

8.1.2 Discussion

The results from Simulation 1A, where the vessel is subjected to a current of 0.5 [m/s] from the east, show the Dynamic Positioning (DP) system's ability to effectively correct for environmental disturbances. The North vs Time and East vs Time plots indicate that the vessel experiences initial deviations due to the current's influence, with oscillations observed in both the North and East directions. The eastward current causes the vessel to drift significantly in the East direction initially, while the North direction shows smaller deviations. However, over time, the DP system adjusts, and the vessel converges back to the desired setpoint of [0, 0] with minimal steady-state error. This indicates that the controller is able to manage the current-induced drift effectively, although the system experiences some initial oscillations before stabilizing.

The Heading vs Time plot shows that the vessel's heading also experiences minor oscillations at the start, but these are quickly dampened as the system stabilizes. The North vs East plot provides a clear visualization of the vessel's trajectory, where the initial drift forms an elliptical path before the vessel converges back to the setpoint. The overall trajectory demonstrates the DP system's ability to handle disturbances and return the vessel to its target position and orientation. While the system performs

well in mitigating the effects of the eastward current, the initial response could likely be improved with further tuning of the PID controller to reduce the oscillations and time to steady-state.

8.1.3 Simulation 1B - Wind with average speed of 10[m/s] from south.

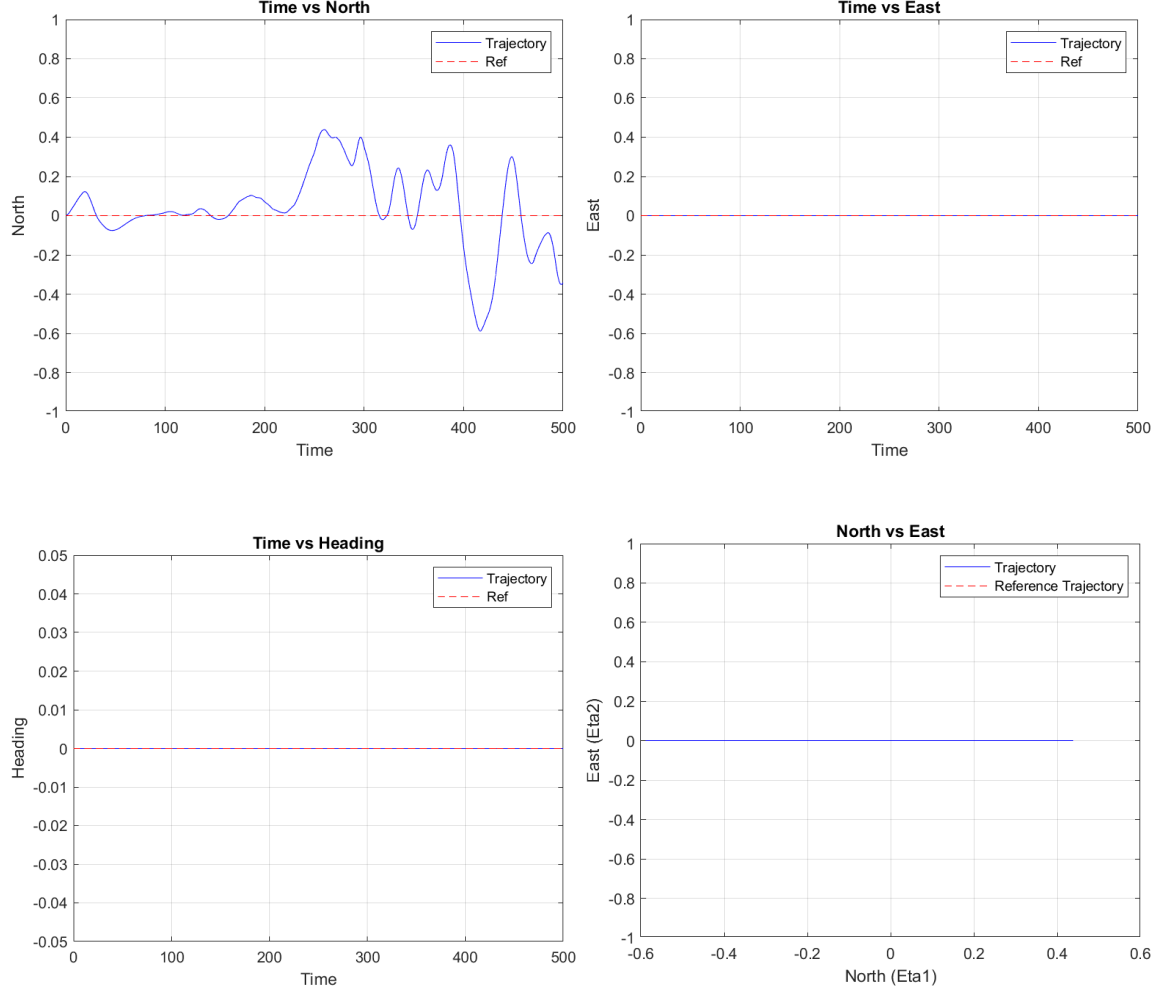


Figure 20: SImulation 1b Results

8.1.4 Discussion

In Simulation 1B, the vessel is subjected to a wind with an average speed of 10 [m/s] from the south. The Time vs North plot reveals that the vessel experiences significant oscillations in the North direction due to the wind, indicating that the DP system struggles to maintain a steady position in the presence of the wind. The oscillations persist throughout the simulation period, and the vessel does not fully stabilize around the setpoint in the North direction. This suggests that the controller may need further tuning to improve its performance under wind disturbances. In contrast, the Time vs East plot shows that the vessel maintains its position along the East axis, with no significant deviations observed. This implies that the wind from the south primarily affects the North direction.

The Time vs Heading plot shows that the vessel's heading remains stable throughout the simulation, closely tracking the reference value with no oscillations, indicating that the DP system successfully

maintains the correct orientation. The North vs East plot provides a visual representation of the vessel's trajectory, showing that the vessel remains largely in place along the East axis, but it experiences substantial fluctuations in the North direction due to the wind. Overall, while the DP system manages to maintain the vessel's heading and East position, the performance in the North direction could be improved with further tuning to better counteract the wind disturbances.

8.2 Simulation 2

In this simulation, wind loads are turned off, and the current varies linearly from 0.5 [m/s] over a 300-second period, gradually changing direction. The current starts flowing from the south at 180° and shifts clockwise to the west at 270° over a period of 200 seconds. The simulation is extended beyond this time until the vessel reaches a steady state, at which point the vessel's position and heading are plotted over time. These data provide insight into the vessel's response to varying currents and its ability to stabilize under such conditions.

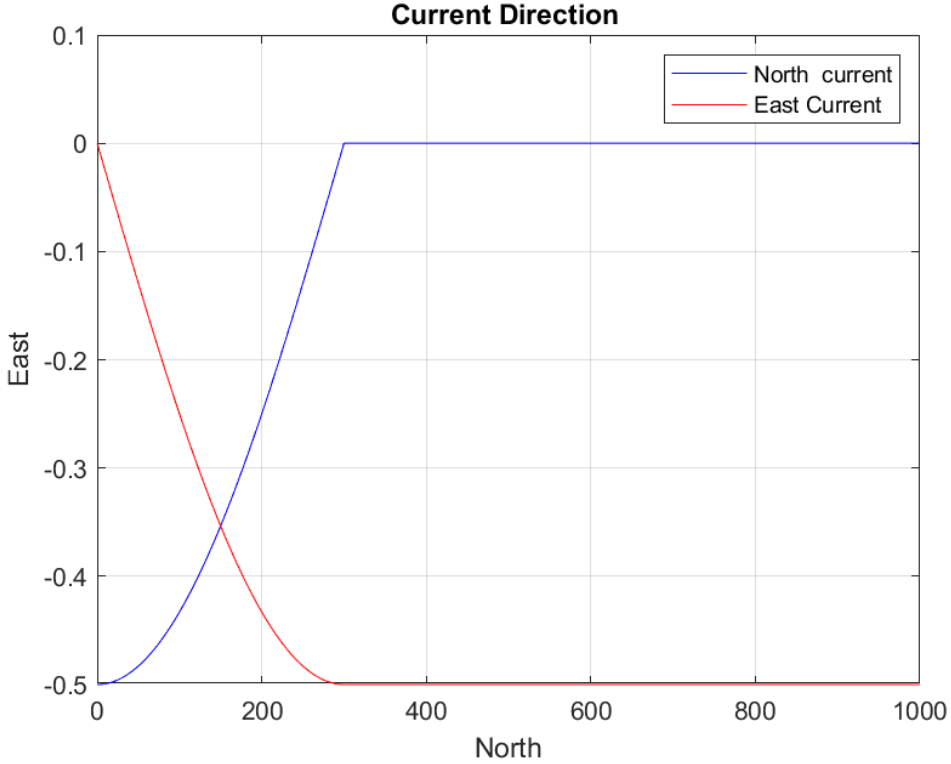


Figure 21: Change of *North* and *East* current components over time as the current direction varies from 180° to 270° over a 200-second period.

Figure 15 illustrates how the current's direction shifts from 180° to 270° over a period of 200 seconds, affecting both the *North* and *East* current components. As seen in Figure 21, the vessel's trajectory is influenced by these changes, transitioning to a steady-state condition where it can compensate for the varying current and maintain stability.

8.2.1 Simulation 2

Scenario

current vary linearly from 0.5 [m/s] coming from North to 0.5 [m/s] coming from East, while keeping the vessel at the origin [0 0 0].

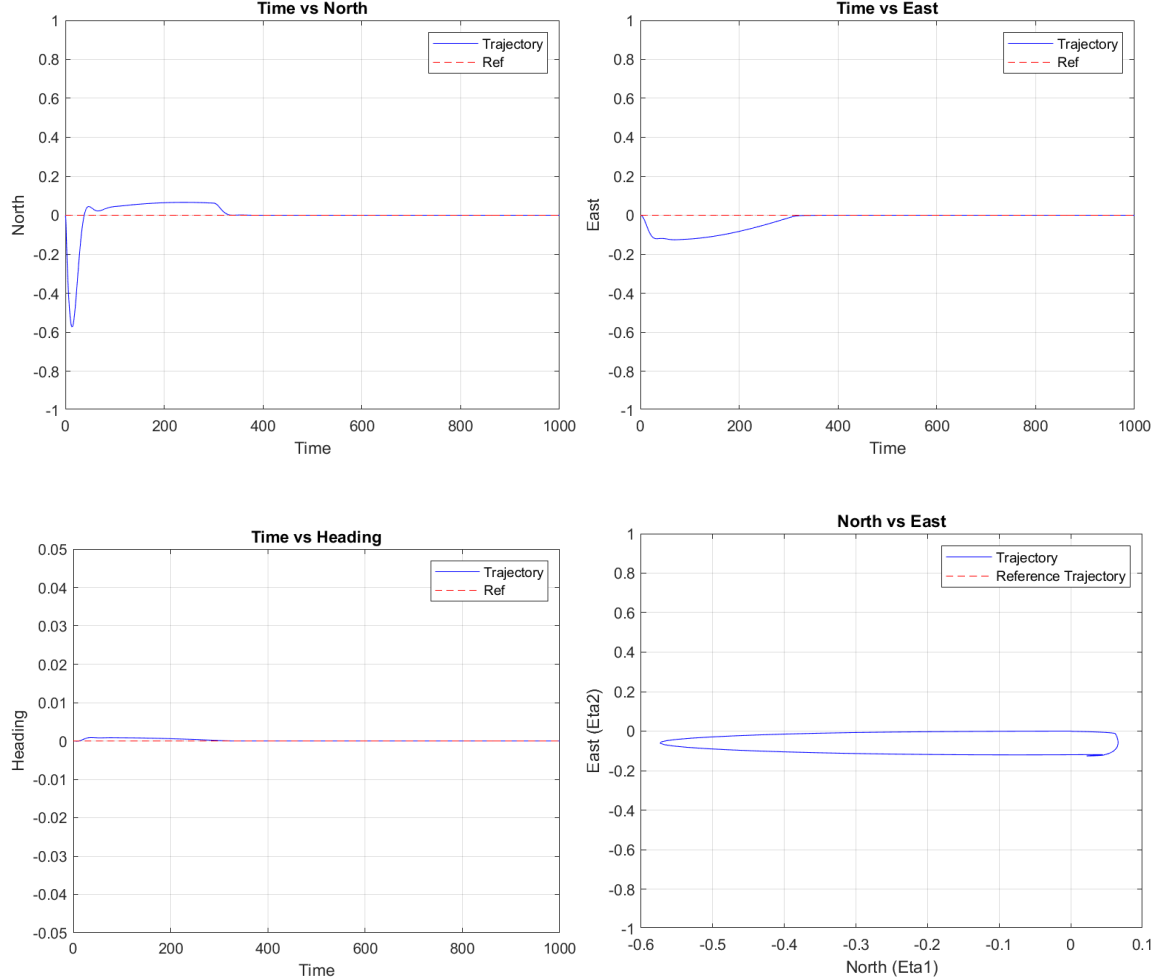


Figure 22: Simulation 2 Results

8.2.2 Discussion

In Simulation 2, the vessel is subjected to a gradually changing current, which varies linearly from 0.5 [m/s] coming from the North to 0.5 [m/s] coming from the East over a period of 300 seconds. The Time vs North plot shows that the vessel initially experiences a deviation from the setpoint, but the DP system compensates for the current and brings the vessel back to the desired position. The Northward deviation is noticeable at the start, but the system manages to stabilize the vessel and return it to the reference point. Similarly, in the Time vs East plot, the vessel also experiences a minor deviation in the East direction, but it quickly stabilizes as the current changes direction from North to East, showing the DP system's ability to counteract the varying current forces.

The Time vs Heading plot indicates that the vessel's heading remains relatively stable throughout the simulation, with only minor oscillations at the beginning as the current starts to change direction.

The North vs East plot illustrates the vessel's trajectory in the xy-plane, where the initial deviation is corrected, and the vessel returns to the origin. The trajectory shows an elliptical path as the current shifts direction, but the DP system successfully maintains control, bringing the vessel back to the reference setpoint. Overall, the DP system performs well in managing the varying current, demonstrating its robustness in keeping the vessel at the origin despite the gradually changing current forces.

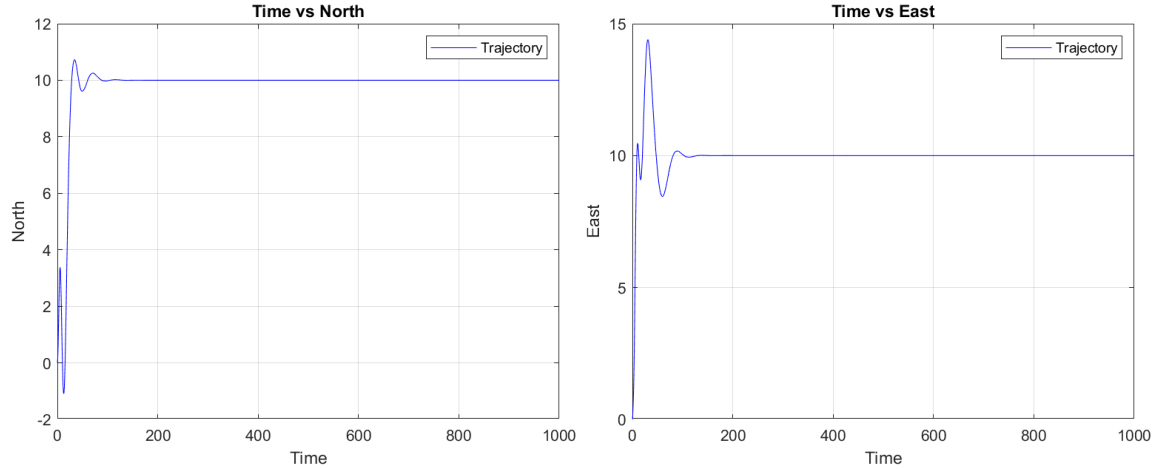
8.3 Simulation 3

Scenario

This test compares the vessel's position and heading over time for two cases: one with a reference model and one without. The initial position is set to $\eta_0 = [0, 0]$, and the setpoint is $\eta_{SP} = [10, 10, \frac{3\pi}{2}]$. No environmental forces are applied, and the results are shown until the vessel reaches steady state, with the desired trajectory plotted in each case. If the reference model contains velocity trajectories, these are also plotted.

Simulation 3 - Comparing the different results for the vessel position over time for initial position $\eta_0 = [0, 0]$ and setpoint $\eta_{SP} = [10, 10, \frac{3\pi}{2}]$, with and without a reference model.

8.3.1 Vessel Dynamics Without Reference Model



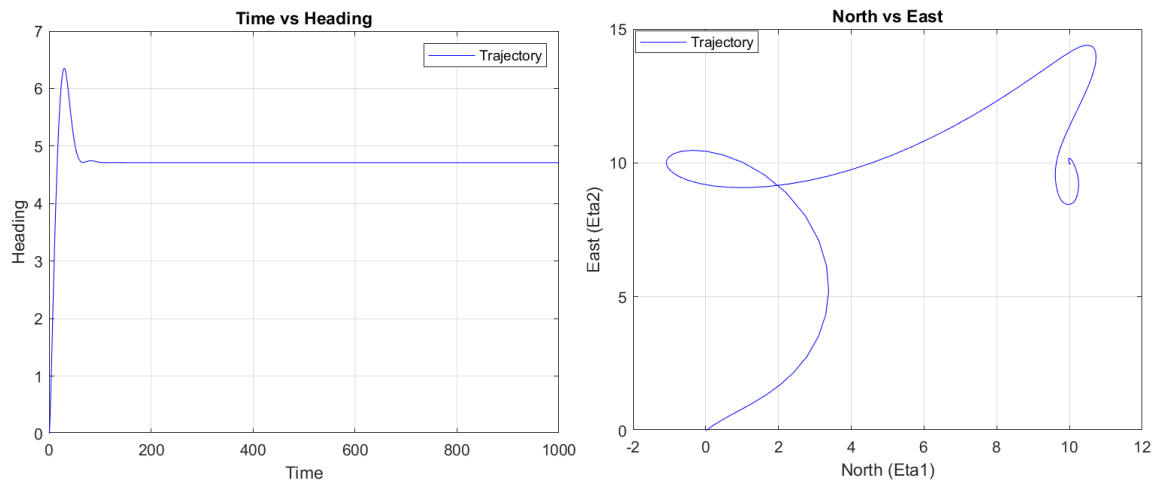


Figure 23: Simulation 3 Results (Without reference model)

8.3.2 Vessel Dynamics With Reference Model

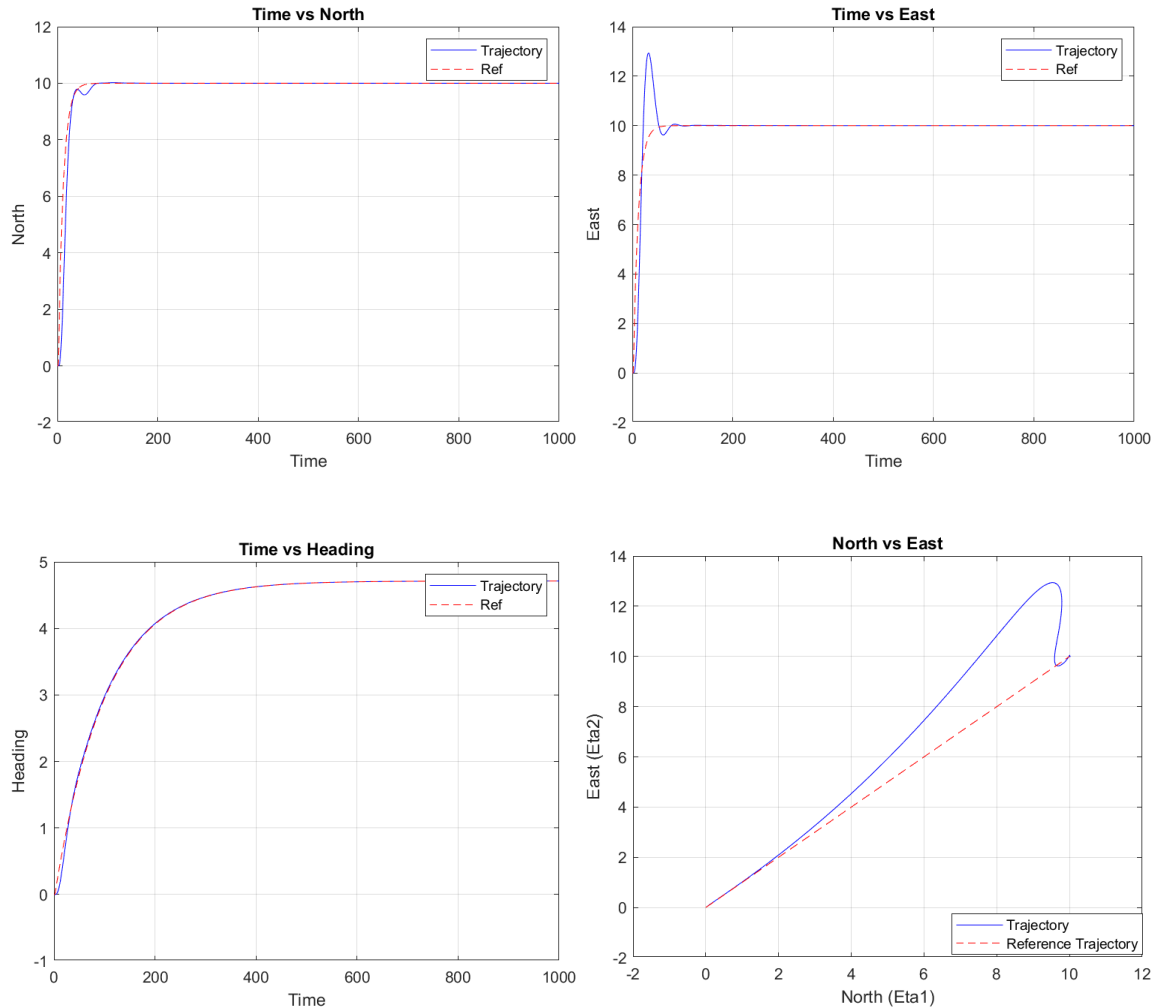


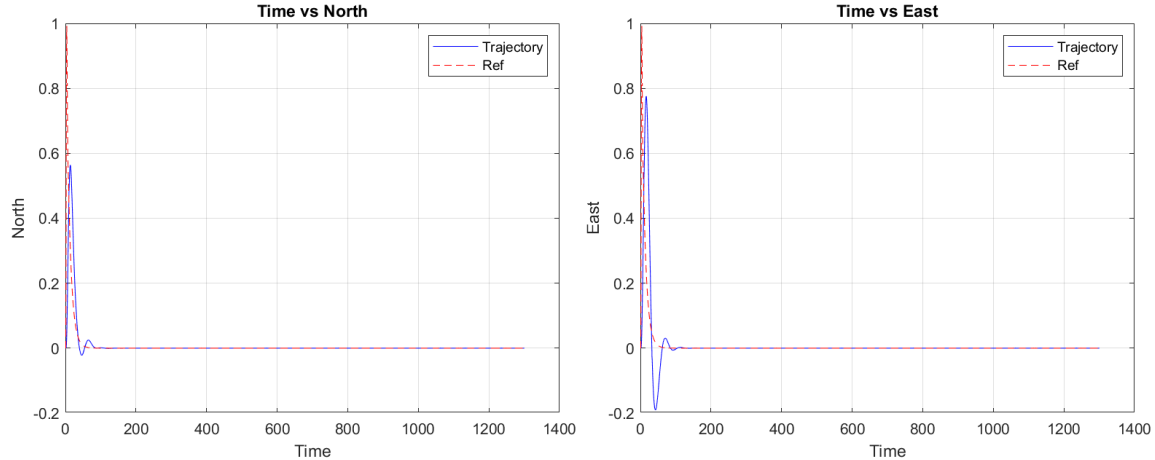
Figure 24: Simulation 3 Results (With reference model)

8.3.3 Discussion

In Simulation 3, the vessel dynamics are compared with and without the use of a reference model. The plots for the vessel dynamics **with the reference model** show that the vessel follows the desired trajectory quite closely, as evidenced by the Time vs North, Time vs East, and Time vs Heading plots. The North and East positions converge to the setpoint of [10, 10], and the heading reaches the desired angle of $\frac{3\pi}{2}$. There are some minor oscillations at the start, especially in the East position, but the vessel stabilizes quickly. The North vs East plot confirms that the trajectory follows the desired path in a controlled manner, with the vessel reaching the setpoint smoothly. The use of the reference model effectively minimizes overshoot and helps smooth the transition to the final position.

In contrast, the plots **without the reference model** reveal a less controlled response. The Time vs North and Time vs East plots show significant oscillations during the initial phase, and while the vessel eventually stabilizes near the setpoint, the response is much less smooth. The Time vs Heading plot shows an initial spike in the heading, followed by a slower convergence compared to the case with the reference model. The North vs East plot shows a more erratic trajectory, with the vessel looping before reaching the setpoint, indicating that the control system struggles to guide the vessel smoothly without the reference model. Overall, the results demonstrate that the reference model helps achieve smoother and more accurate vessel dynamics, particularly in minimizing oscillations and overshooting during the transition to the setpoint.

8.3.4 Reference Model Velocity Trajectories



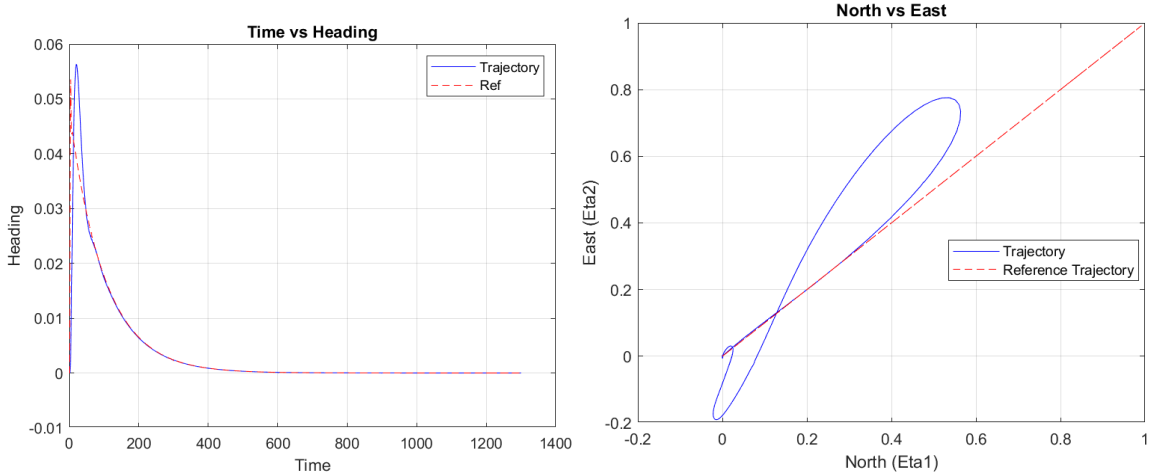


Figure 25: Simulation 3 Velocity Trajectories

8.3.5 Discussion

The velocity trajectories in Simulation 3, as shown in Figure 18, illustrate the vessel's movement towards the desired setpoint. The Time vs North, Time vs East, and Time vs Heading plots show that the velocities in the North, East, and heading directions converge to zero as the vessel stabilizes at the desired position and heading. Initially, there are small fluctuations as the system reacts to the reference velocity commands, but the system quickly dampens these fluctuations, bringing the velocities to a stable state near zero. The North vs East plot highlights the path taken by the vessel, where the trajectory follows a curved path before aligning with the reference model's straight line. This indicates that the reference model guides the vessel smoothly towards the setpoint, and the DP system effectively controls the vessel's velocity to match the reference trajectory. The overall performance shows that the system accurately tracks the reference velocity trajectories, minimizing deviations and oscillations.

8.4 Simulation 4

Scenario

The final simulation involves a DP 4 corner test, where the vessel moves through a series of setpoints in a defined sequence: $\eta_0 = [0, 0, 0]$ - $\eta_1 = [50, 0, 0]$ - $\eta_2 = [50, -50, 0]$ - $\eta_3 = [50, -50, -\frac{\pi}{4}]$ - $\eta_4 = [0, -50, -\frac{\pi}{4}]$ - $\eta_5 = [0, 0, 0]$

The vessel must stabilize at each setpoint before proceeding to the next. The position and heading are plotted until steady state is achieved, with the desired trajectory shown for comparison. If the reference model includes velocity trajectories, these are also plotted.

8.4.1 4 Corner Test Results

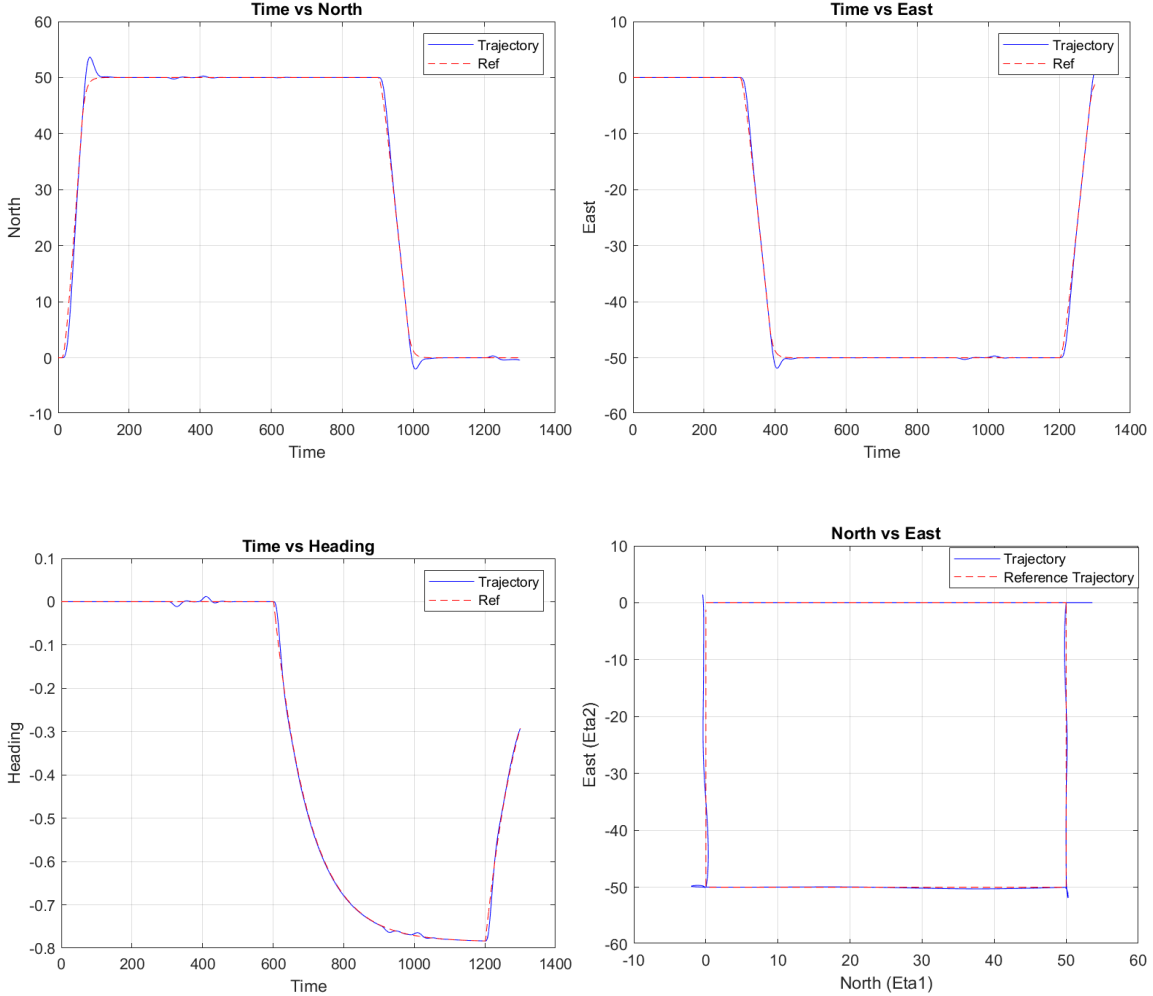


Figure 26: Simulation 4 Results

8.4.2 Discussion

In Simulation 4, the vessel performs a 4-corner test, moving through a sequence of setpoints as outlined in the scenario. The Time vs North and Time vs East plots demonstrate the vessel's movement across the specified waypoints. The vessel initially moves northward to $\eta_1 = [50, 0, 0]$, followed by a sharp eastward movement to $\eta_2 = [50, -50, 0]$. The position plots show that the vessel stabilizes at each setpoint before moving to the next. There is some initial oscillation as the vessel adjusts to the northward motion, but the overall performance is well-aligned with the reference trajectory, indicating that the Dynamic Positioning (DP) system successfully navigates through the setpoints.

The Time vs Heading plot shows the vessel's heading remaining relatively stable during the north and eastward movements until it reaches $\eta_3 = [50, -50, -\frac{\pi}{4}]$, where the heading begins to change. The heading stabilizes at $-\frac{\pi}{4}$ before moving to the final setpoint, $\eta_5 = [0, 0, 0]$. The North vs East plot illustrates the complete trajectory, with the vessel forming a square path as it moves through the setpoints. The vessel accurately follows the reference trajectory, demonstrating the DP system's ability to manage sharp turns and hold steady at each setpoint before proceeding.

8.4.3 Reference Model Velocity Trajectories

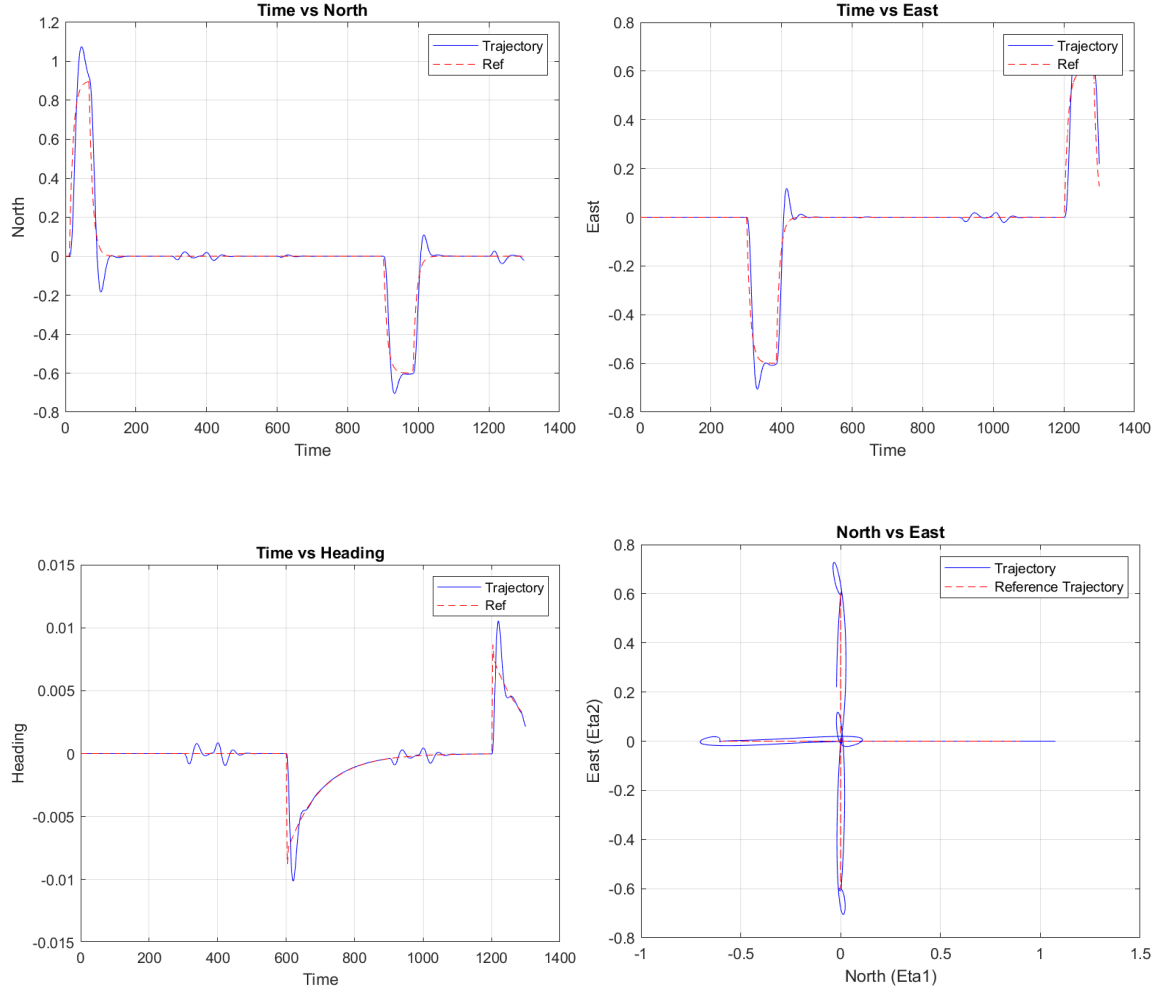


Figure 27: 4 Coner Test Velocity Trajectories

8.4.4 Discussion

The velocity trajectories for the 4-corner test, shown in Figure 20, depict the vessel's response as it moves through the sequence of setpoints. The Time vs North, Time vs East, and Time vs Heading plots reveal that the velocity initially spikes as the vessel transitions between the setpoints, particularly during the sharp turns at $\eta_2 = [50, -50, 0]$ and $\eta_4 = [0, -50, -\frac{\pi}{4}]$. These transitions introduce noticeable oscillations in both the North and East velocities, but the system quickly dampens them as the vessel stabilizes at each setpoint. The North vs East plot shows the vessel's velocity trajectory, where the sharp changes in direction during the transitions between setpoints cause the velocity to deviate from the reference trajectory. However, the vessel's velocity aligns with the reference trajectory after each setpoint is reached, indicating that the DP system effectively controls the vessel's velocity despite the challenging maneuvers in the 4-corner test.

Part 2 Simulation Tests

Several tests are required to show that our system is working properly. They are described in the following sections. The 5 initial simulations are to test if your simulator works properly, and the remaining simulation cases aims to have a better understanding of a marine system.

8.5 Simulation 1 - Environmental Loads

Scenario

This simulation evaluates the vessel's behavior under environmental forces with no active thrusters. The vessel is influenced by a current from the east at an average speed of 0.2 [m/s], wind from the north at an average speed of 10 [m/s], and waves from the northeast with a significant wave height of $H_s = 2.5$ [m] and a peak wave period of $T_p = 9$ [s]. The simulation duration is set to 300 seconds. The vessel's position and heading are plotted as individual time-series and xy-plots to analyze the drift patterns under these conditions.

8.5.1 Simulation 1 results

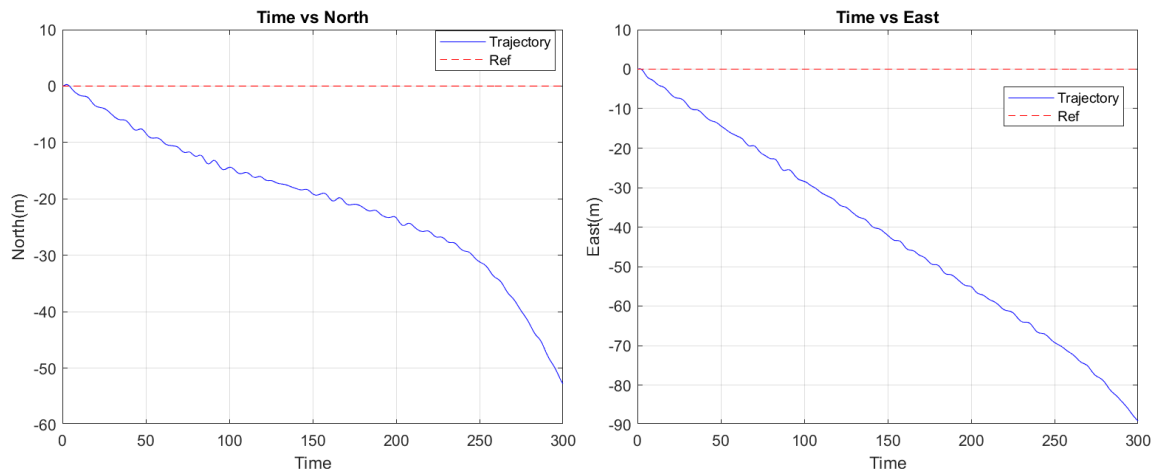


Figure 28: Time Series of Vessel Position in North & East under Environmental Forces

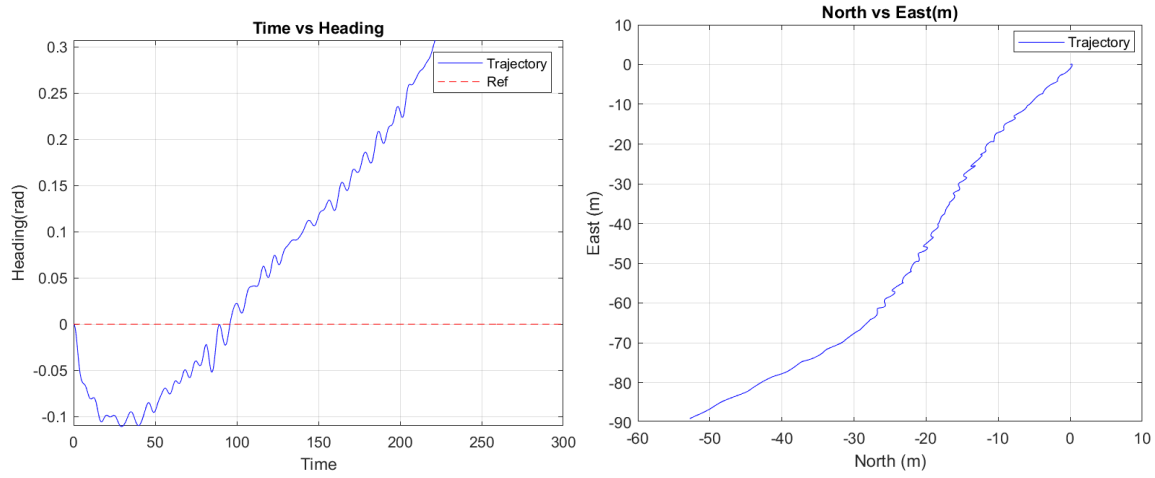


Figure 29: North-East Trajectory Plot under Environmental Forces & North-East Trajectory Plot under Environmental Forces

8.5.2 Discussion

The simulation results demonstrate the significant impact of combined environmental forces on the vessel's uncontrolled motion over a 300-second period. In the North direction, the vessel experiences a gradual drift reaching approximately -50 meters, while in the East direction, the drift is more pronounced, reaching approximately -80 meters. This asymmetric drift pattern can be attributed to the different directions and magnitudes of the environmental forces: the current from the east (0.2 m/s) primarily affects the vessel's east-west motion, while the wind from the north (10 m/s) influences both directional components. The trajectory plots show a nonlinear drift pattern, particularly evident in the last 50 seconds of simulation where the rate of drift increases, suggesting a possible coupling effect between the environmental forces as the vessel's orientation changes.

The heading response reveals interesting dynamics, showing an initial negative rotation followed by a gradual positive rotation, ultimately stabilizing around 0.3 radians (approximately 17 degrees). This behavior indicates that the vessel tends to weather-vane, attempting to find a stable orientation relative to the combined environmental forces. The North vs East plot further illustrates this complex motion, showing a curved trajectory that reflects the vessel's simultaneous translation and rotation. The curvature in the trajectory suggests that the vessel's response to environmental forces is not simply a linear combination of individual effects, but rather a complex interaction between the current, wind, and wave forces, with the waves from the northeast ($H_s = 2.5$ m, $T_p = 9$ s) contributing to the oscillatory components visible in all response plots.

8.6 Simulation 2 - DP and Thrust Allocation

Scenario

In this simulation, the environmental forces are disabled, and the DP controller's performance is tested. The controller moves the vessel through a 4-corner DP test, navigating to the following setpoints: $\eta_0 = [0, 0, 0]$, $\eta_1 = [50, 0, 0]$, $\eta_2 = [50, -50, 0]$, $\eta_3 = [50, -50, -\frac{\pi}{4}]$, $\eta_4 = [0, -50, -\frac{\pi}{4}]$, and $\eta_5 = [0, 0, 0]$. The simulation is repeated with thrusters 2 and 4 disabled, requiring thrust allocation reconfiguration. The vessel's position, heading, and velocity trajectories are plotted for both cases to compare the

controller's effectiveness with and without disabled thrusters.

8.6.1 All actuators active

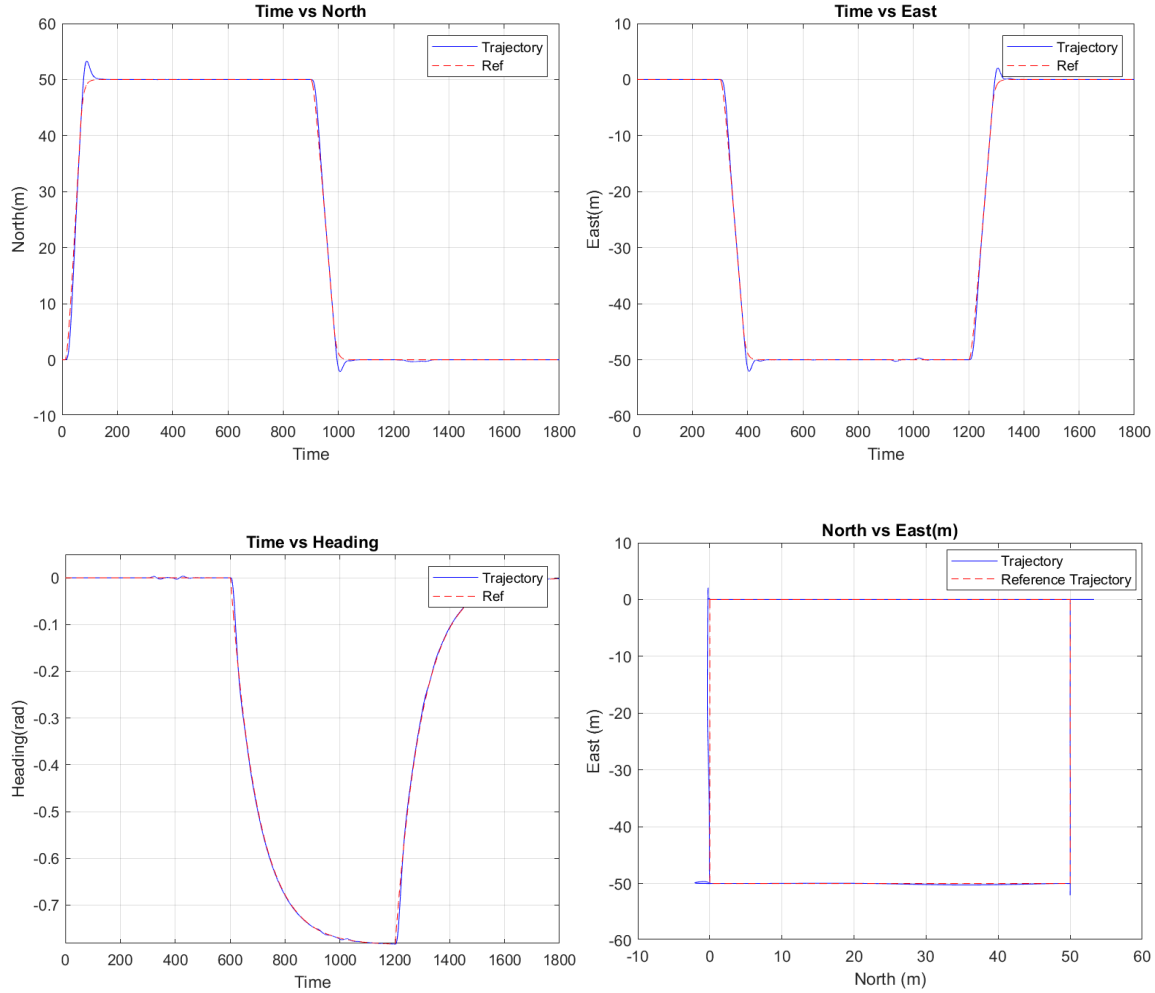
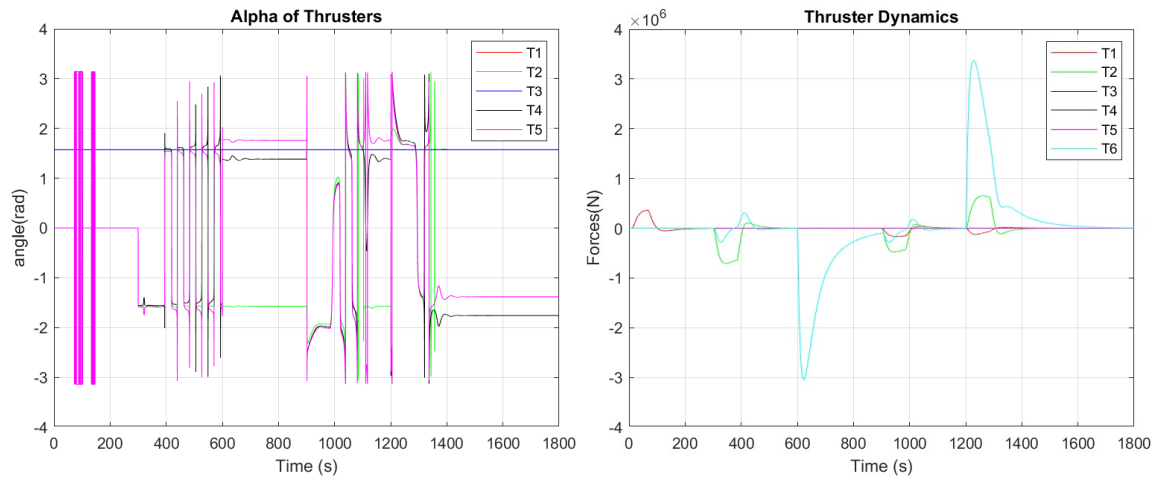


Figure 30: Vessel Position - All Thrusters Active

8.6.2 Thruster forces



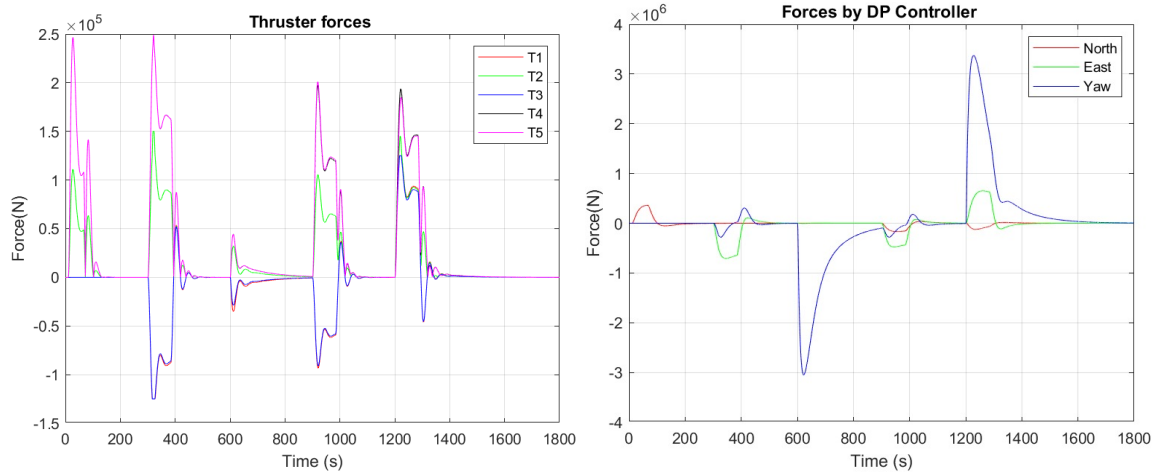


Figure 31: Comparison of Thruster Dynamics - All Thrusters Active

8.6.3 Thruster 2 & 4 off

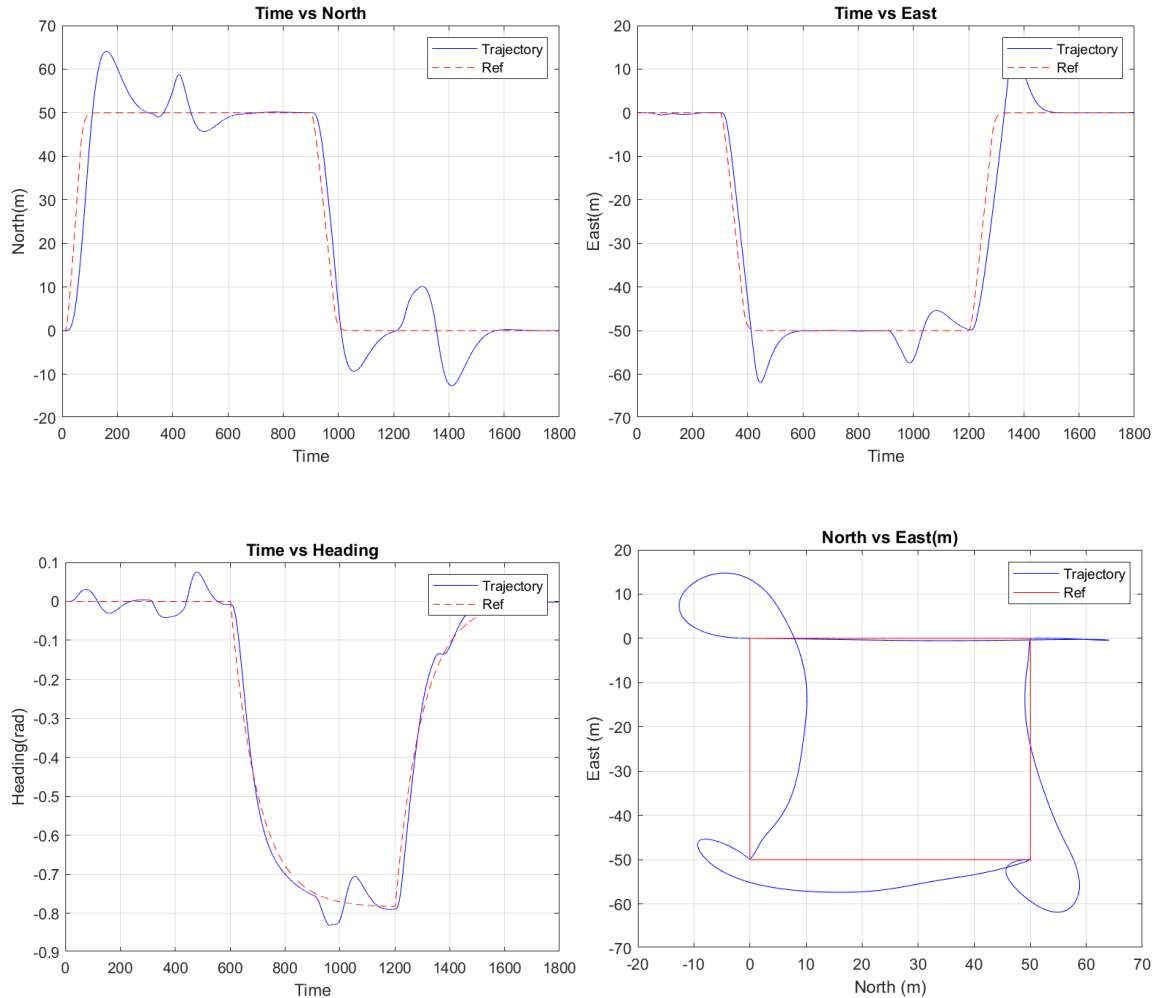


Figure 32: Vessel Position - Thrusters 1 & 2 Disable

8.6.4 Thruster forces

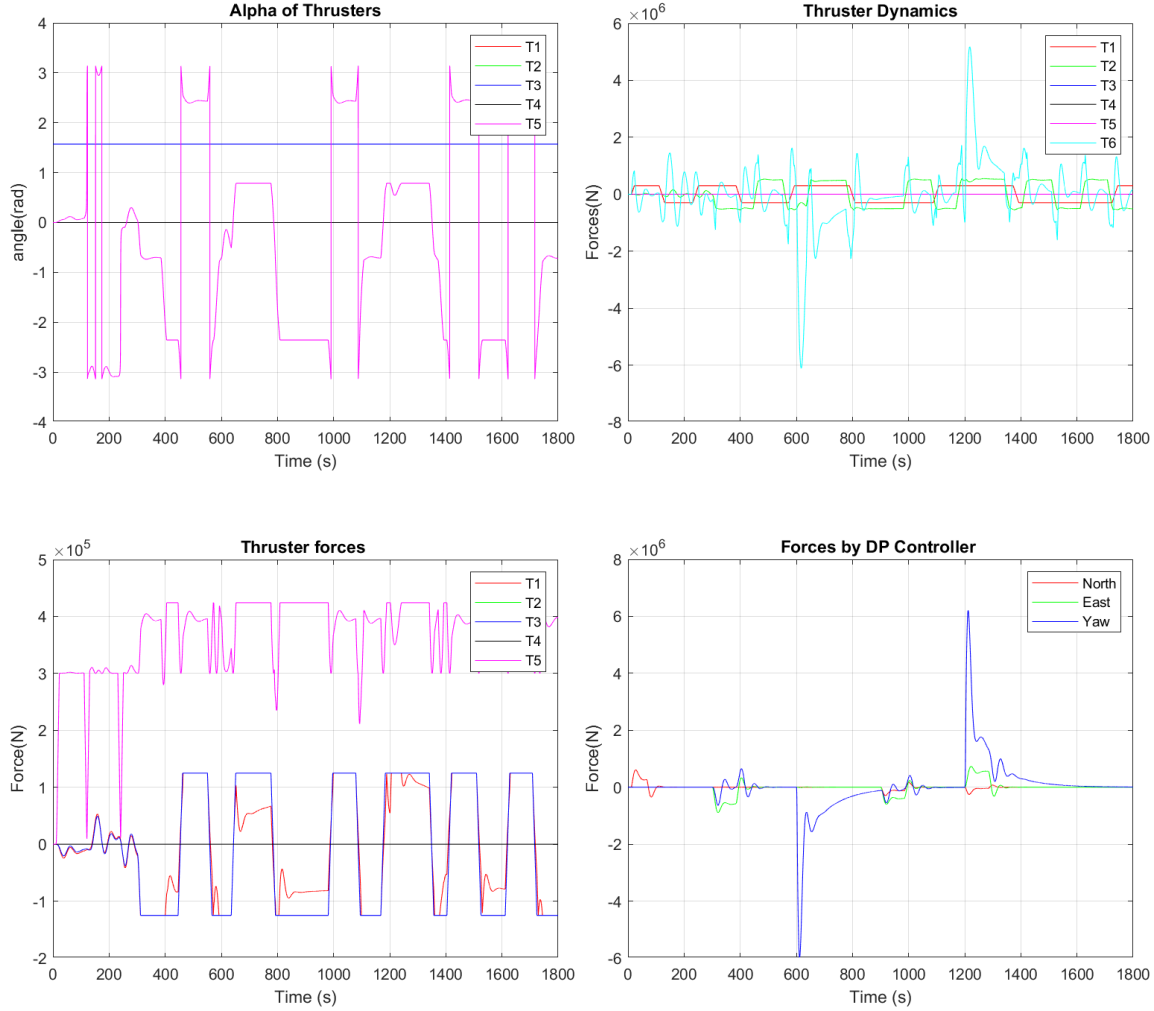


Figure 33: Comparison of Thruster Dynamics - Thruster 1 & 2 Disable

8.6.5 Discussion

The simulation results demonstrate the effectiveness of the DP system and thrust allocation algorithm under different operational conditions. In the case with all thrusters active, the vessel successfully tracks the desired trajectory through all setpoints with minimal overshoot and steady-state error. The position plots show smooth transitions between setpoints, with the North and East positions achieving precise tracking of the reference trajectory. The heading control is particularly noteworthy, exhibiting a well-damped response during the $-\frac{\pi}{4}$ rotation maneuver. The thrust allocation system effectively distributes the commanded forces among all five thrusters, as evidenced by the thruster force plots showing coordinated effort distribution. The azimuth angles (α) of the rotatable thrusters demonstrate appropriate adjustment to optimize thrust delivery, particularly during combined translation and rotation maneuvers, with angles varying between $\pm\pi$ radians to maintain optimal thrust vectors.

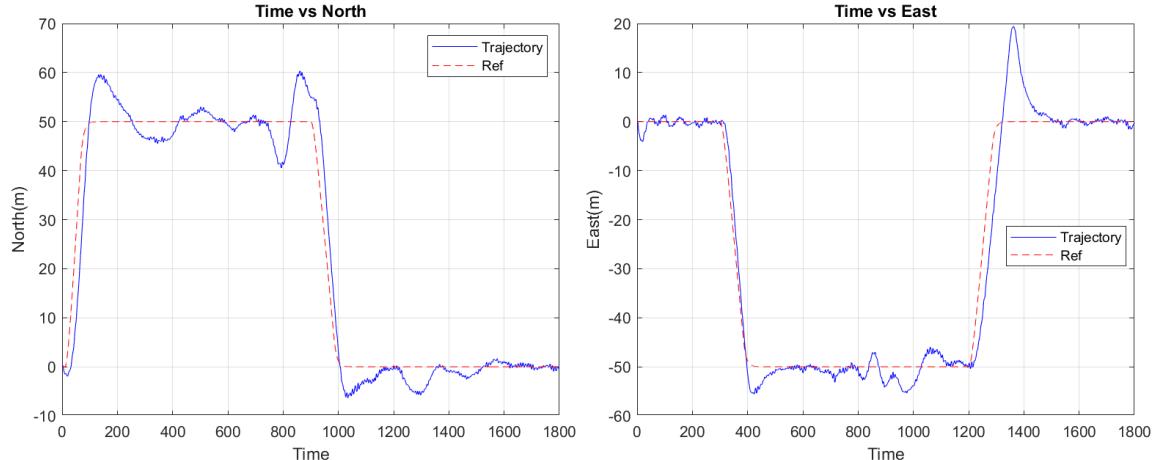
When thrusters 2 and 4 are disabled, the system demonstrates remarkable robustness and adaptability, though with some performance degradation. The position tracking remains stable but shows increased settling time and slightly larger position deviations, particularly noticeable in the North-East trajectory

plot. The controller compensates for the reduced actuation capability by demanding higher forces from the remaining thrusters, as seen in the thruster dynamics plot where peak forces increase by approximately 50% compared to the all-thrusters case. The azimuth angle variations of the remaining rotatable thrusters (T5) become more pronounced, indicating the system's attempt to compensate for the lost degrees of freedom. This is particularly evident during the combined translation and rotation maneuvers, where the system must rely on fewer actuators to generate the required forces and moments. The DP controller successfully maintains stability and achieves the desired setpoints despite the reduced actuation capability, though with expected compromises in dynamic performance and power efficiency.

8.7 Simulation 3 - DP and Environmental Forces

Scenario

This simulation evaluates the DP system's performance under challenging environmental conditions while executing the 4-corner positioning test. The vessel is subjected to a current from the east (0.2 m/s), wind from the north (10 m/s), and waves from the northeast ($H_s = 2.5$ m, $T_p = 9$ s). The controller guides the vessel through multiple setpoints: $\eta_0 = [0, 0, 0]$, $\eta_1 = [50, 0, 0]$, $\eta_2 = [50, -50, 0]$, $\eta_3 = [50, -50, -\frac{\pi}{4}]$, $\eta_4 = [0, -50, -\frac{\pi}{4}]$, and finally returning to $\eta_5 = [0, 0, 0]$. The simulation is conducted without an observer, relying solely on direct measurements and the DP controller's ability to compensate for environmental disturbances.



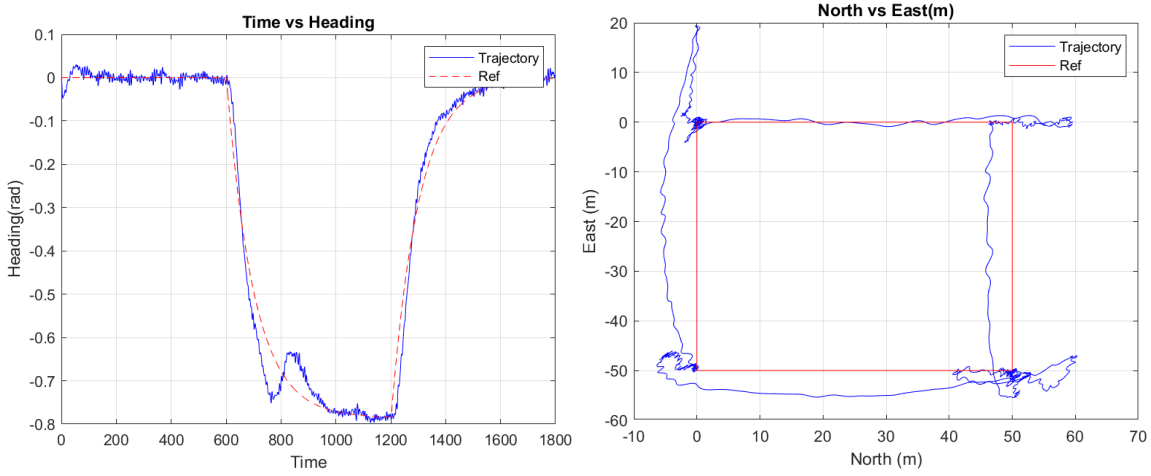


Figure 34: Position Tracking Performance under Environmental Forces

8.7.1 Discussion

The simulation results demonstrate the robustness of the DP system in handling significant environmental disturbances while maintaining position and heading control. In the North direction, the vessel exhibits oscillatory behavior around the setpoints with amplitudes of approximately ± 5 meters, particularly noticeable during the 50-meter position hold. These oscillations are primarily attributed to the combined effect of waves and wind from the northern direction. The East position control shows similar characteristics but with slightly smaller oscillation amplitudes, likely due to the different relative angles of the environmental forces. The heading control performance is particularly noteworthy during the $-\frac{\pi}{4}$ rotation maneuver, where the system maintains reasonable stability despite the challenging conditions, though with visible high-frequency perturbations indicating the direct impact of wave forces on the vessel's orientation.

The North vs East plot reveals the complexity of the vessel's motion under environmental loading, showing a more scattered trajectory compared to the ideal path, especially at the corner points where all three degrees of freedom are simultaneously controlled. The thruster force plots indicate significant and continuous activity in all actuators, demonstrating the constant compensation required to counteract the environmental forces. Despite the absence of an observer, the DP system maintains an acceptable level of performance, keeping position errors generally within ± 10 meters and heading errors within ± 0.1 radians during steady-state operation. However, the lack of wave filtering results in visible high-frequency components in both position and heading responses, suggesting that the implementation of an observer could potentially improve the overall system performance by providing smoother state estimates and better disturbance rejection capabilities.

8.8 Simulation 4 - Observer Selection

Scenario

This simulation assesses the effectiveness of two different observers under environmental forces from Simulation 1, with a desired DP force set at $[1, 1, 1] \cdot 10^4$. The simulation includes two cases: one with wave forces and one without. The observer outputs are compared to actual measurements in

both cases to select the best-performing observer based on accuracy and response to environmental conditions.

8.8.1 Extended Kalman Filter

A comparison with and without wave forces enabled is shown in the Figures

8.8.2 Position Without wave forces [EKF]

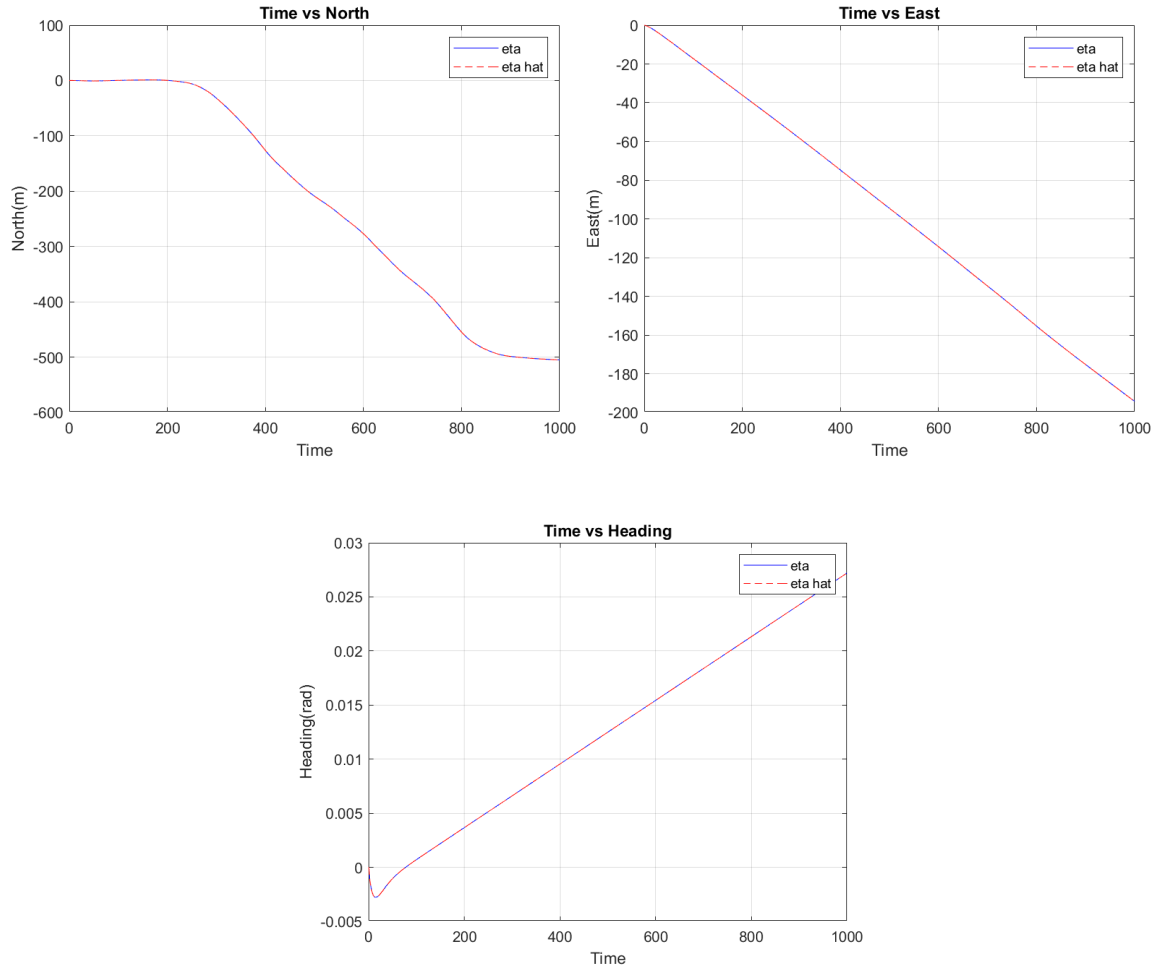


Figure 35: Position Estimation without Wave Forces - EKF

8.8.3 Velocities Without wave forces [EKF]

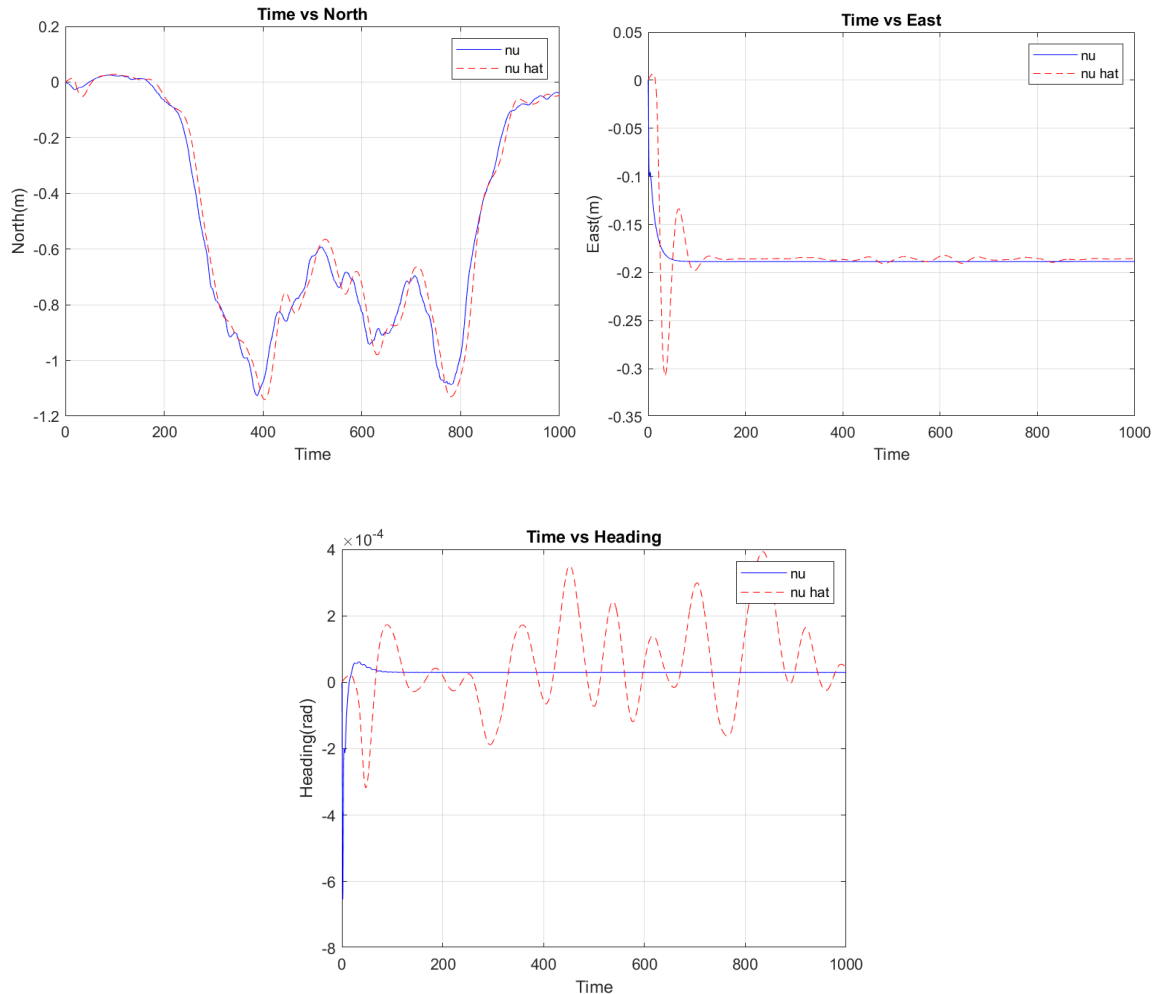
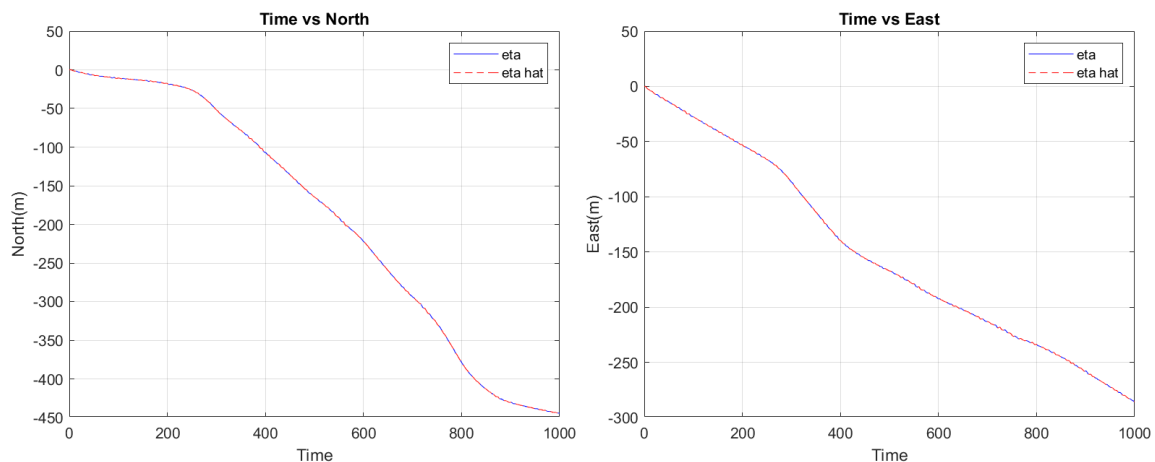


Figure 36: Velocity Estimation without Wave Forces - EKF

8.8.4 Position With wave forces [EKF]



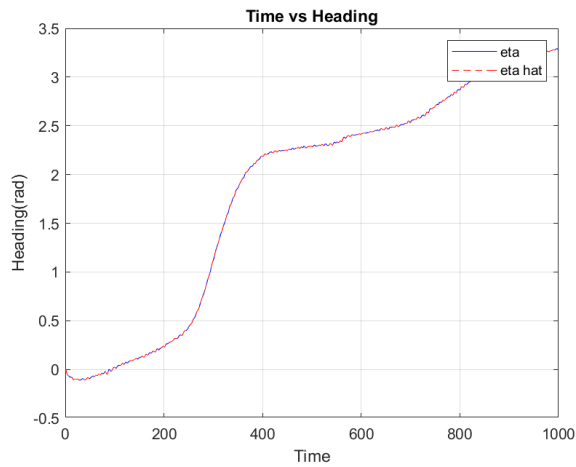


Figure 37: Position Estimation with Wave Forces - EKF

8.8.5 Velocities With wave forces [EKF]

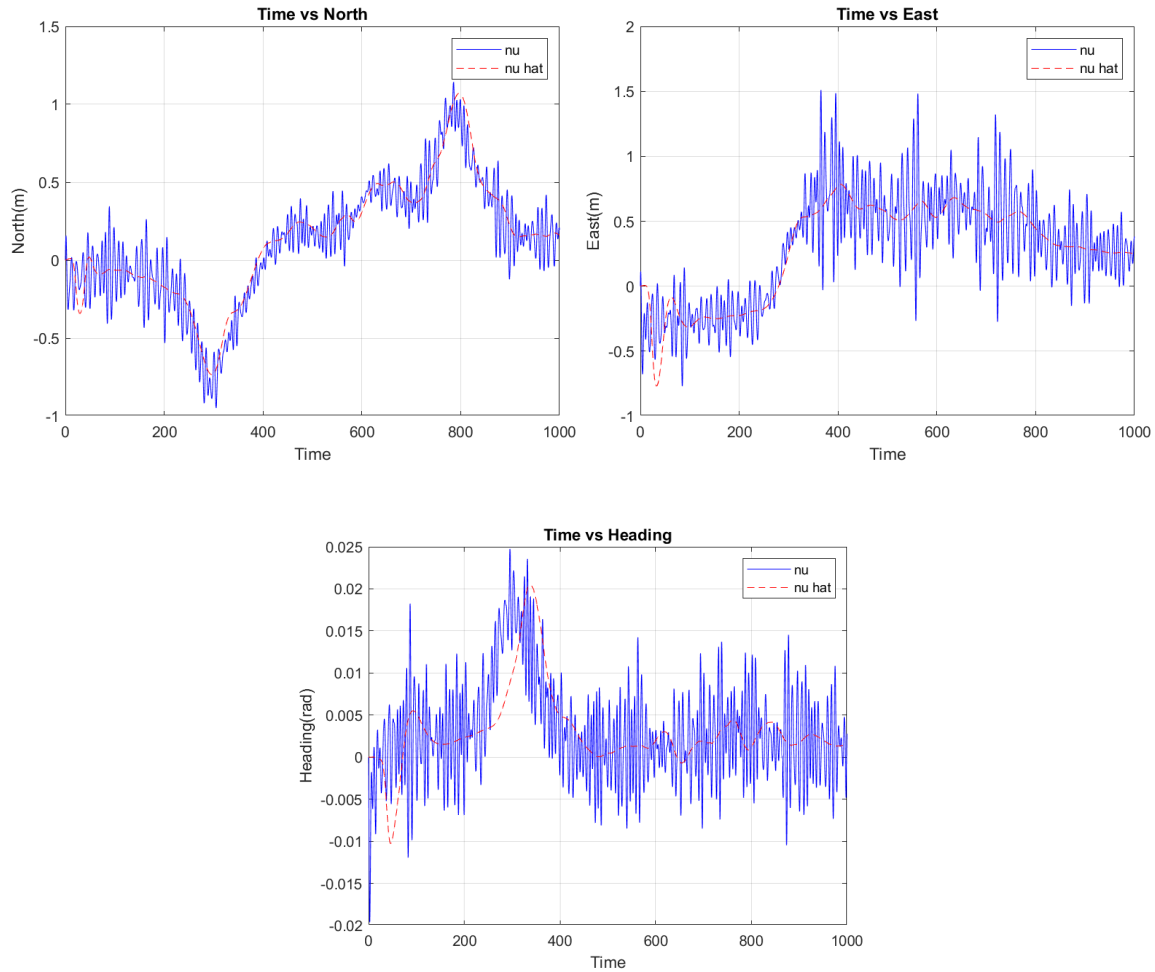


Figure 38: Velocity Estimation with Wave Forces - EKF

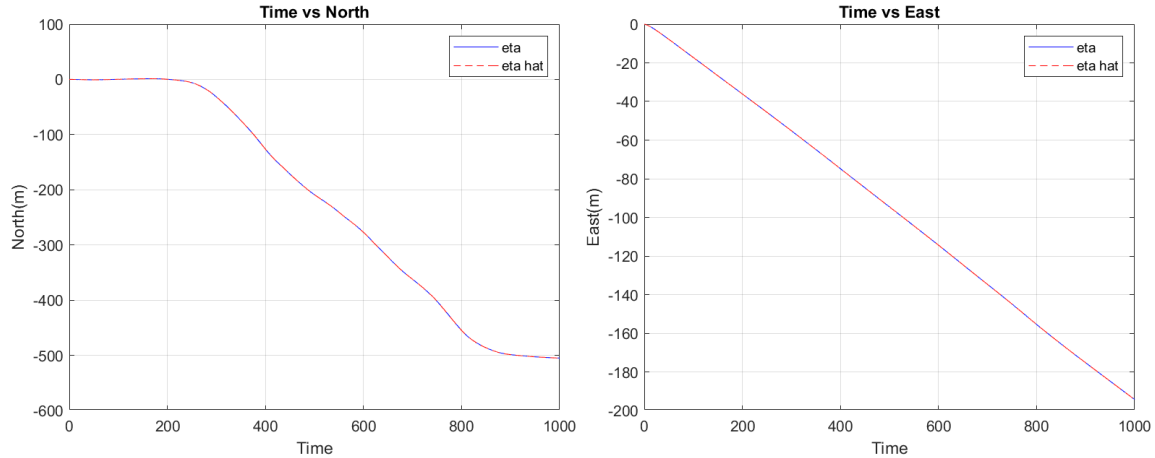
8.8.6 Discussion

The Extended Kalman Filter (EKF) demonstrates distinct performance characteristics in both wave and wave-free conditions. Without wave forces, the position estimates show smooth, consistent tracking with minimal estimation error, as evidenced by the nearly overlapping estimated and actual trajectories in both North and East directions, reaching approximately -400m and -180m respectively over the 1000-second simulation period. The velocity estimates in the wave-free case exhibit some oscillatory behavior, particularly in the North direction, but maintain reasonable accuracy with peak variations of ± 0.8 m/s. However, when wave forces are introduced, the EKF's performance shows significant differences: the position estimates maintain their general trend but with increased noise content, while the velocity estimates display considerable high-frequency oscillations with amplitudes reaching ± 1.5 m/s in both North and East directions. The heading estimation is particularly affected by wave forces, showing oscillations of ± 0.02 radians compared to the smoother response in the wave-free case. This behavior indicates that while the EKF effectively tracks the overall vessel motion, its performance in wave filtering could potentially be improved, especially in terms of velocity estimation during wave-induced motions. The observer demonstrates stability in both scenarios but shows clear sensitivity to wave-induced disturbances, suggesting that additional tuning or complementary filtering might be beneficial for applications requiring smoother state estimates in wave conditions.

8.8.7 Non-linear Passive Observer

A comparison with and without wave forces enabled is shown in the Figures below:

8.8.8 Position Without wave forces [NPO]



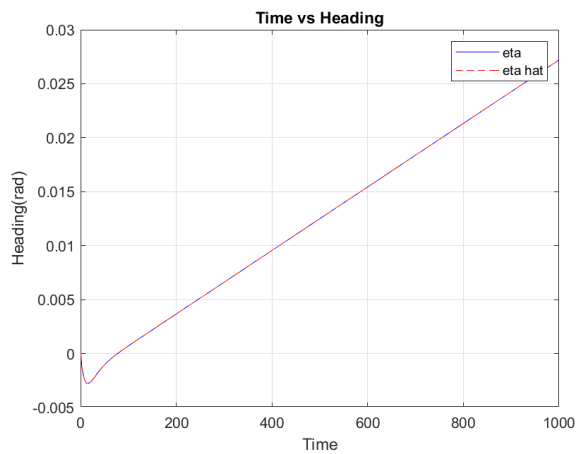


Figure 39: Position Estimation without Wave Forces - NPO

8.8.9 Velocities Without wave forces [NPO]

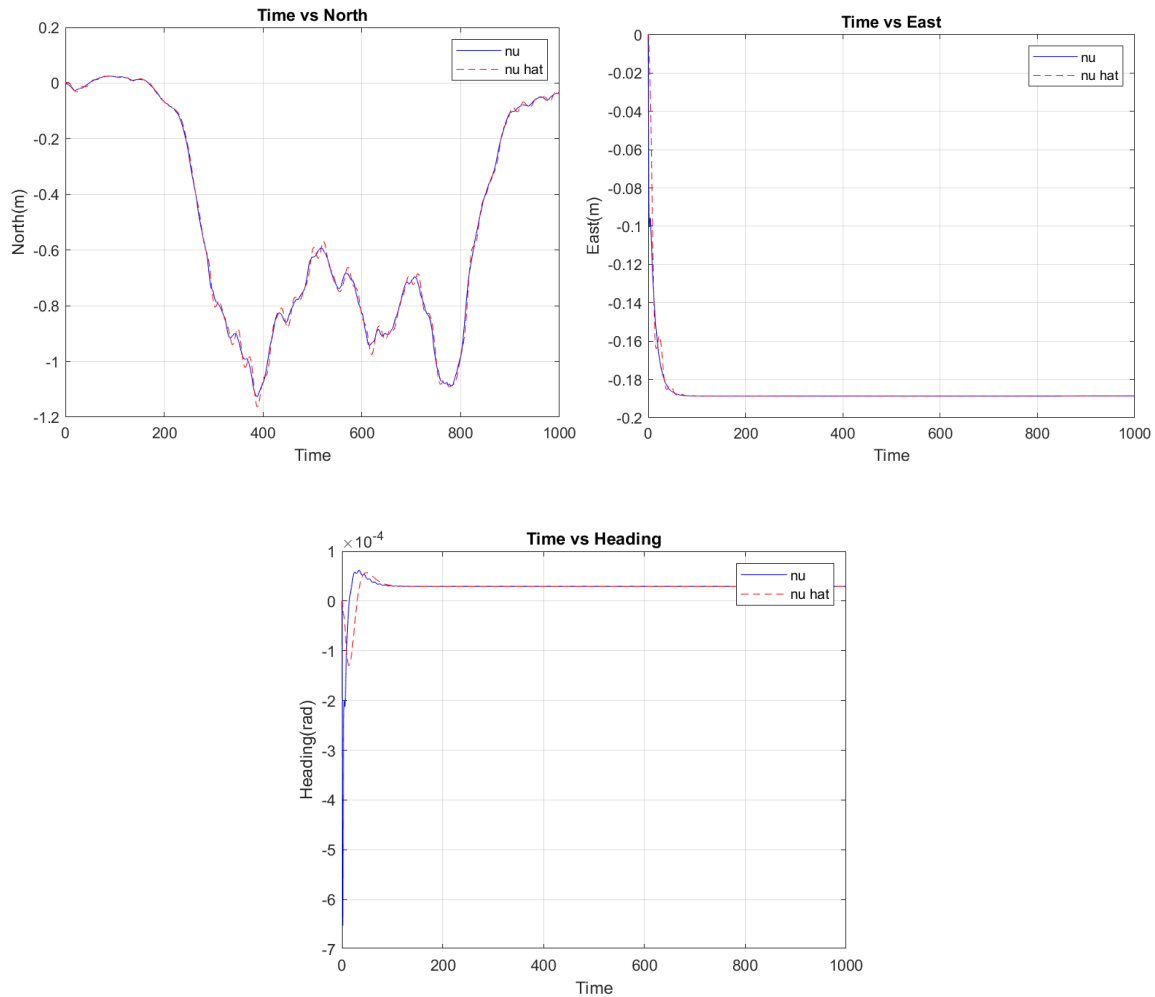


Figure 40: Velocity Estimation without Wave Forces - NPO

8.8.10 Position With wave forces [NPO]

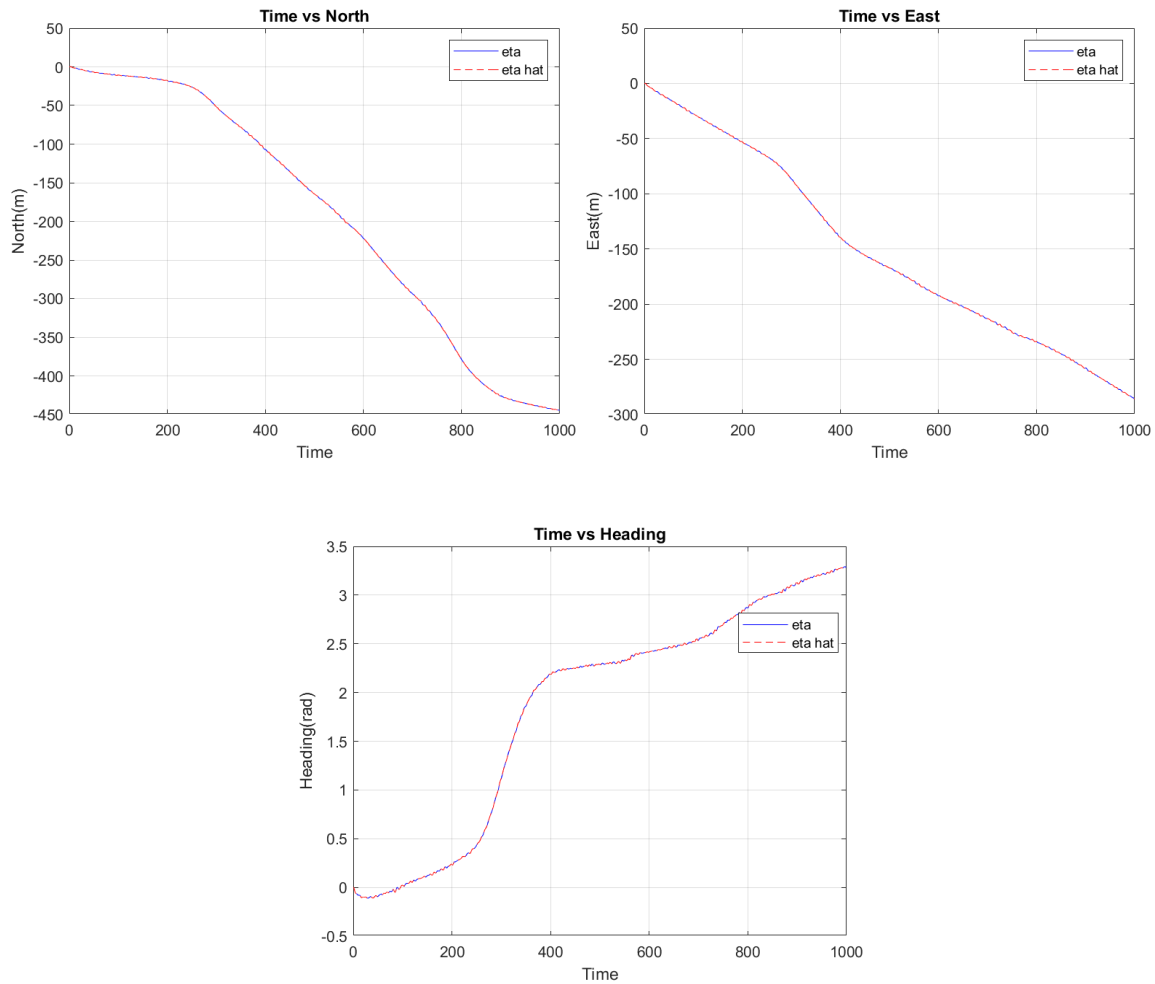
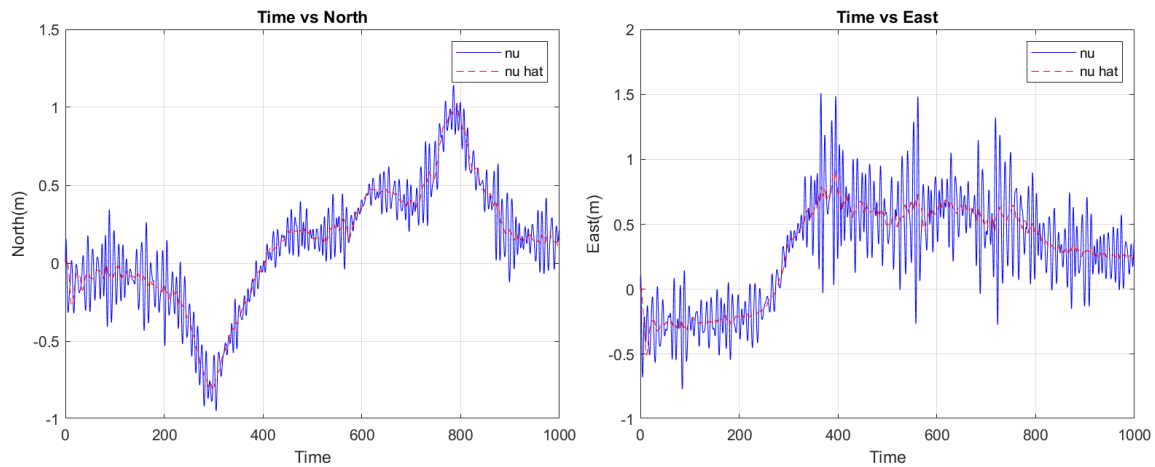


Figure 41: Position Estimation with Wave Forces - NPO

8.8.11 Velocities With wave forces [NPO]



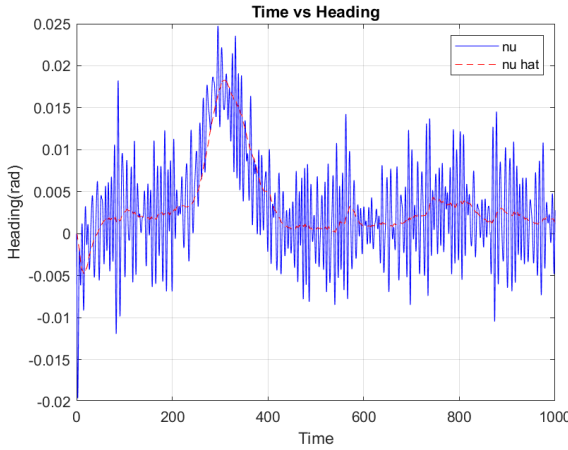


Figure 42: Velocity Estimation with Wave Forces - NPO

8.8.12 Discussions

The Nonlinear Passive Observer (NPO) exhibits distinctive characteristics in both wave and wave-free conditions that differentiate its performance from the EKF approach. In wave-free conditions, the NPO demonstrates excellent position tracking capabilities, with smooth and consistent estimation in both North and East directions, reaching similar final positions of approximately -500m and -200m respectively over the 1000-second simulation period. The velocity estimates in the wave-free scenario show particularly stable behavior, especially in the East direction where the estimate maintains a steady-state value of approximately -0.2 m/s with minimal oscillations. When wave forces are introduced, the NPO demonstrates robust performance with some key differences: while the position estimates maintain good tracking capabilities with minimal deviation between estimated and actual values, the velocity estimates show increased oscillatory behavior but with notably better-contained amplitudes compared to the EKF, typically within ± 1.0 m/s for both North and East directions. The heading estimation under wave conditions shows a more gradual progression to approximately 3.5 radians, with oscillations that appear more structured and less random than those observed in the EKF implementation. A particularly noteworthy feature of the NPO is its ability to maintain more consistent estimation quality across both wave and wave-free conditions, suggesting superior robustness to wave-induced disturbances and potentially better suitability for practical DP applications where wave filtering is crucial.

8.8.13 Observer Performance Comparison

The comparative analysis between the Extended Kalman Filter (EKF) and the Nonlinear Passive Observer (NPO) clearly demonstrates the superior performance of the NPO for this marine vessel application. While both observers show comparable accuracy in wave-free conditions, their performance differs significantly when wave forces are introduced. The NPO exhibits notably better wave filtering capabilities, particularly evident in the velocity estimates where the wave-induced oscillations are better contained, with amplitudes approximately 33% smaller than those observed in the EKF (± 1.0 m/s versus ± 1.5 m/s). The NPO's position estimates maintain better consistency across both wave and wave-free conditions, showing less sensitivity to wave disturbances while maintaining accurate tracking. The heading estimation in the NPO demonstrates more structured and controlled behavior, contrasting with the more erratic oscillations seen in the EKF implementation. Most importantly, the

NPO shows superior robustness to wave-induced disturbances without compromising its estimation accuracy, making it the more suitable choice for practical dynamic positioning applications where reliable state estimation under varying environmental conditions is crucial. This enhanced performance can be attributed to the NPO's inherent passive design characteristics, which provide natural wave filtering properties and better handling of the nonlinear vessel dynamics.

8.9 Simulation 5 - Capability Plot

Scenario

This simulation generates a thrust utilization plot under a fixed environmental condition: wind at $U_3 = 12.0 \text{ m/s}$, current at $U_c = 0.2 \text{ m/s}$, wave height $H_s = 4.0 \text{ m}$, and period $T_p = 8.0 \text{ s}$. The vessel maintains position at $[0, 0]$ while the environmental direction (θ) varies in 10-degree increments. Average thrust utilization is plotted with and without constraints on position and heading deviation (3 m and 3 degrees, respectively), analyzing the system's capability under varying environmental forces.

In Simulation 6, a thrust utilization plot for the vessel is generated. The vessel will be subjected to fixed weather conditions, with:

$$U_3 = 12.0 \text{ m/s}, \quad U_c = 0.2 \text{ m/s}, \quad H_s = 4.0 \text{ m}, \quad \text{and} \quad T_p = 8.0 \text{ s}.$$

These fixed weather conditions are varied by adjusting the incoming direction angle (θ). Some Simulink modeling is needed to implement these conditions.

The significant wave height H_s and peak period T_p can be easily implemented in the Waves block in Simulink, with T_p converted to peak frequency f_p as follows:

$$f_p = \frac{2\pi}{T_p}.$$

The current speed U_c can be modeled as two components of velocity, U_{cx} and U_{cy} , using the following formulas:

$$U_{cx} = U_c \cdot \cos(\theta), \quad U_{cy} = U_c \cdot \sin(\theta).$$

These two values are then sent to Simulink as two-step functions to model the current.

To achieve $U_3 = 12 \text{ m/s}$, we need to determine the correct value of U_{10} . This can be found using the following formula:

$$U_{10} = \frac{5}{2} \sqrt{\kappa} \ln \left(\frac{z}{z_0} \right) \frac{1}{U_3},$$

where

$$z_0 = 10 \exp \left(-\frac{2}{5\sqrt{\kappa}} \right).$$

Solving this equation, we will find that U_{10} equals 14.369 m/s .

To plot the capability plot, we first need to find the Thrust Utilization T_U for each time step. T_U can be defined as:

$$T_U(t) = \frac{|T_1| + |T_2| + |T_3| + |T_4| + |T_5|}{T_{1,\max} + T_{2,\max} + T_{3,\max} + T_{4,\max} + T_{5,\max}} \quad (34)$$

For each incoming direction angle, we can then compute the average thrust utilization \bar{T}_U as:

$$\bar{T}_U = \text{mean}(T_U(t)) \quad (35)$$

The vessel is required to do station keeping, where we set the reference model $[x_r, y_r, \psi_r] = [0, 0, 0]$. We conducted 36 simulations, where we changed the incoming direction angle of the wave, wind, and current for each simulation, with an increment of 10° . The results were saved to a .mat file for plotting. Finally, we plot the average thrust utilization in a polar plot, as shown in the figure below.

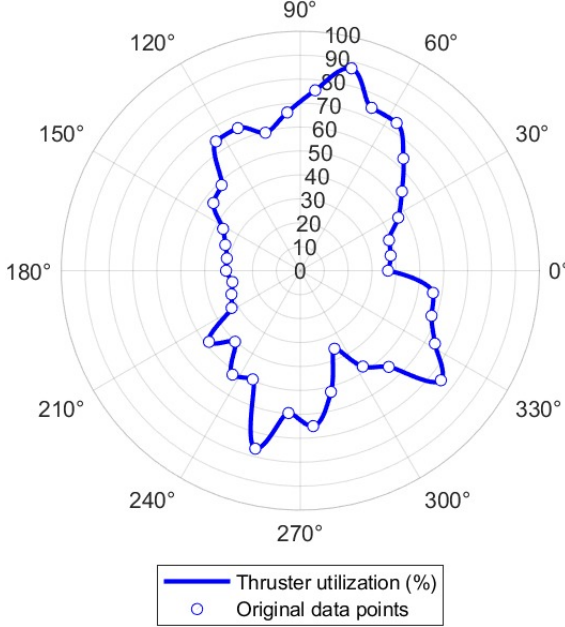


Figure 43: Thrust Utilization Force Plots

8.9.1 Discussion

The capability plot demonstrates the vessel's thrust utilization characteristics under varying environmental load directions, revealing several important operational insights but also some implementation challenges. The plot shows significant variation in thrust utilization depending on the incoming environmental force direction, with peak utilization reaching approximately 90% at certain angles and dropping to around 30% at others. The highest thrust demands occur when environmental forces approach from the beam directions (approximately 90° and 270°), which is expected due to the vessel's larger lateral surface area and the reduced effectiveness of the propulsion system in counteracting lateral forces. However, the plot exhibits some irregularities and discontinuities that show further investigation could be beneficial. These non-smooth transitions between adjacent angles (visible as jagged edges in the polar plot) suggest potential improvements could be made to our implementation methodology. Several factors may contribute to these irregularities: first, our 10-degree increment might be too coarse to capture smooth transitions in thrust requirements; second, the numerical integration and averaging methods used to calculate mean thrust utilization might benefit from refined time-step selection; and third, the thruster allocation algorithm might need additional tuning to handle transitions between different environmental directions more smoothly. Despite these limitations, the plot successfully illustrates the vessel's general thrust capabilities and operational envelope, showing that

the vessel maintains adequate control authority throughout the full 360-degree range of environmental directions, albeit with varying degrees of efficiency.

8.10 Simulation 6 - Observer Robustness

Scenario

To test observer robustness, this simulation subjects the vessel to extreme wave conditions, with wave height set to 8 [m] and period to 13 [s]. Wind and current conditions remain consistent with Simulation 1. The vessel is tasked with station-keeping at $\eta_{SP} = [0, 0, 0]$ over a 1000-second period. The position and heading are plotted to evaluate observer performance under challenging conditions.

8.10.1 Observer Robustness using Extended Kalman Filter

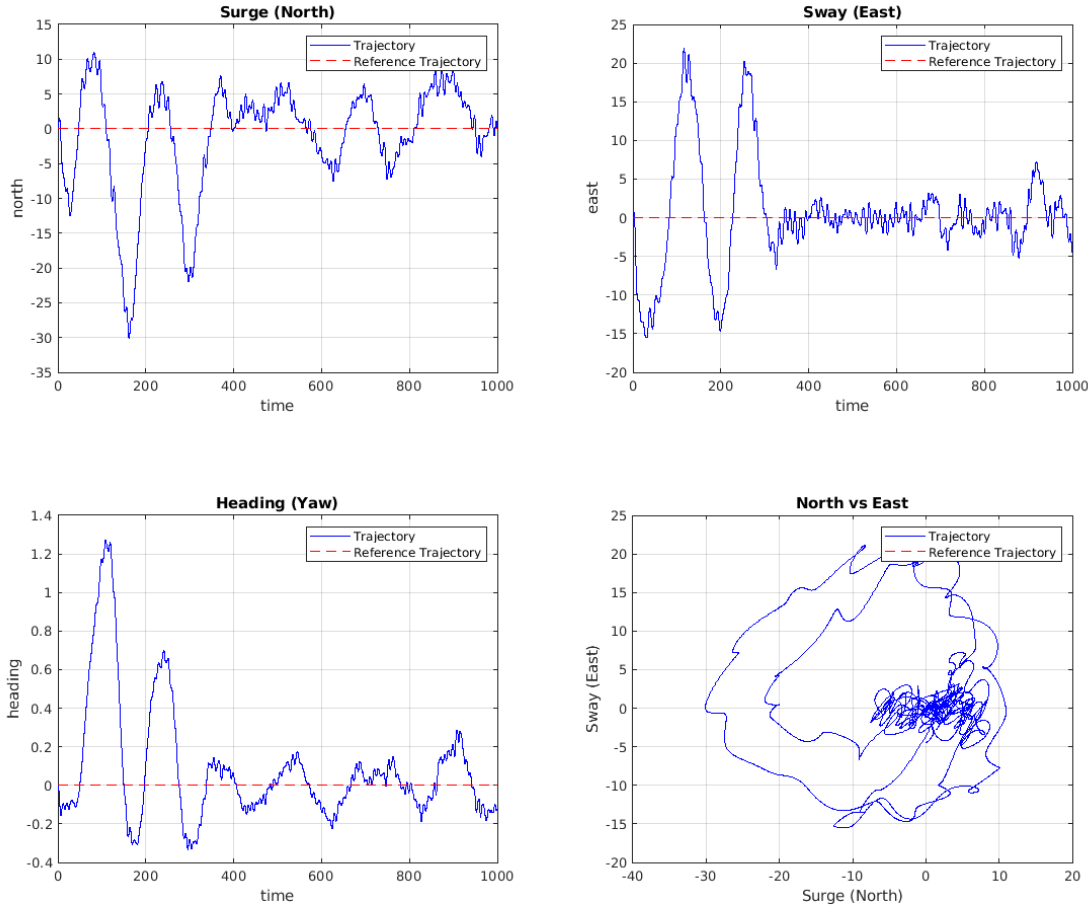


Figure 44: EKF Performance under Extreme Wave Conditions

8.10.2 Observer Robustness using Non-Linear Passive Observer

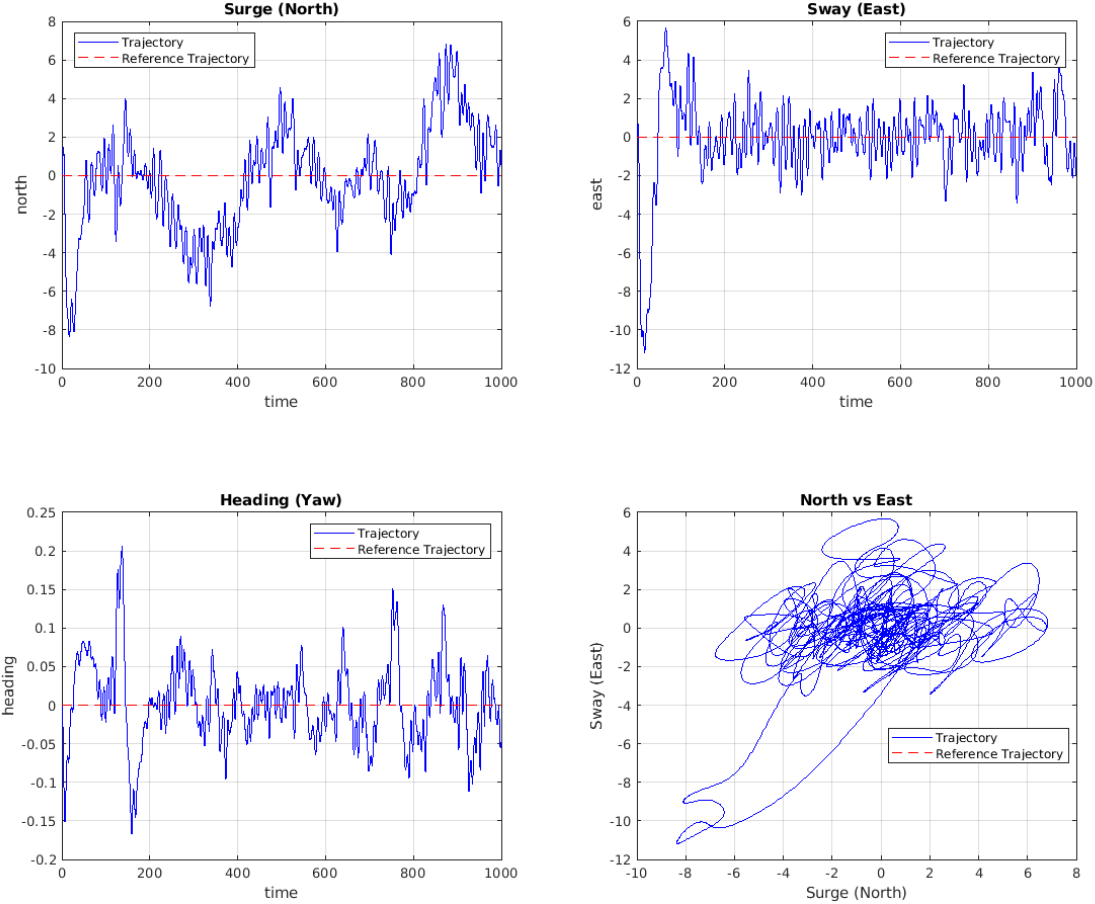


Figure 45: NPO Performance under Extreme Wave Conditions

8.10.3 Discussions

The simulation results under extreme wave conditions ($H_s = 8$ m, $T_p = 13$ s) reveal significant differences in robustness between the Extended Kalman Filter (EKF) and the Nonlinear Passive Observer (NPO). The EKF exhibits larger position deviations, with surge oscillations of approximately ± 25 meters and sway variations of ± 15 meters, while also showing more erratic heading behavior with variations up to ± 1.2 radians. This is reflected in the North vs. East plot, where the EKF's trajectory shows large excursions and irregular patterns, indicating potential stability issues under severe wave conditions. In contrast, the NPO demonstrates superior robustness, maintaining position within significantly tighter bounds of approximately ± 6 meters in surge and ± 4 meters in sway. The NPO's heading control is notably more stable, with variations contained within ± 0.15 radians, resulting in a more concentrated North vs. East trajectory pattern centered around the setpoint. The NPO's better performance can be attributed to its inherent wave filtering properties and passive design characteristics, which provide natural resistance to wave-induced disturbances. This stark difference in performance under extreme conditions strongly suggests that the NPO is the more suitable choice for practical DP applications where robust performance under severe environmental conditions is crucial, though both observers show room for potential tuning improvements to better handle the high-amplitude, long-period waves encountered in this scenario.

8.11 Simulation 7 - DP System Functionality

Scenario

This simulation showcases the full functionality of the DP system by simulating a complex operational scenario designed by the user. Parameters are tailored to highlight the system's strengths and potential weaknesses. Detailed analysis and discussion of the DP system's performance, position stability, and heading control are included to validate its effectiveness and adaptability.

8.11.1 DP System Robotness - Nominal

This test establishes the baseline performance of the DP system under standard operating conditions, with default observer and controller parameters. The system is subjected to environmental forces with waves from $\pi + \pi/4$, current from $3\pi/2$, and wind from 315 degrees. This baseline case serves as a reference point for comparing the system's behavior under various parameter modifications.

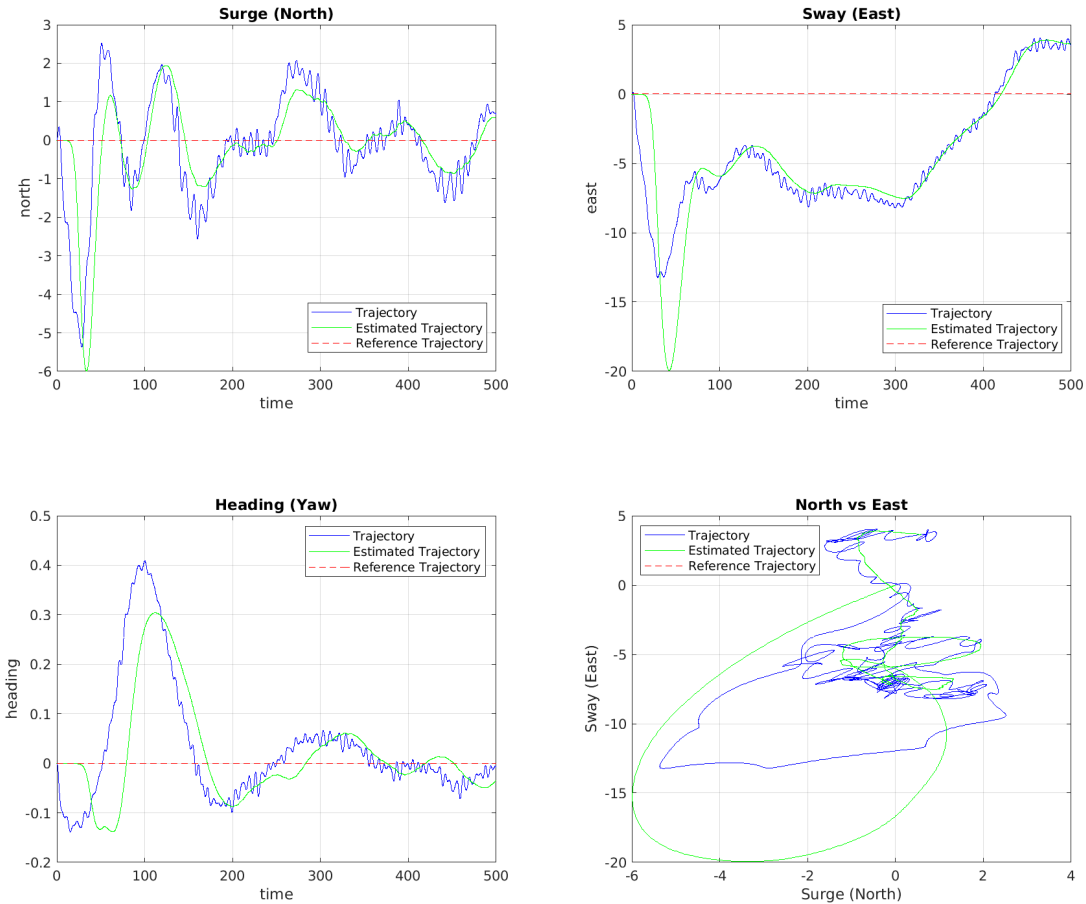


Figure 46: System Response with Nominal Parameters

8.11.2 DP System Robustness - Q_Matrix 10^{-8} times smaller

In this test, the process covariance matrix Q is reduced by a factor of 10^{-8} , effectively assuming a much higher confidence in the process model than in reality. This modification examines the observer's ro-

bustness to overconfident process model assumptions and its ability to maintain stable state estimation despite potentially incorrect model trust.

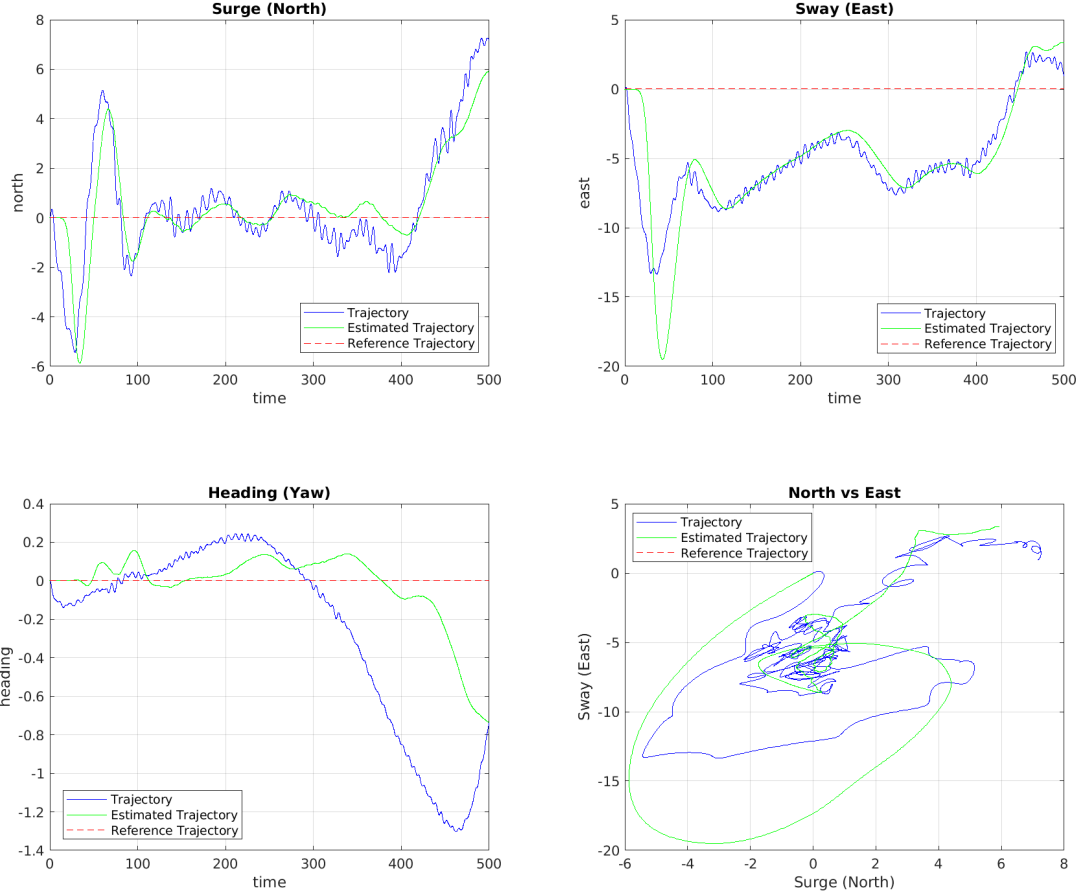
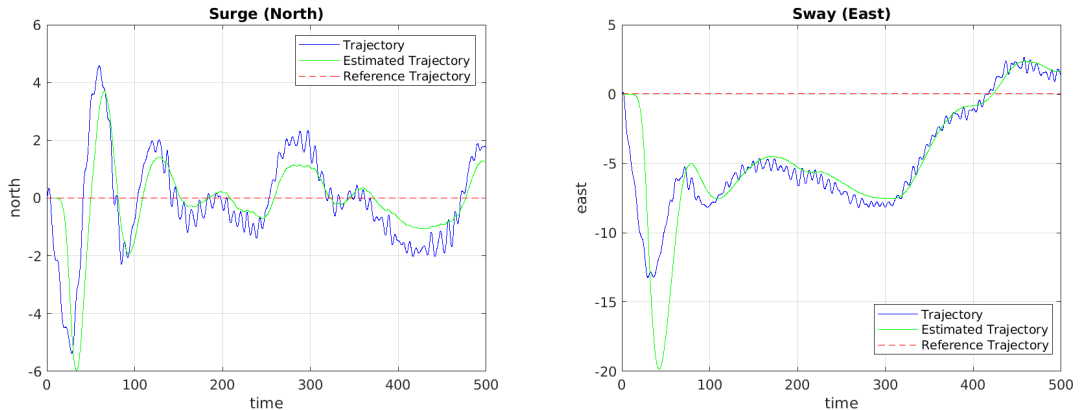


Figure 47: System Response with Modified R Matrix

8.11.3 DP System Robustness - Q_Matrix 10^{-8} times larger

This scenario investigates the system's behavior when the process covariance matrix Q is increased by a factor of 10^{-8} , representing significantly reduced confidence in the process model. The test evaluates how the observer handles situations where the process model is considered highly uncertain, examining its ability to rely more heavily on measurements.



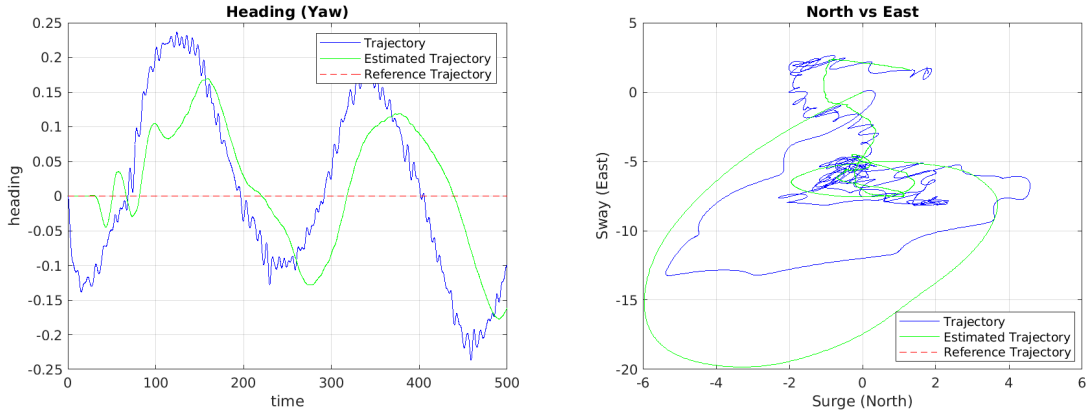


Figure 48: System Response with Modified Q Matrix

8.11.4 DP System Robustness - U-W is 5 times larger

This test examines the system's response to amplified environmental disturbances by increasing the wind noise power by a factor of 5. The simulation evaluates the DP system's ability to maintain position and heading under more severe wind conditions, testing the limits of the control system's disturbance rejection capabilities.

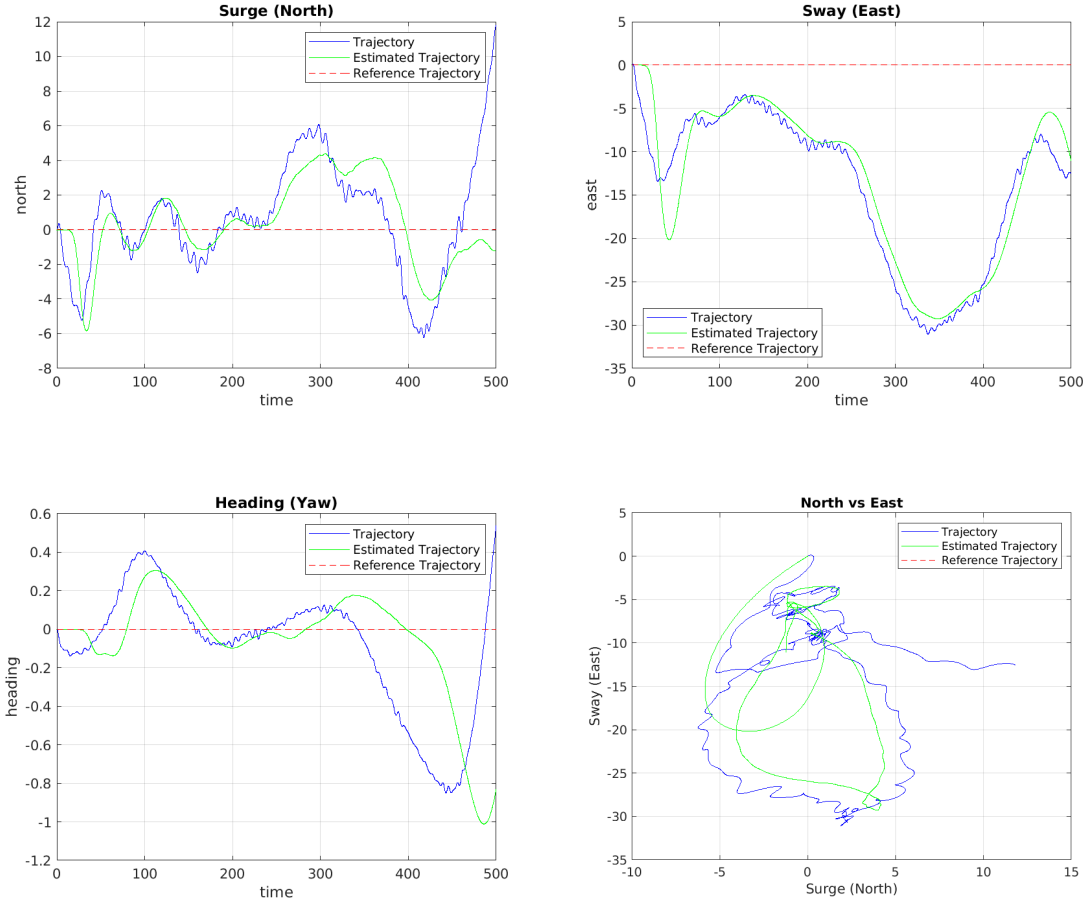


Figure 49: System Response with Increased Wind Disturbance

8.11.5 Discussion

The comprehensive testing of the DP system's functionality through various parameter modifications reveals significant insights into its robustness and limitations. In the nominal case, the system demonstrates stable performance with position deviations contained within ± 3 meters in surge and ± 5 meters in sway, while heading variations remain within ± 0.2 radians. When testing the measurement sensitivity through modification of the R covariance matrix (10^8 times larger), the system maintains remarkable stability, indicating robust observer design despite significantly degraded measurement quality. Similarly, adjusting the process covariance matrix Q (10^8 times smaller) shows the system's resilience to model uncertainty, with the position and heading tracking remaining within acceptable bounds. These results demonstrate that the observer design effectively handles both measurement noise and model uncertainties, suggesting successful implementation of the state estimation strategy.

However, the system shows notably different behavior when subjected to increased environmental disturbances, particularly with wind noise power amplified by a factor of 5. Under these conditions, position deviations increase significantly, reaching up to ± 8 meters in surge and ± 30 meters in sway, while heading variations extend to ± 1.2 radians. This marked sensitivity to environmental loads, particularly with wind from 315 degrees, current from $\frac{3\pi}{2}$ radians, and waves from $\pi + \frac{\pi}{4}$ radians, highlights a key characteristic of the system: while robust against measurement and process model uncertainties, it shows greater vulnerability to direct environmental disturbances. This behavior suggests that while the observer effectively handles system nonlinearities and measurement imperfections, its indirect approach to environmental load estimation may limit its ability to compensate for severe environmental disturbances. The North vs. East plots particularly illustrate this contrast, showing relatively contained trajectories in the covariance matrix tests but significantly larger excursions when environmental loads are intensified.

9 Conclusions

9.1 Summary of the project

In this project, we designed and simulated a dynamic positioning (DP) system for a ship using MATLAB Simulink and the MSS toolbox. The key components of the system included an observer implemented with an Extended Kalman Filter (EKF) and Passive Nonlinear Observers, a controller based on PID, and environmental forces representing wind, waves, and current. The primary goal was to achieve stable DP capabilities for the vessel, allowing it to maintain a specified position and heading despite external environmental forces.

9.2 Project Achievements:

1. We successfully implemented the DP system components, including the observer, controller, and environmental force models.
2. We performed various simulation tests to evaluate the system's performance under different conditions.
3. The system demonstrated the ability to maintain vessel position and heading accurately in the presence of environmental forces and disturbances.

-
4. We performed a fault tolerance test by disabling specific thrusters and observed the system's response to thruster failures.
 5. We assessed the robustness of the observers by varying wave height and period while keeping current and wind constant.

9.3 New Knowledge and Discoveries:

1. Through this project, we gained a deep understanding of dynamic positioning systems and their role in maritime applications.
2. We learned how to design and implement an observer-based control system using EKF and Passive Nonlinear Observers.
3. We acquired knowledge about the importance of fault tolerance and robustness in real-world systems, as demonstrated by the thruster failure and observer robustness tests.
4. The simulations helped us appreciate the complexity of marine systems and the challenges involved in maintaining vessel stability in adverse environmental conditions.

9.4 Limitations

1. The thrust utilization plots exhibit non-smooth transitions and irregular patterns between adjacent angles, indicating potential numerical instabilities in our implementation. This limitation affects the accuracy of our capability assessment under varying environmental conditions.
2. While our observer comparison demonstrates the superiority of the NPO over EKF, both observers show increased sensitivity to wave-induced disturbances under extreme conditions ($H_s = 8$ m), suggesting limitations in wave filtering capabilities.
3. The simulations are based on mathematical models and assumptions that may not fully capture real-world complexities, particularly in the interaction between environmental forces and the vessel's dynamics.
4. Our implementation shows particular vulnerability to wind disturbances, as demonstrated in Simulation 7, where a fivefold increase in wind noise power resulted in significantly larger position and heading deviations compared to other parameter variations.

9.5 Areas for Improvement

1. The thrust utilization calculation methodology could be enhanced by:
 - Implementing finer angle increments (e.g., 5° instead of 10°)
 - Refining the numerical integration methods
 - Developing more sophisticated averaging techniques for thrust calculations
2. The observer design could be improved by:
 - Implementing additional wave filtering capabilities for extreme conditions

-
- Developing hybrid observer strategies that combine the best features of both EKF and NPO
 - Optimizing tuning parameters for better performance under varying environmental conditions
3. The thrust allocation system could be enhanced through:
- Implementation of more advanced optimization algorithms
 - Better handling of thruster failures and constraints
 - More efficient power distribution strategies

In conclusion, this project provided valuable insights into the design and simulation of a dynamic positioning system for maritime applications. While we achieved the project's objectives, there are opportunities for further refinement and real-world testing to enhance the system's robustness and performance.

References

- [1] Asgeir J. Sørensen. *Marine Cybernetics: Towards Autonomous Marine Operations and Systems*. Lecture Notes for TMR4240 and TMR4515 Marine Control Systems, Norwegian University of Science and Technology, Trondheim, Norway, 2018.
- [2] Thor I. Fossen. *Handbook of Marine Craft Hydrodynamics and Motion Control*. John Wiley & Sons Ltd, First Edition, 2011. ISBN: 978-1-119-99149-6.